博士論文

Growth of high-quality graphene by alcohol CVD method

(アルコール CVD 法による高品質グラフェンの合成)

陳　嘯

Growth of high-quality graphene by alcohol CVD method

(アルコール CVD 法による高品質グラフェンの合成)

Xiao Chen

陳　嘯

A thesis presented in partial fulfillment of
the requirements for the degree of
Doctor of Philosophy

Department of Mechanical Engineering
The University of Tokyo

東京大学大学院工学系研究科機械工学専攻

August 2014

Acknowledgements

With the utmost gratitude I would like to thank my supervising professor, Shigeo Maruyama, for his persistent support, and enduring guidance during the past three years. His enthusiasm in education and research, along with his experience and knowledge has led me to become a full-fledged researcher. His inspiring encouragement and insightful advice brought me to success. I feel very fortunate to have him as my supervisor, and the precious experiences will be irreplaceable assets in my life.

I would like to thank Professor Shohei Chiashi for his motivating advices. His insightful teaching has greatly expanded my interest and enriched my knowledge.

I express my appreciation to Doctor Pei Zhao and Doctor Rong Xiang for their guidance as senior members of our group. Their experience and attitude toward research help me to establish my own position and interest in the field of graphene growth.

I owe deep thanks to all the other members in the Maruyama-Chiashi laboratory for being dependable and supportive, and all the friends in Shiomi laboratory for sharing opinions and knowledge.

I would like to thank the Global COE program and the SEUT program for their multiple financial supports.

Lastly, I would like to give my special thanks to my parents and fiancée for their support, understanding and love.

Contents

List of figures

Chapter 1
Introduction

1.1 A brief history of graphene

Graphene is the newest member of this already fascinating family of carbon allotropes. The study of carbon allotropes have always been an important issue in the fields of experimental physics, material science, and dynamics. Beautiful shinning and extremely hard diamonds, dark but smooth graphite (Figs. 1.1a and b), carbon allotropes have been well known, utilized, and studied by human for centuries. In

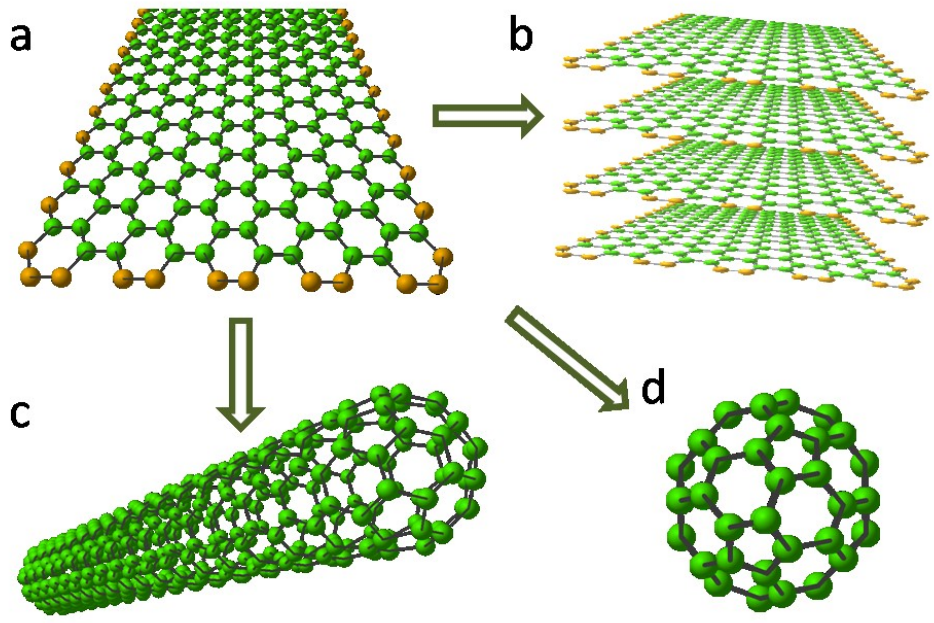

Figure 1.1, Forms of carbon allotropes that share the same honeycomb sp^2-bond structure. a) graphene b) graphite c) carbon nanotube d) buckyball fullerene

recent years, two newly found carbon materials, namely fullerenes and carbon nanotubes (Figs. 1.1c, d), have brought the research of carbon materials to a new era of excitement and fantasy. These three are composed by orbital hybridizations of sp2 bonds, which are called the graphitic materials.

Fullerenes were discovered in 1985 by Robert F. Curl, Sir Harold W. Kroto, and Richard E. Smalley [8], and it was a breakthrough for which they were awarded the Nobel prize in chemistry in 1996. The most well known fullerene is the "buckyball", or C_{60}. Due to its spherical symmetry and small size (consisting of 60 atoms), it is nearly a zero-dimensional (0D) material, also known as a quantum dot. Another great breakthrough is the finding of a 1D carbon allotrope, known as a carbon nanotube (CNT), which was discovered in 1993 [9-10]. Before graphene, buckyball fullerene and CNTs have already showed the world a spectacular future of extreme strength and excellent electronic properties that was supported by sp^2-bonded carbon atoms. So upon the discovery of graphene, which was exfoliated from graphite by K. S. Novoselov and A. K. Geim [11], the tremendous attention and enthusiasm towards it seemed only fair and natural.

Graphene shares the same basic structure as buckyball fullerenes and CNTs. It can be stacked into 3D graphite, rolled into 1D carbon nanotubes, or wrapped into 0D

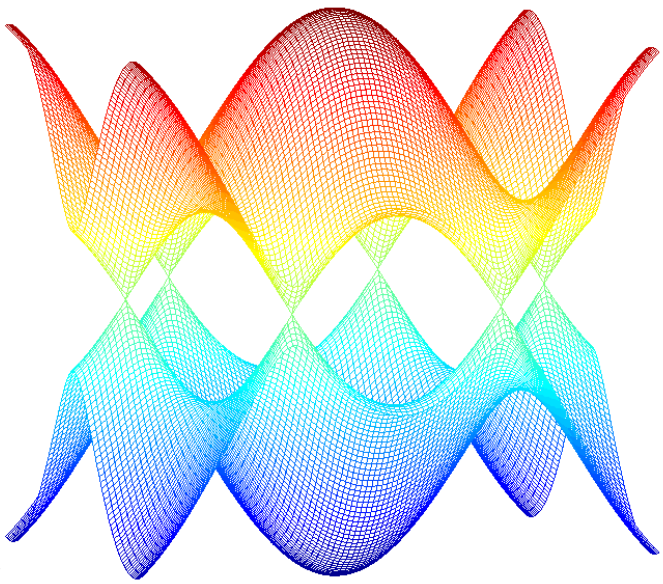

Figure 1.2. Electronic band structure of graphene

fullerenes [12]. In narrow sense, graphene is only defined as a single 2D hexagonal sheet of carbon atoms (Fig. 1.1e), more than one layer should be named as graphite. But because double layers and few layers possess similar characters as single-layer graphene (SLG), in broad sense, the concept graphene also include double layers and few layers, namely bi-layer graphene (BLG) and few-layer or multi-layer graphene (MLG). Few-layer graphen have 3 to 10 layers of such 2D graphene sheets. Graphene containing more than 10 layers is considered as thick graphene sheet and is of little scientific interest.

1.2 Graphene properties

Many interesting properties come with the single-atom-thick nature and the sp^2-bonded honeycomb carbon structure of graphene. For example, graphene is almost transparent, with the transmittance ratio of about 97% for light with the incite wavelength of 550 nm. Half-integer quantum Hall effect at room temperature has also been observed in single-layer graphene. [13]

One of the most interesting properties of graphene is that there is a tiny overlap between valence and conductance bands (Figure 1.2), resulting in the metallic electrical performance.

The charge carriers in these structures are more naturally described by the Dirac equation rather than the Schrodinger equation, which are known as massless Dirac fermions. These quasiparticles can be seen as electrons that lost their rest mass or as neutrons that acquired the electron charge. Hence, very strong ambipolar electric field effect can be induced by applying gate voltage, such that carrier mobility exceed to more than 20,000 $cm^2V^{-1}S^{-1}$ (on Si/SiO_2 substrates), which is the highest among all materials in ambient conditions. For suspended graphene, the carrier mobility exceeds to more than 200,000 $cm^2V^{-1}S^{-1}$ [14], surprising number for any semi-conductive material. In 2010, C. Dean and colleagues proved that hexagonal boron nitride (h-BN) is a much more suitable high-k dielectric material than silicon dioxide for graphene, and reported a carrier mobility of more than 25,000 $cm^2V^{-1}S^{-1}$ for graphene on h-BN. [15]

Another important feature is the extreme strength that graphene shows [16]. The sp^2 bonds that connect carbon atoms in graphene are extremely strong, possessing

energy of 7.4 eV per atom, much higher that between graphene layers or carbon-metal, which is roughly 100 meV per atom. This makes graphene the strongest material ever, as demonstrated by C. Lee *et al.*[17], through the experiment in which an atomic force microscope (AFM) probe is utilized to push graphene sheet through on a perforated substrate. The break force of graphene is higher than any material ever measured, and it is roughly 300 times the strength of steel.

1.3 Graphene synthesis methods

Since graphene first isolated by K. S. Novoselov and A. K. Geim in 2004, the method they used, mechanical exfoliation by using scotch tape, has been the most widely used method even till now, due to its extreme simplicity, which surprised most scientists when it was first reported. Typically, Kish graphite or highly oriented pyrolytic graphite (HOPE), which is considered as many layers of graphene due to their excellent crystalline, is used as raw material. By sticking some graphite on scotch tape, and repeatedly folding and opening the tape area with graphite, very thin layers of graphene can be produced. Then place the tape on substrates (usually Si/SiO_2), use a pencil eraser to gently rub the back of scotch tape, and slowly rip the tape off. Thus, some thin graphite would be left on the substrate, and by observation

Table 1.1. Comparison of early graphene synthesis methods

	Advantage	Disadvantage
Micromechanical exfoliation	Simple and extremely high-quality	Small sized and hardly repeatable or controllable
Epitaxial growth on SiC	High-quality	Requiring high temperature and high vacuum, hard to control layer number.
Reducing graphene oxide	Efficient, simple.	Low-quality, lack control of morphology

using optical microscope, one may find SLG on this substrate.

Many groups utilize this method because the tools needed are so easy, and the resultant SLG is extremely high in quality. The highest carrier mobility of graphene with SiO_2 substrates derived in this way is more than 20,000 $cm^2V^{-1}S^{-1}$, higher than that obtained from any other methods. But the disadvantages of this method are also very obvious. The yield of SLG is very low, and even if one can find a piece of SLG, the size of it is often less than 100 micron. Although in recent years some effort has been made to increase the size of graphene by mechanical exfoliation, such as heating the graphite to decrease Van der Waal's force, ripping off scotch tape from substrates in special angle and speed, the sizes of SLG produced in this way are often still around tens of microns, even for experienced researchers. High-yield synthesis of graphene films was urgently needed.

Another interesting way to produce graphene is the thermal desorption of Si in single-crystal SiC. This method has been known to be able to produce graphite for over 40 years [18], [19], but only after 2004, people began to optimize this procedure to produce graphene. Typically, using the (0001) facet of single-crystal SiC, after surface preparation by H_2 etching or oxidation, oxidation is removed by heating the samples in very high vacuum with electron bombardment. This oxidize-and-deoxidize procedure must be conducted several times to improve the surface quality of SiC. After the final remove of oxide, the sample is heated to more than 1200 ˚C for several minutes to desorb Si, leaving thin graphene layers [20]. There are mainly two drawbacks of this method: the experiment conditions and equipment used are difficult to reach; the control over numbers of layers of graphene is insufficient. Without a proper solution of these two problems, after some initial published works, most groups decided not to follow this method.

The third method that I would like to mention is the reduction of exfoliated graphene oxide (GO) [21-22]. Graphite is first treated with an oxidative procedure to reduce the electronic conjugation by methods developed by Brodie, Staudenmeier, and Hummers, respectively, then reduced by hydrazine hydrate. In this way, graphene small flakes can be produced, but the size and quality of them are not eligible for most applications.

Comparing the three early graphene synthesis methods mentioned above, we can

easily find out their advantages and disadvantages, as shown in Table 1.1. It is very clear that none of these three early methods are suitable for large-scale application or even for many scientific researches. In ideal method should be able to synthesize large-size, uniform, flat, low-defect graphene in a simple and low-cost procedure. These are the reason that chemical vapor deposition (CVD) of graphene was developed and well accepted.

1.4 Chemical vapor deposition growth of graphene

The idea of graphene growth on metal surface is very old. One of the earliest observations of graphene was in 1965, the low energy electron diffraction pattern showed the evidence of graphene on Pt (100) surface [23]. At that time, surface scientists were often troubled by the carbon layers on metal surfaces, so before they took a deep look into this material, they developed a method to remove it [24]. So after SLG was identified in 2004, it became very straight forward to turn back to CVD as a method for graphene synthesis. The basic idea is: decomposition of carbon source in high temperature provides carbon which is adsorbed on metal surface, and the carbon adatoms form graphene structure epitaxially on metal surfaces (although later evidences prove that graphene growth on Cu is not really epitaxial). In the first graphene CVD paper, Alpha T. N'Diaye and collaborators showed that by deposition of the decomposition product of ethylene on the (111) face of single-crystal Ir, graphene single-crystals can be synthesized [25].

Later, more transition metals are reported to be suitable for graphene-growth substrates [26-29]. Among them, Ni and Cu [30], became popular for graphene synthesis substrates. In 2009, R. Alonso, J. Kong and collaborators provided a proto procedure for graphene growth on Ni substrate using methane as carbon source [31]. In this paper, they transfer the graphene with wet etching of metal substrates using PMMA as mediator, and this method became a standard transfer technique. But in their work, the yield of real SLG was considerably low. Soon afterwards, K. S. Kim and collaborators published a much better result from a similar procedure, with carrier mobility of 3700 $cm^2V^{-1}S^{-1}$ [32], which made graphene growth on Ni popular for a while.

Parallel to this work, X. Li and R. Ruoff conducted and published their work in

which Cu foils were utilized as substrates for CVD growth of graphene on Cu [33]. They showed that with Cu substrates, the resulting graphene was very homogeneously single layer.

1.5 Objective of this thesis

Despite all the excellent work done by former studies, there are still remaining challenges:

First, the control on number of layers was not sufficient. For graphene growth on Ni, SLG, BLG and FLG were often found on the same sample. Even for Cu substrate, which was generally considered in favor of homogeneous graphene, still some bi-layer region could be observed.

Second, the defect level was still higher than that of mechanically exfoliated ones. For mechanical exfoliated graphene, the carrier mobility on SiO_2 was over 20,000 $cm^2V^{-1}S^{-1}$, but in CVD derived graphene, carrier mobility was no more than 5,000 $cm^2V^{-1}S^{-1}$. There was often some D-band in the Raman spectroscopy for CVD derived graphene, while for mechanical exfoliation, the D-band in graphene was always zero.

Third, the mechanism behind this growth procedure was still not clear. In previous works, researches roughly summarized the growth mechanism for both Ni and Cu substrate. In the case of Ni, it was believed that a dissolving and precipitating procedure dominated the growth of graphene, due to high solubility of C in Ni [34]. As for Cu, the growth was a strict surface procedure, due to the low solubility of carbon in Cu. But the detailed mechanism was not sufficiently discussed, such as the catalytic role of Cu and Ni, how the nucleation formed, the expansion rate of graphene flakes during growth, and how the carbon atoms attacked on the edges of graphene flakes, etc.

Before I started this research, almost all the successful studies in this field were conducted using methane as carbon source, for its simplicity in CVD reaction. Some other carbon sources are reported, such as ethane [35], ethanol [36-37] or even solid materials[38-39] but their results are far from good enough to compare with that of methane. Considering the history of our lab, in which we demonstrated that due to the extra O atom in each ethanol molecule, very clean and single-walled

carbon nanotubes can be grown [40-41] we hope that this advantage would allow us to grow very clean and single-layer graphene, and the more complex decomposition products of ethanol would let understand the mechanism. Ultimately, we hope that we can grow large, low-defect, single-crystal graphene from ethanol.

1.6 Organization of this thesis

After a brief introduction on the structure, properties, and former synthesis methods of graphene, the ACCVD method, which is the main experiment procedure in this work, is introduce in Chapter 2. The characterization methods, especially Raman spectroscopy, is also explained and summarized in detail. In chapter 2, some of our initial work about graphene growth on Ni substrates is also reported.

Chapter 3 and Chapter 4 are the main contents of this thesis, in which I would explain in detail about how we manage to gradually improve the quality of graphene growth on Cu using ethanol precursor. Many problems with the quality of graphene are resolved by the optimization of CVD processes. Finally, high-quality large single-crystal graphene is synthesized by alcohol CVD method. The influence of each CVD factor is systematically studied and the quality of graphene films are confirmed through different characterization methods. A mechanism model emphasizing the role of surface oxygen is proposed. Moreover, we fabricated and tested the graphene/n-Si solar cells, and demonstrated the extraordinary performance brought by the improvement in graphene growth.

Chapter 2

Synthesis and characterization methods

2.1 Raman spectroscopy of graphene

Several basic characterization methods for graphene were developed before the proposal of its CVD synthesis. For example, graphene films with different layer numbers show obvious contrasts under microscopy when they are transferred onto Si wafer with the right thickness of oxide layers (such as 300 nm). Atomic force microscopy (AFM) was also used to judge the existence of graphene based on its uniform height. But these methods are circumstantial and unreliable, providing no information on the quality of atomic level. Soon after, Raman spectroscopy became a major method for the characterization of graphene, for its detailed and direct information on the local chemical structure of materials.

Raman spectroscopy has historically played an important part in the structural

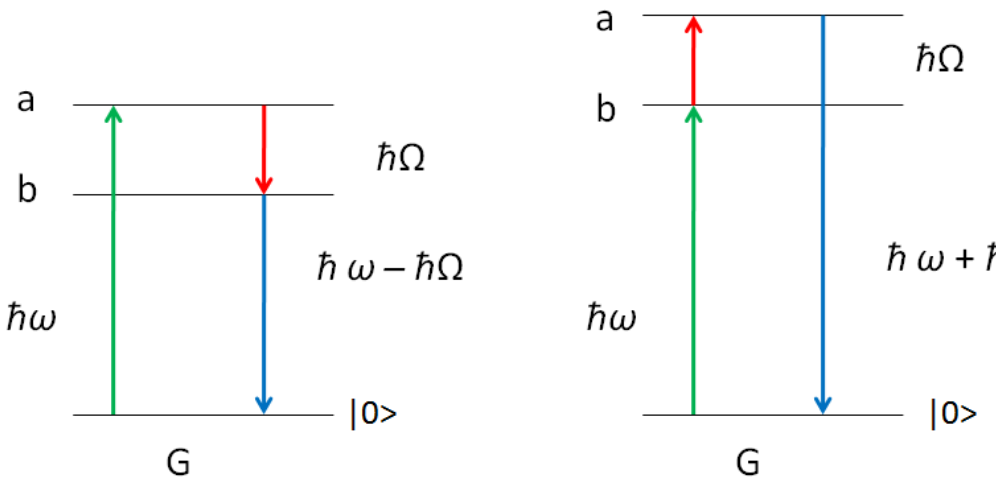

Figure 2.1 Raman processes of a) Stokes scattering and b) anti-Stokes scattering

characterization of graphitic materials, especially carbon nanotubes (CNTs), for its thorough information about the charality, defect level, diameters, etc. Since graphene share the same basic structure as CNTs, the characterization method should be similar.

The principle of resonance Raman spectroscopy is the inelastic scattering of photon, which is phenomenon of change of frequency when light is scattered by molecules. When a light wave reaches a solid material or a molecule, most photons are elastically scattered, which means there is almost no energy difference between incident and scattered light, and this process is called Rayleigh scattering. However, there is a small fraction of light (approximately 1 in 10^7 photons) that is inelastically scattered, with a different frequency from the incident photons, which is called Raman scattering. If the energy level of the molecule is already above its lowest energy, then an encounter with a photon would make it obtain a transition to a lower energy, thus the photon is scattered with an increased frequency. Hence, we can conclude that the Raman shifts have such characteristic that they are equivalent to the energy changes involved to transitions of the scattering species, although Raman shifts are caused by rotational transitions of the scattering molecules, rather than

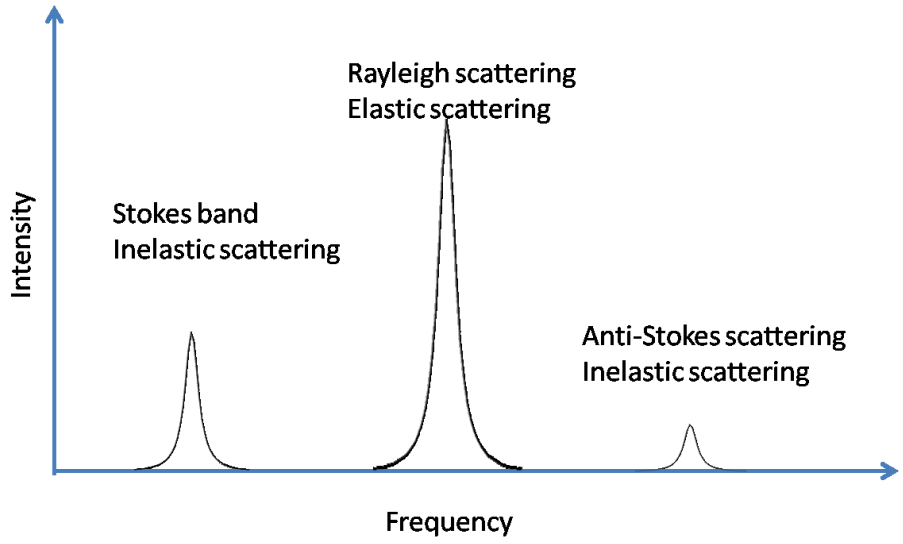

Figure 2.2. Spectrum of photon transition from elemental ground level to virtual states.

absorbed the photon perturbs the molecule and induces this phenomenon. In resonant Raman scattering, three processes occur as shown in Figure 2.1. Firstly, after absorbing a photon, an electron is excited from the valence energy band to the conduction energy band. Then the excited electron is scattered by emitting or absorbing phonons. In the end the electron relaxes to the valence band by emitting a photon. During the above procedure, if the scattered photon has lower frequency than incident photon, which means losing energy to phonons, then the phenomenon is called Stokes Raman scattering. Otherwise, if the scattered photon has higher frequency (gaining energy from phonons), it is called anti-Stokes Raman scattering.

We can obtain a Raman spectrum by plotting the intensity of scattered light as a function of energy difference marked as "Raman shift" (in unit cm^{-1}), as shown in Fig. 2.2. In Raman spectroscopy, the Stokes and anti-Stokes scattering signals are symmetric, and the Rayleigh scattering is displayed centrally (Raman shift = 0). This is because they all indicate the same phonon energy of the material. Raman

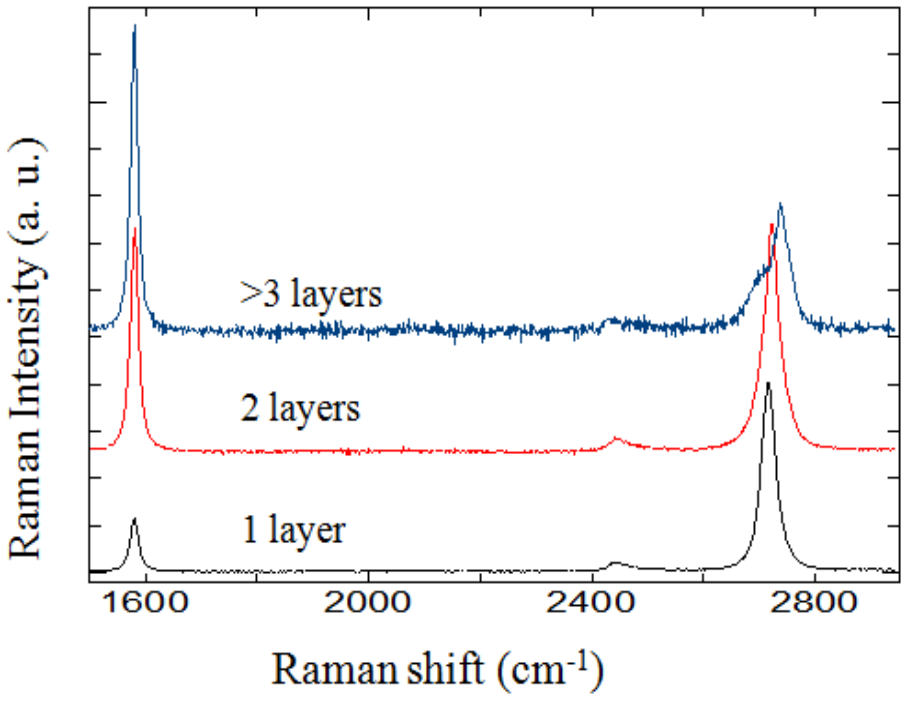

Figure 2.3. Raman spectra of single-layer, double-layer and few-layer graphene

intensity is proportional to the number of phonons, which can be described by Boltzmann distribution, therefore we obtain more intense signals in Stokes Raman scattering and usually only plot them in Raman spectra. Raman spectra reveal phonon explicitly, being independent of the electronic structure of materials and excitation laser energy, and in weak intensity. However, the scattering efficiency is largely enhanced when incident phonon matches the energy separation between two electronic states, and this process is called resonance Raman spectroscopy (RRS). This technique has become widely used to improve the S/N (signal-to-noise ratio) in Raman spectra.

The main features in the Raman spectra of carbon materials are the so-called G and D peaks, which lie at around 1580 and 1360 cm^{-1} respectively for blue light (488 nm) excitation. For graphene, a special third peak called the G' peak is also very important. Since it is located at ~2700 cm^{-1}, nearly twice the Raman shift of the D peak, this G' peak is also referred as the 2D peak. The G band is caused by the E2g vibrational mode, and the 2D band is a second-order two-phonon mode. The third feature, the D band at ~1360 cm−1, is not Raman active for pristine graphene but can be observed where symmetry is broken by edges or in samples with a high density of defects. It is the changes in the positions and the relative peak heights of the G and 2D bands that serve to indicate the number of layers for a given flake. The location of the G peak for single-layer graphene is 3-5 cm^{-1} higher than that for bulk graphite, while its intensity is roughly the same (In Figure 2.3, the curves are normalized with 2D peaks for the convenience in comparison).[42]

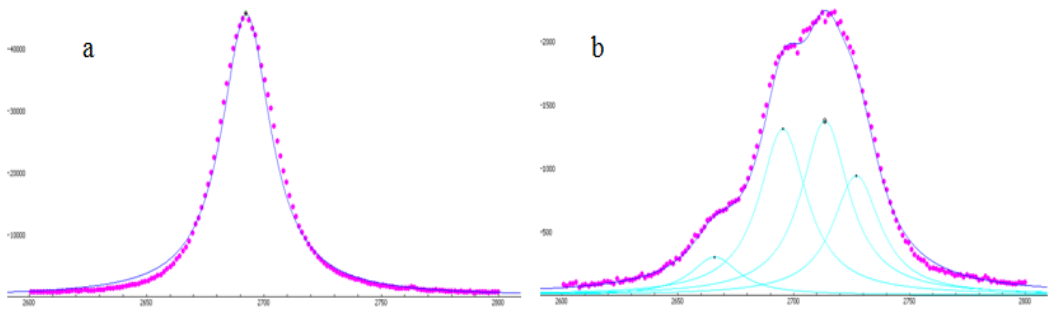

Figure 2.4. 2D bands of a) single-layer graphene, b) bi-layer graphene.

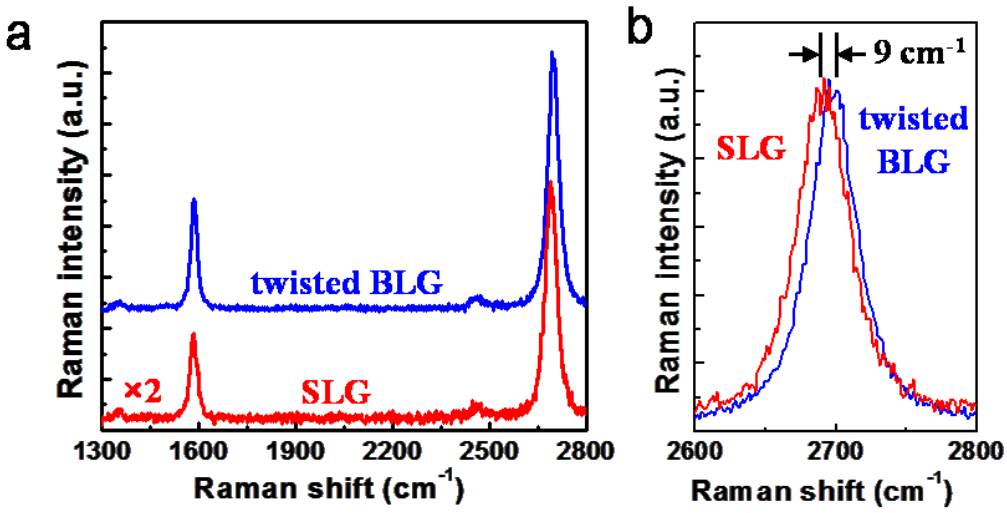

Figure 2.5. a) Raman spectra and b) 2D bands of twisted bi-layer graphene and single-layer graphene.

The 2D peak in graphene is due to two phonons with opposite momentum in the highest optical branch near the K point of the Brillouin zone. It can be split into four components, and each represents one possible choice of phonon scatter, due to the splitting in both valence band and conductance band. For single-layer graphene, there is no splitting in either the conductance band or the valence band, thus the 2D peak exhibits a strong and symmetric Loranzian (Figure 2.4 a). The intensity of 2D band of single-layer graphene is almost twice the intensity of G band, thus this is a convenient signature for the detection of single-layer graphene. The 2D peak shows a significant change in both shape and intensity as the number of layers is increased. For double-layer graphene, the 2D band is a combination of 4 individual components with different Raman shifts, so the intensity of 2D-band is decreased, and its width enlarged, with a unsymmetrical shape (Figure 2.4 b). Its intensity is almost the same as G band. For graphene with 3 layers or more, the 2D band consists of more components, its intensity becomes lower, and the shape is more complex.(Figure 2.3) [43-44]

The 2D band for bi-layer graphene discussed above is only referring to

AB-staking BLG. For there is a chance that the orientations of two layers of graphene are normal to each other, and the stacking order is not AB Bernal-stacking. We refer to this kind of bi-layer graphene as twisted BLG. For twisted BLG, the valence and conductance bands are not split, so the 2D band is also strong and symmetric just like the 2D band of SLG (Figure 2.5 a), so the general Raman spectra for twisted BLG and SLG are very alike. But if observed more closely, there is a little shift (~9 cm^{-1}) between the 2D band of twisted BLG and that of SLG (Figure 2.5 b). This little shift allows us to confirm the number of layers accurately. These results about twisted bi-layer grphene are mainly discussed by A. MacDonald and colleagues [45], and Z. Ni and colleagues [46].

Due to these very special wave-shape characteristics of the Raman spectra of single-layer, bi-layer and multi-layer graphene, Raman spectroscopy becomes a very easy and accurate way not only to decide their layer numbers but also their qualities. More specific studies regarding the features for twisted bi-layer graphene with different twist angles, graphene edges, graphene with chemical doping, graphene under mechanical strain, are also conducted, providing us with thorough information for graphene characteristics [47-57]. In this thesis, unless mentioned otherwise, all Raman spectroscopy is conducted using a incite laser wavelength of 488 nm.

2.2 Alcohol CVD method

The synthesis of graphene on metal substrates is progressing quickly, but many challenges are still remaining. Many reported works have proved that CVD procedure is effective in synthesizing graphene from a variety of hydrocarbons such as methane, ethylene, acetylene and benzene, but the quality of the resultant graphene is in doubt. Besides, the mechanism of this CVD growth is not completely understood. So far, most of the works on graphene large single crystals have been conducted using methane as carbon source, following the initial successful trial reported by the Ruoff group in 2009 [33]. For its structural simplicity, methane is suitable for the on-going study about nucleation and graphene-edge attachment of C atoms. But some other hydrocarbons with more complex structures may prove to be more suitable for the growth of single-crystal graphene in future industrial

manufacture (such as lower temperature). Our group has shown that very clean and single-walled CNTs can be synthesized from ethanol, which is considered a benefit from its decomposition products [40-41]. Here I employ alcohol as carbon source, not only to take beneficial trial to see if all the excellent advantages in synthesizing CNTs still apply in producing graphene but also to learn the mechanism of CVD growth in a subtly different point of view.

The schematic of an ACCVD system in our lab is shown in Fig. 2.6. This system can provide a minimum pressure of 15 Pa and a maximum temperature of 1200 ˚C. Liquid ethanol is contained in a stainless-steel tank. The reaction chamber is a quartz tube, and we can load the sample in it through each end of the tube. The tube is surrounded by an electrical furnace to create a designed temperature for CVD reaction. During a CVD procedure, the ethanol vapor diluted by Ar/H_2 is pumped in to the quartz tube, ethanol would decompose into many products to provide carbon, and these carbon species would be adsorbed on the substrate to form carbon nanotubes or graphene, depending on the substrates and reaction conditions.

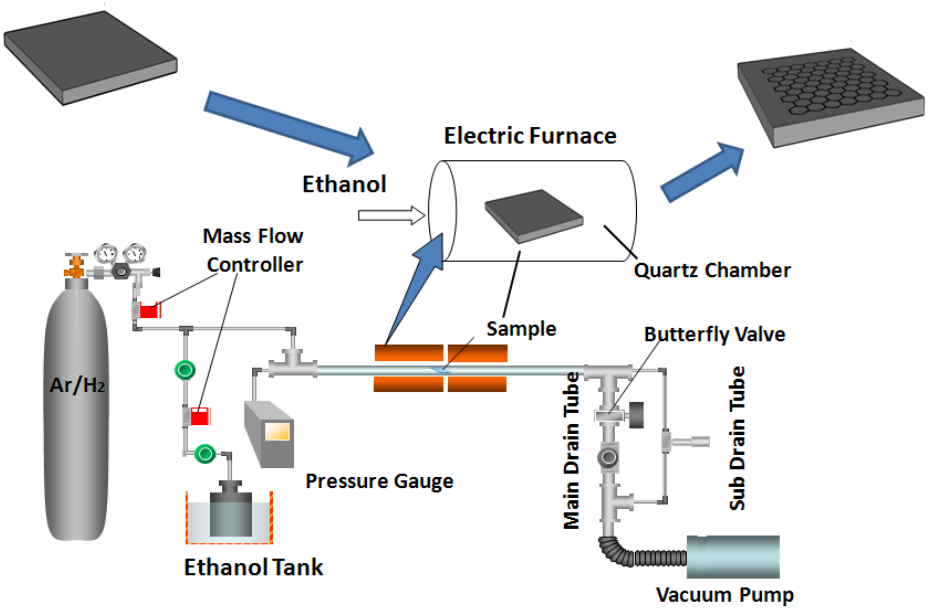

Figure 2.6. Schematic of ACCVD system for graphene growth. Note that mass flow of ethanol vapor is controlled with a mass flow controller, rather than a bubbling system.

2.3 Graphene synthesis on Ni using ethanol precursor

2.3.1 Background

It has been known for decades that CVD of hydrocarbons on reactive Ni or transition-metal-carbide surfaces can produce thin graphitic layers. The mechanism has been discussed since then, and a most accepted model is summarized as follows: hydrocarbons would be decomposed in a high-temperature environment, to provide carbon atoms, and these carbon atoms isolated would dissolve into bulk Ni. Then as temperature decreases, carbon atoms would precipitate out of the surface of Ni foil to form a graphite-like layer. This procedure is shown by Figure 2.7. So the key point on produce graphene on Ni foils should be reducing the massive carbon atom quantity dissolved in Ni surface. To achieve that, flow rate of carbon source should be low, and the pressure should be very low; besides, some groups claimed that very thin metal film would contribute in the same way.

Our work about graphene growth on Ni is mainly inspired by K. Kim et al [32] and A. Reina et al. [31]. They reported the growth of wafer-scale graphene films on Ni substrates using methane as carbon source. The carrier mobility in their graphene is more than 3,700 $cm^2V^{-1}S^{-1}$, which is very high considering all the other graphene synthesis works at that time, but there is still room for improvement. They show that their graphene films is not homogeneous, consisting of single-layer,

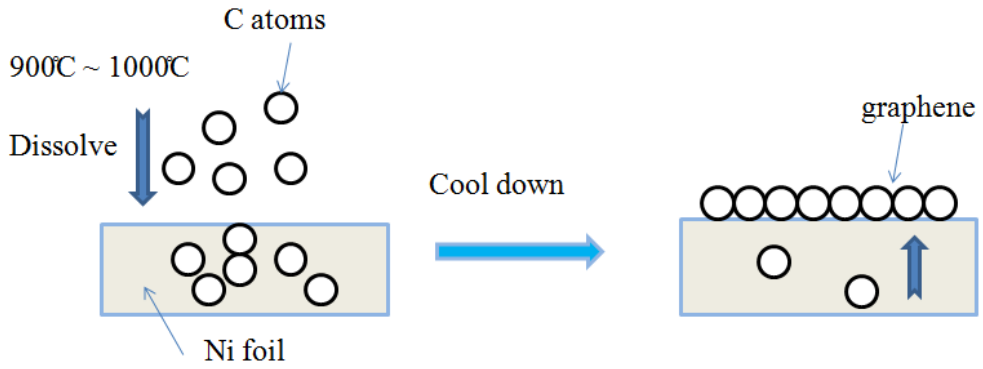

Figure 2.7.Schematic of graphene growth mechanism on Ni substrates

bi-layer and multi-layer graphene, which seems to be unavoidable considering the dissolution-and-segregation growth mechanism. We would very much like to see if ethanol can prove to be a better carbon source in realizing homogeneous single-layer graphene.

Parallel to our research, Miyata et al. published the first work using ethanol as carbon source on Ni substrate.[37] But their work is more of an initial trial, the resulting graphene in very inhomogeneous, with a very large D-band intensity indicating very strong defect level. They specifically emphasizing on the importance of fast cooling process at the end of a CVD procedure to successfully synthesize graphene, corresponding to the dissolution-segregation-precipitation mechanism.

2.3.2 Experiment procedure and characterization

Based on previous work, we explore our own growth procedure. Both commercial Ni foils (The Nilaco Corporation) with different thickness and deposited Ni film on Si/SiO_2 substrates are employed as substrates for graphene growth. The typical CVD processes are shown in Figure 2.8. In order to lower the numbers of layers, after many trials, major improvement has been made at the aspects of smaller vapor flow of ethanol and shorter CVD durations. Other CVD parameters, such as the reaction temperature, pressure, etc., are optimized as well. The typical procedure of synthesis is as follows:

The sample is loaded into the quartz tube, and is heated to 900°C, with a reduction gas flow of 300 sccm H_2/Ar during the heating. Because the carbon source needed is very little, we flow alcohol at a rate of 50 sccm for merely 2 s. Then a

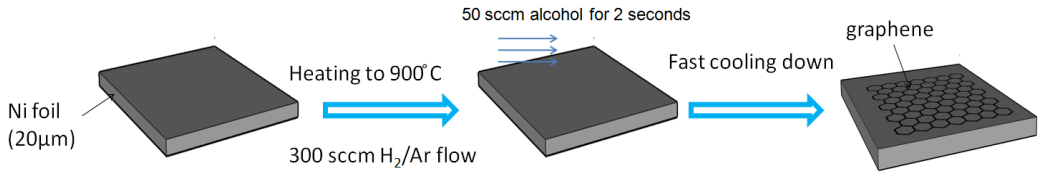

Figure 2.8. Schematic of graphene growth procedure on Ni substrates using ethanol as carbon source

cooling down procedure with normal cooling rate (about 10 °C per second) is applied.

Raman spectroscopy helped to detect the existence of graphene (Figure 2.9). To set a reference for the Raman features of graphene with different layer numbers, mechanical exfoliation was employed to produce graphene with the best quality, and their Raman spectra is shown in Figure 2.10. For their obvious contrast under microscopy, their layer numbers are accurately distinguished, and the Raman spectra from them can be used to identify all the graphene films from CVD method. Note that in Figure 2.9, the Raman spectrum of double-layer graphene and single-layer graphene taken directly on Ni substrates have quite similar profiles, unlike the Raman spectrum taken on Si/SiO_2 substrates after transferred (Figure 2.10). In order to get the homogeneity of graphene films directly on Ni substrates we have to scrutinize the wave shape of the 2D peaks to confirm whether the synthesized graphene is single-layer or double-layer. By using the same data used to

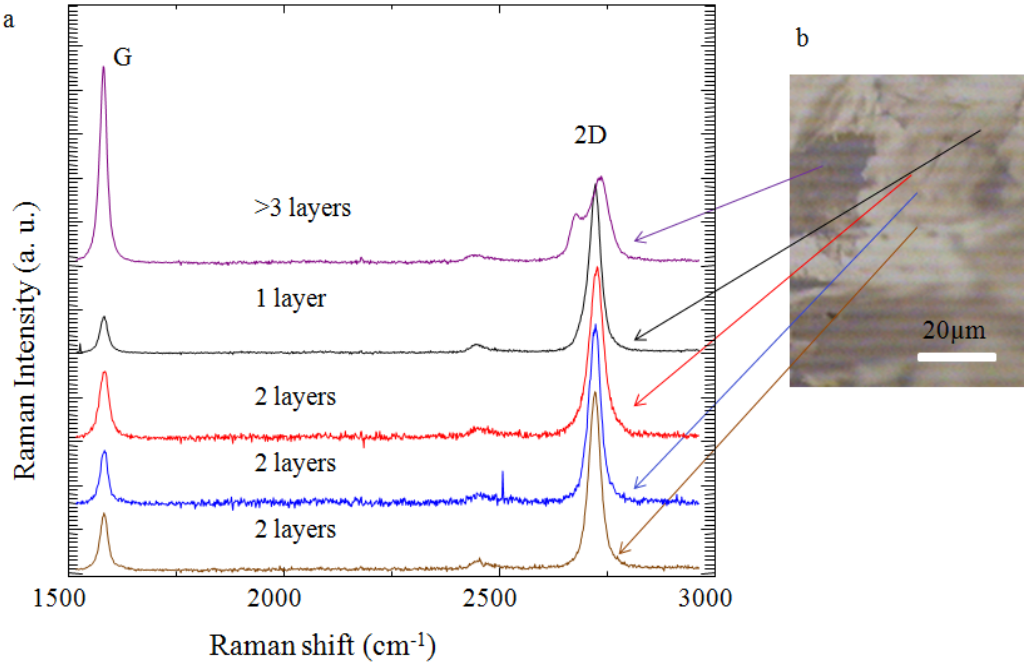

Figure 2.9. (a) Raman spectra of single-layer, double-layer and multi-layer graphene taken directly on Ni substrates. (b) optical image of graphene on Ni

plot Figure 2.9, I fitted the 2D peaks with Lorentzians. The 2D peak of single-layer graphene is perfectly symmetric and can be fitted by a single Lorentzian with a full-width at half-maximum (FWHM) of ~25 cm^{-1}; the 2D peak of double-layer graphene can be exactly fitted by four Lorentzians, each with a FWHM of ~25 cm^{-1}. The optical image in Figure 2.9 is not very clear because of a little curvature of the Ni film. Also, Figure 2.9-b clearly shows that the graphene film on Ni substrates is very inhomogeneous, and the same speculation is confirmed by Raman spectroscopy, as shown in Figure 2.9-a. Single layers, double layers, few layers coexist on Ni substrate.

Optical photos and SEM images of graphene growth on Ni substrates are taken. Before CVD, the pristine Ni foil shows bright, shining, metal color, as shown in Figure 2.11-a. After CVD growth, the Ni foil looks rougher, and a little darker (Figure 2.11-b). SEM images show that graphene cover the whole surface of the Ni foil. Some spots, contaminations and other kinds of imperfection can be observed

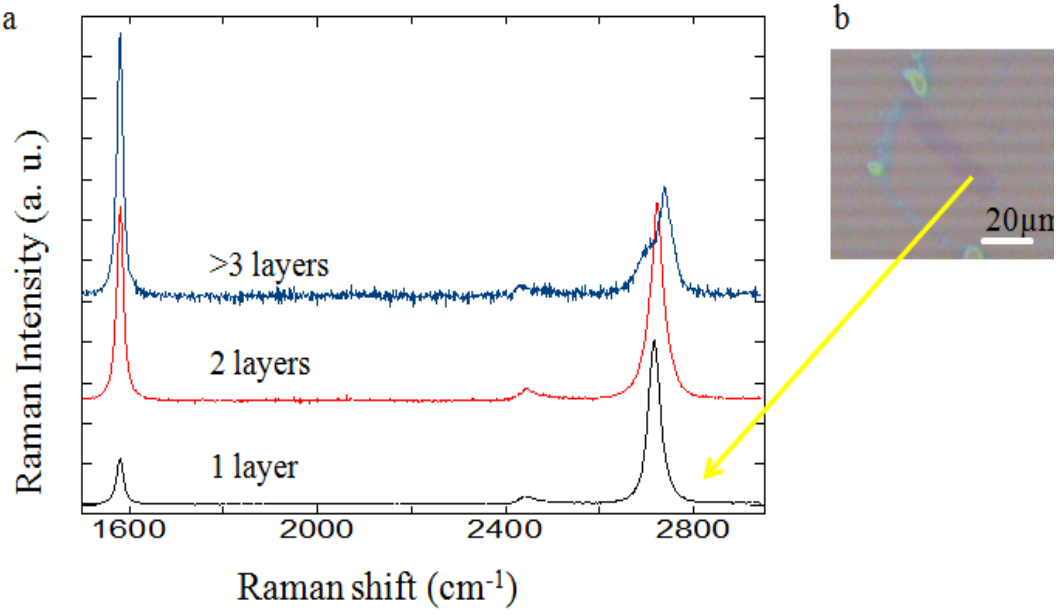

Figure 2.10. (a) Raman spectra of single-layer, double-layer and multi-layer graphene after transfer onto Si/SiO_2 substrates. (b) Optical image of graphene on Si/SiO_2 substrates.

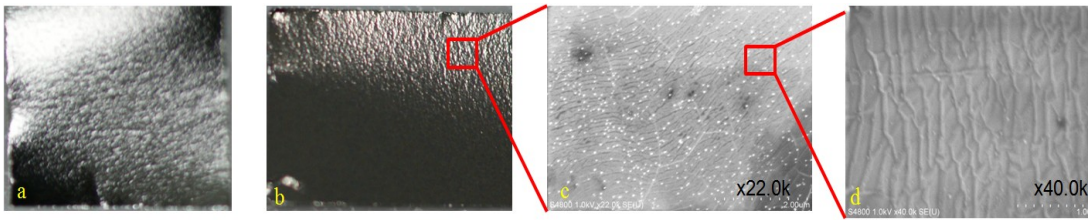

Figure 2.11. Photograph of the Nickel foil (a) before and (b) after undergoing CVD reaction along with SEM images (c and d) of graphene on Ni substrate.

on the graphene surface (Figure 2.11-c). Higher magnification reveals that there are many wrinkles in the graphene film, which may caused by the thermal expansion of the underlying Ni.

More specific Raman characterization was conducted after graphene film was transferred to Si/SiO_2 substrates. As explained in 2.1, the intensity ration of G peak/D peak reflects the defect level of the graphene film, and the very weak D peak in our result (Figure 2.12) suggests that our single-layer graphene has few defects (G/D ratio is ~ 10), while a later published result could not achieve results as desirable as ours.[37]

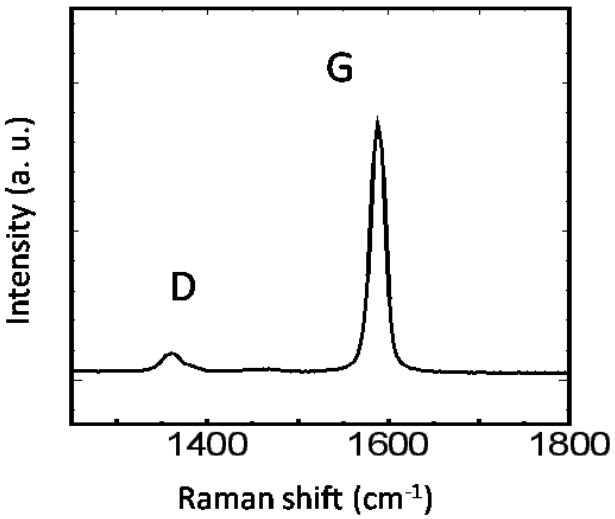

Figure 2.12. A typical Raman spectrum of our graphene film showing the area of D band and G band. The G/D ratio is about 10 for many measured sites.

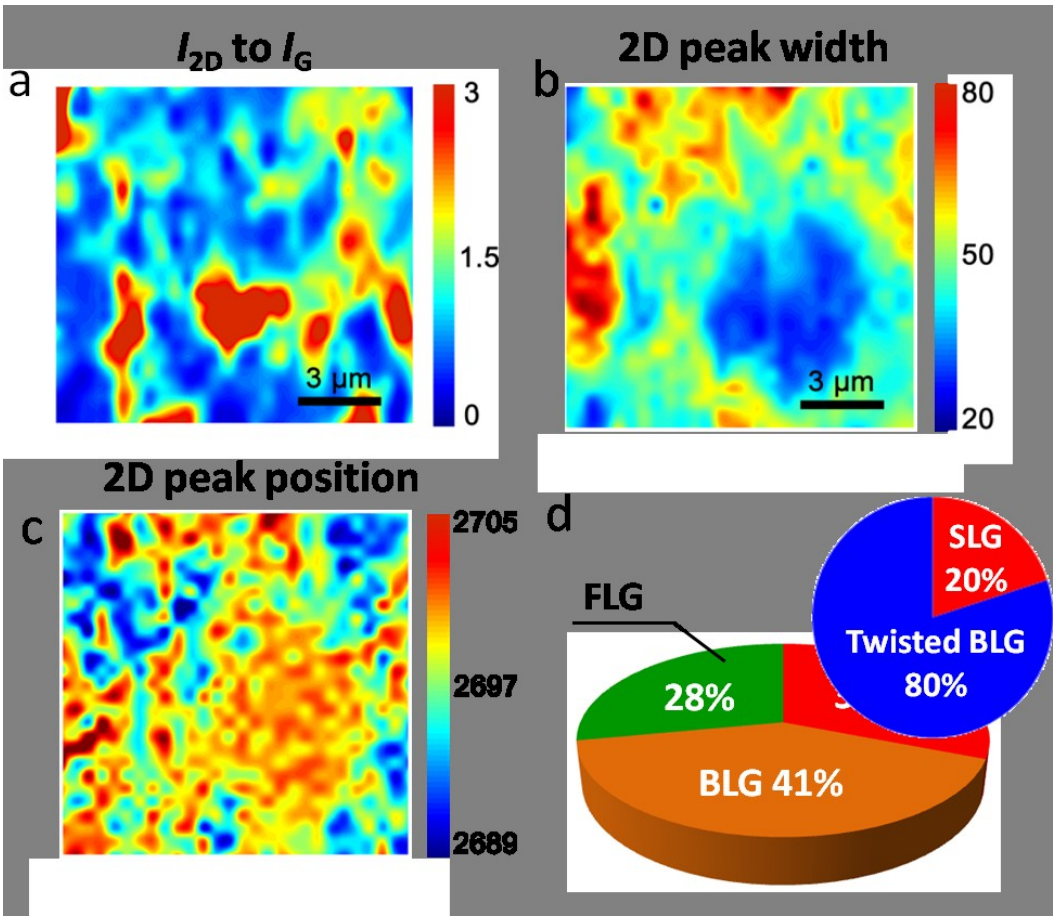

Figure 2.13. Scanning Raman spectra of graphene sample transferred to Si/SiO_2 substrates. a) 2D to G intensity ration map. b) 2D width map. c) 2D peak position map. d) the ratio of different layer numbers.

To further demonstrate the quality of our graphene film, we employ scanning Raman spectroscopy. We scan an area of 15 μm × 15 μm, after we transfer the graphene film onto Si/SiO_2 substrate. The map of 2D to G ratio and the 2D width are drawn in Figure 2.13-a, b. Here we roughly decide that if the 2D to G ratio is higher than 1.5, and the 2D width is smaller than 35 cm^{-1}, then we believe this area is singe-layer. By this principle, we count in Figure 2.13 a and b, and come to the conclusion that 31% of the area that we scan with Raman spectroscopy is single-layer graphene, 41% is bi-layer graphene, and the rest 28% is few-layer graphene. The ratio of SLG and BLG we acquired is among the best ever results on Ni substrates so far.

But on a closer observation, we find ourselves too optimistic. As discussed in 2.1, the 2D band of twisted bi-layer graphene exhibits the same characteristic as single-layer graphene. So the 31% single layer that we decided upon observation of 2D to G intensity ration and the width of 2D is inaccurate. So we draw another Raman map based on the position of 2D, as shown in Figure 2.13 c. Now with the blue-shift of nearly 10 cm^{-1} of twisted bi-layer graphene from single-layer graphene, we are able to distinguish them. We find that among the 31% area, there is actually 80% twisted bi-layer graphene, and only 20% is the real single-layer (Figure 2.13 d). This suggests that the majority of our graphene film synthesized on Ni films is double-layer graphene. Both commercial Ni foils and deposited Ni films are applied as substrates, and they exhibit no obvious difference.

We also studied the influence of CVD temperatures on the synthesized graphene. We selected 5 points randomly on 5 samples synthesized at different temperatures and mapped out the relationship between 2D/G ratio and temperature. 2D/G ratio is used as an approximate parameter to determine the amount of graphene layers at each point. Because this Raman spectrum is directly taken from Ni substrates, single-layer graphene could be confirmed only when 2D/G ratio is around 5. If 2D/G

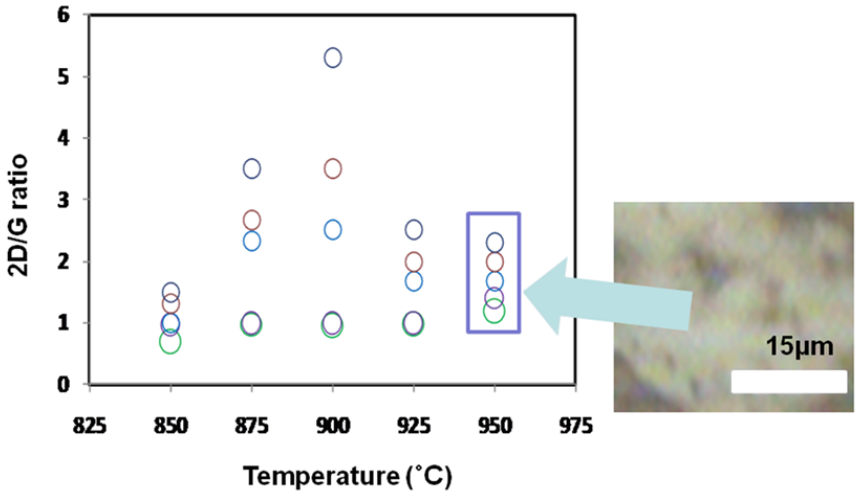

Figure 2.14. The study of homogeneity with different growth temperatures. At each temperature, we selected five random locations, for Raman observation, and plot the 2D to G ratios.

ratio is between 2 to 4, the laser spot may cover the boundary of double-layer graphene and triple layer graphene. On the when the 2D/G ratio is close to 2, the synthesized graphene is double-layer. From Figure 2.14, we see that only when the CVD temperature is around 900°C, single-layer graphene could be synthesized, but the graphene film is very inhomogeneous. Since we are not able to synthesize a majority of single-layer graphene, homogeneity of a double layer may also be important. When CVD temperature is 950 ˚C, the dispersion of 2D/G ratio is narrow and close to 2, suggesting the graphene film under this temperature is relatively uniform double-layer, and its optical image is shown in the inset of Figure 2.14. On the other hand, when temperature is lower than 875 ˚C, a majority of multi-layer graphene is observed.

Conventional view believes that there are two key points to synthesize SLG on Ni substrates: the very low thickness of Ni (less than or equal to 300 nm) foils and the fast cooling rate (around 10°C per second) after CVD reaction. So we also tried to grow graphene on 300 nm deposited Ni foils and apply a slow cooling rate (less than or equal to 1°C per second) after CVD reaction. The synthesized graphene samples have no much difference from the result obtain under previous proposed conditions.

2.3.3 Study of growth mechanism by carbon isotope labeling

Since we proved that the fast cooling rate may not be necessary for graphene growth on Ni using ethanol as the carbon source, we believe the mechanism of this growth may be other than the conventional dissolution-segregation-precipitation. Some other researchers also reported that with optimized conditions, uniform single-layer graphene can be formed by local saturation of carbon species on Ni surfaces, and Ni only act as a mediating carbon sink [58]. This is consistent with our results, for the fact that in our experiments, bulk Ni foils (20 μm thick) and deposited Ni thin films (300 nm thick) exhibit no much difference as substrates.

In order to study the mechanism, we did four experiments using carbon isotope labeling. Because ^{13}C ethanol is very expensive, a no-flow procedure for graphene growth is developed. This procedure is almost the same as the proposed one except that after heating the sample to 900°C, instead of flowing alcohol at a constant rate, we add in a preset amount of alcohol into the sealed tube at one time. After keeping the CVD reaction running for ten minutes in a closed environment we then cool

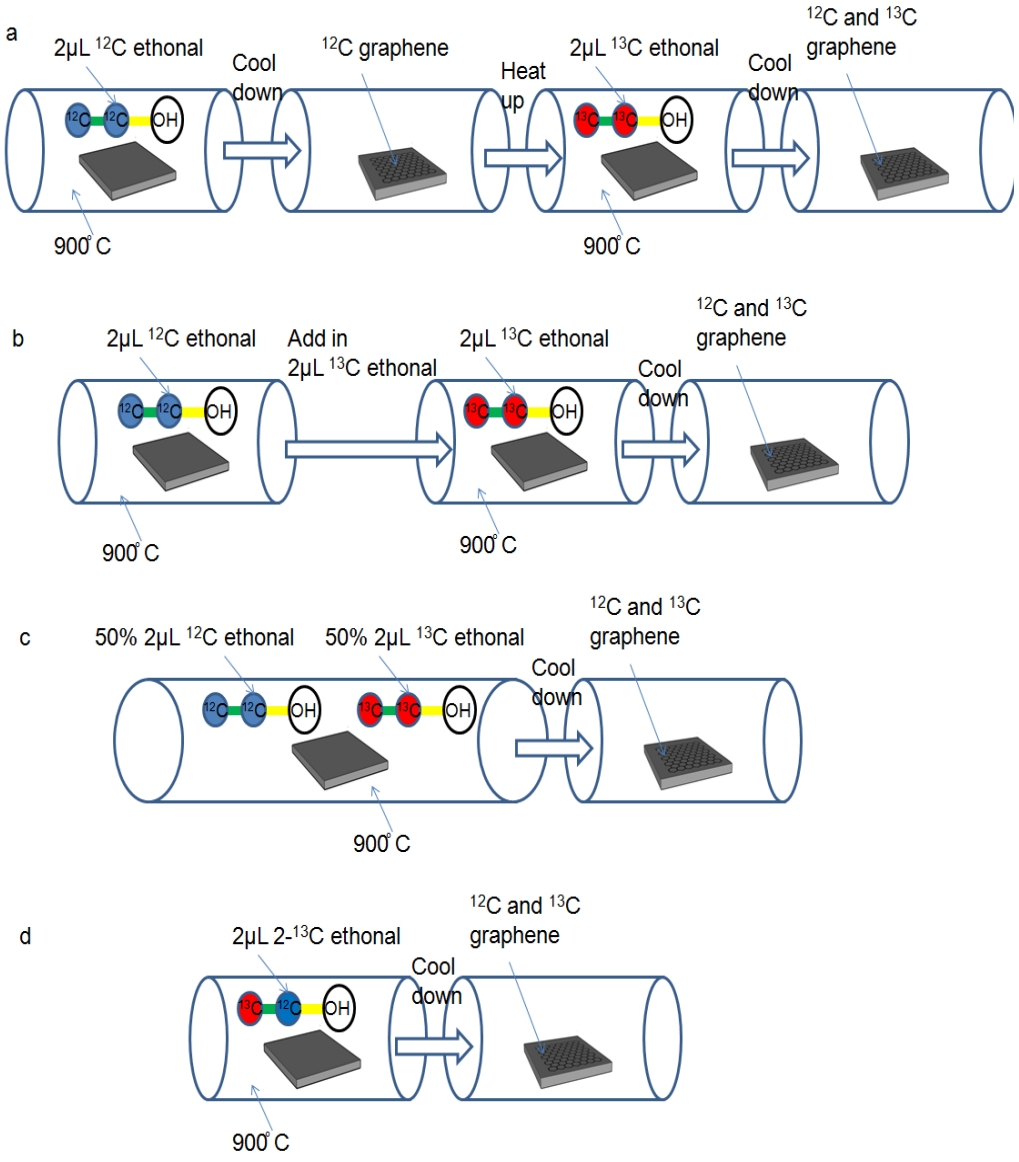

Figure 2.15. Schemes of isotope-labeling experiment processes

down the tube. This process makes it possible for us to precisely control the amount of carbon source or the ratio of different carbon sources. In this case, we involve three kinds of ethanol, ^{12}C, ^{13}C and 2-^{13}C. The procedures of these three experiments are shown as below.

Experiment **a**:

Firstly we provide an amount of 2μL ^{12}C ethanol to react with the Ni foil, then we cool the tube down to ambient temperature, so that graphene synthesized from ^{12}C ethanol could be formed. In the second step, we heat the tube to 900°C again and add in 2μL ^{13}C ethanol to react with the sample, then cool down to ambient temperature.

Experiment **b**:

Experiment **b** is almost same as the experiment **a**, except that there is no cooling down process between the two steps. After the reaction with ^{12}C ethanol, we directly add in ^{13}C ethanol without cooling down.

Experiment **c**:

In a no-flow CVD procedure, we use a mixture of 50% ^{12}C ethanol and 50% ^{13}C ethanol to react with the Ni foils. Then cool down to ambient temperature to form graphene.

Experiment **d**:

In a no-flow CVD procedure, we use 2-^{13}C ethanol to react with the Ni foils. Then cool down to ambient temperature to form graphene.

The schemes of these four experiments are shown in Figure 2.13. Besides these four experiments we also grew graphene using ^{12}C ethanol and ^{13}C ethanol separately. By comparing the Raman spectrum of graphene films produced by these four experiments, some interesting ideas can be drawn about the mechanism of CVD process on Ni.

Raman spectra of experiment **c** and **d** along with ^{12}C graphene and ^{13}C graphene are shown together in Figure 2.15. The frequencies of Raman modes are given by (1) with the assumption that the ^{12}C or ^{13}C atoms are randomly mixed and the bond force constants are equal.

$$\omega = \omega_{12}\sqrt{\frac{m_{12}}{n_{12}m_{12} + n_{13}m_{13}}} \qquad (1)$$

Where ω_{12} is the Raman mode frequency of ^{12}C graphene/ graphite, n_{12} and n_{13} are the atomic fractions, and m_{12} and m_{13} are the atomic masses of ^{12}C and ^{13}C, respectively. This equation is definitely applicable to the result of the experiment **c**. We use the center of FWHM of the G band (1585 cm^{-1}) and 2D band (2686 cm^{-1}) of ^{12}C graphene as standard, and compute the theoretical results of 50% ^{12}C graphene and ^{13}C graphene. Comparisons of these theoretical and experimental results are shown in Table 2.1, and there is not much difference between them.

Table 2.1:

	50% ^{12}C G band	50% ^{12}C 2D band	^{13}C G band	^{13}C 2D band
Theoretical	1558 cm^{-1}	2657 cm^{-1}	1522 cm^{-1}	2591 cm^{-1}
Experimental	1558 cm^{-1}	2660 cm^{-1}	1520 cm^{-1}	2590 cm^{-1}

In Fig. 3.11 we can see that the peak position of 2-^{13}C graphene is much closer to ^{13}C graphene than 50% ^{12}C graphene and ^{13}C graphene. This is because that the bond between C atoms in ethanol is weaker than the bond between C atom and O atom, so in experiment **d**, during the decomposing process more ^{13}C atoms than ^{12}C atoms are decomposed. Hence the synthesized graphene consists of more ^{13}C atoms.

Raman spectra of the first three experiments are shown in Fig. 2.16. Both results of experiment **a** and **b** are almost the same as experiment **c**, indicating that all produced graphene consist of equally and uniformly dispersed ^{12}C and ^{13}C atoms.

In experiment **a**, ^{12}C graphene was firstly synthesized before the adding of ^{13}C ethanol, but still the consequential graphene consists of equally and uniformly dispersed ^{12}C and ^{13}C atoms. This can only be explained that the strong sp^2 bonds are broken and ^{12}C graphene is decomposed at 900°C on Ni foil, and releases ^{12}C atoms which are dissolved into Ni foil mixed sufficiently and uniformly with ^{13}C atoms. Later they precipitate together during the second cooling down process to form a

50% ^{12}C graphene film.

In experiment **b**, ^{12}C atoms have completely dissolved into Ni foil before ^{13}C atoms access into the tube. But later they can still precipitate to form a uniformly dispersed 50% ^{12}C graphene film, suggesting that C atoms can be mixed with each other inside the Ni foil regardless the order of their entrances. All that C atoms can move relatively freely in Ni film. These results are consistent with the work of Li Xuesong et al.

By sequentially inducing ^{12}C and ^{13}C ethanol, if the graphene growth follow the conventional principle, i. e., the dissolution/segregation process, we should expect that the ^{12}C and ^{13}C form together during the cooling down process, which would result in randomly dispersed ^{12}C and ^{13}C atoms. Thus, the Raman spectrum of this mixed C isotope graphene should be a combination of ^{12}C and ^{13}C graphene, i. e., there should be a solo G band, with a position in between the pure ^{12}C-graphene G band and ^{13}C-graphene G band.

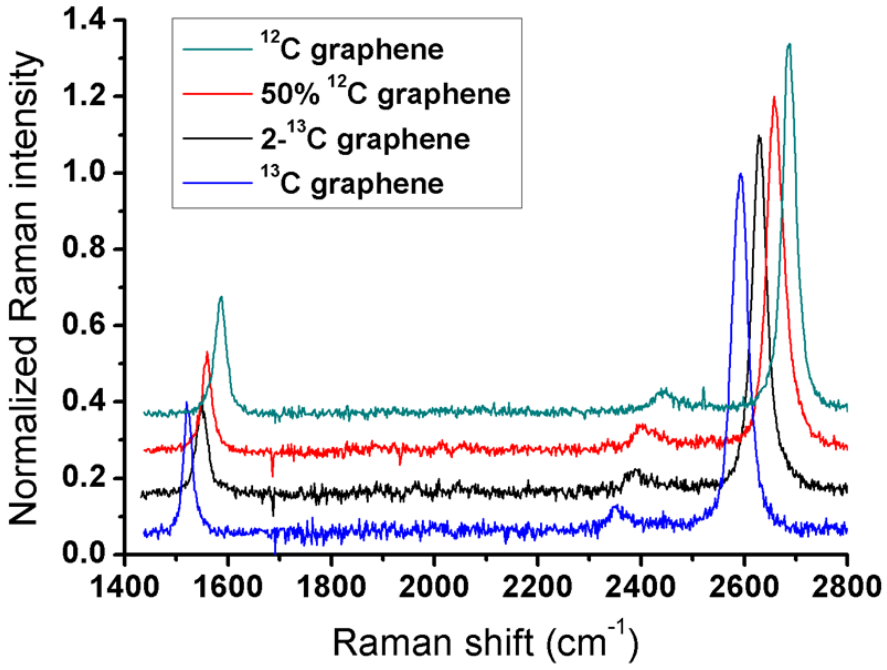

Figure 2.16. Raman spectra of graphene from carbon isotopes

Instead, we always observe the existence of separated ^{12}C-graphene G band and ^{13}C-graphene G band, as shown in Figure 2.17. For our Raman spectroscopy equipment, the size of the laser spot is around 1 μm^2, and it is very big compared with graphene lattice, but very small compared with the graphene film. So in Figure 2.17, the laser spot sometimes covers pure ^{12}C graphene, sometimes it covers both ^{12}C and ^{13}C graphene, and sometimes covers multi-layer graphene, but seldom does it cover graphene layer that consists of randomly mixed ^{12}C and ^{13}C atoms or only pure ^{13}C atoms, as shown in Figure 2.17. Almost all the areas that exhibit ^{13}C signals also show the existence of ^{12}C. From the Raman map

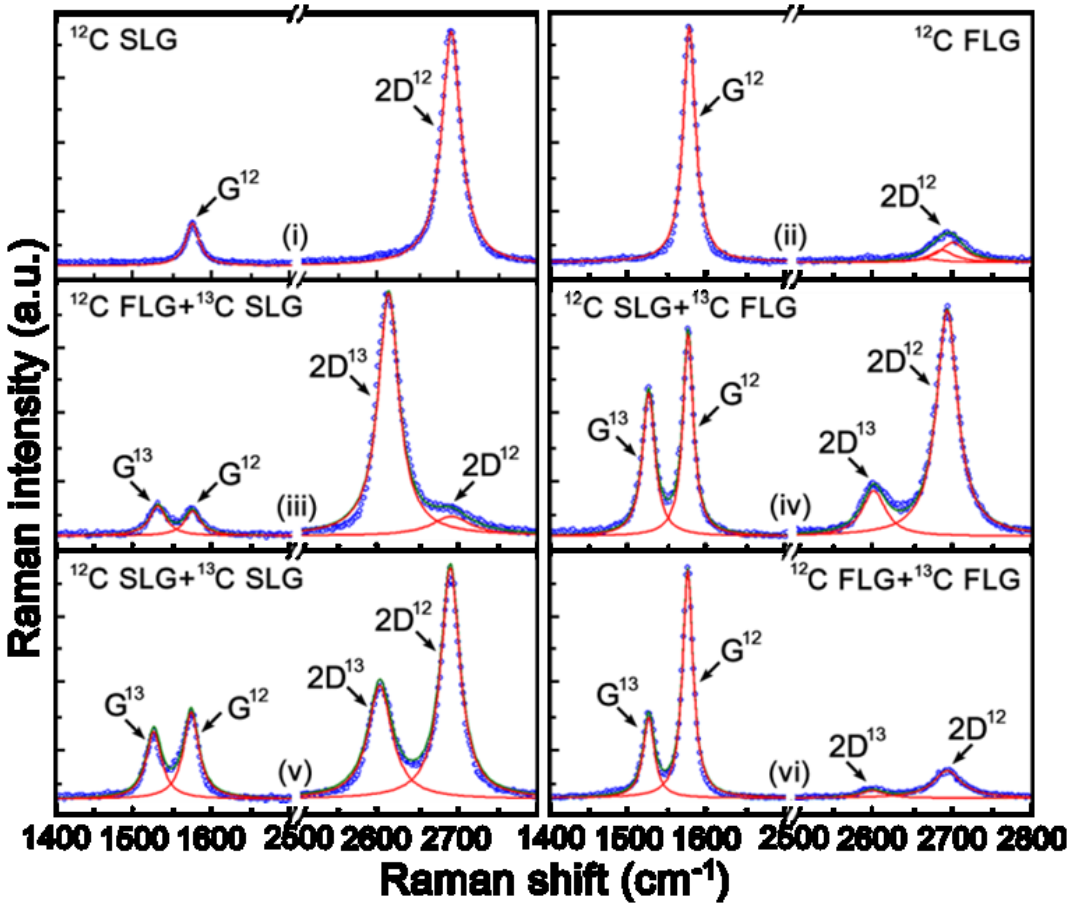

Figure 2.17. Typical Raman spectra for isotopic graphene samples. Spectra of single-layer graphene are shown on the right side, and spectra of few-layer graphene are shown on the left.

observation, we summarize two phenomena: firstly, ^{13}C graphene always coexist with ^{12}C graphene, while ^{12}C graphene can exist alone on the film; secondly, ^{12}C graphene and ^{13}C graphene are always separated, the two types of atoms are seldom evenly mixed.

The second point summarized above proved that the conventional dissolution/segregation process is not applicable for our graphene growth, since during the dissolution process, C atoms, regardless of induced order, must travel with high freedom and mix inside the Ni foils, thus it would without doubt result in a predominant evenly mixed isotopic graphene film. So we suspect that our growth mechanism is a surface procedure.

The first phenomenon proved our suspicion. The fact the growth of ^{13}C

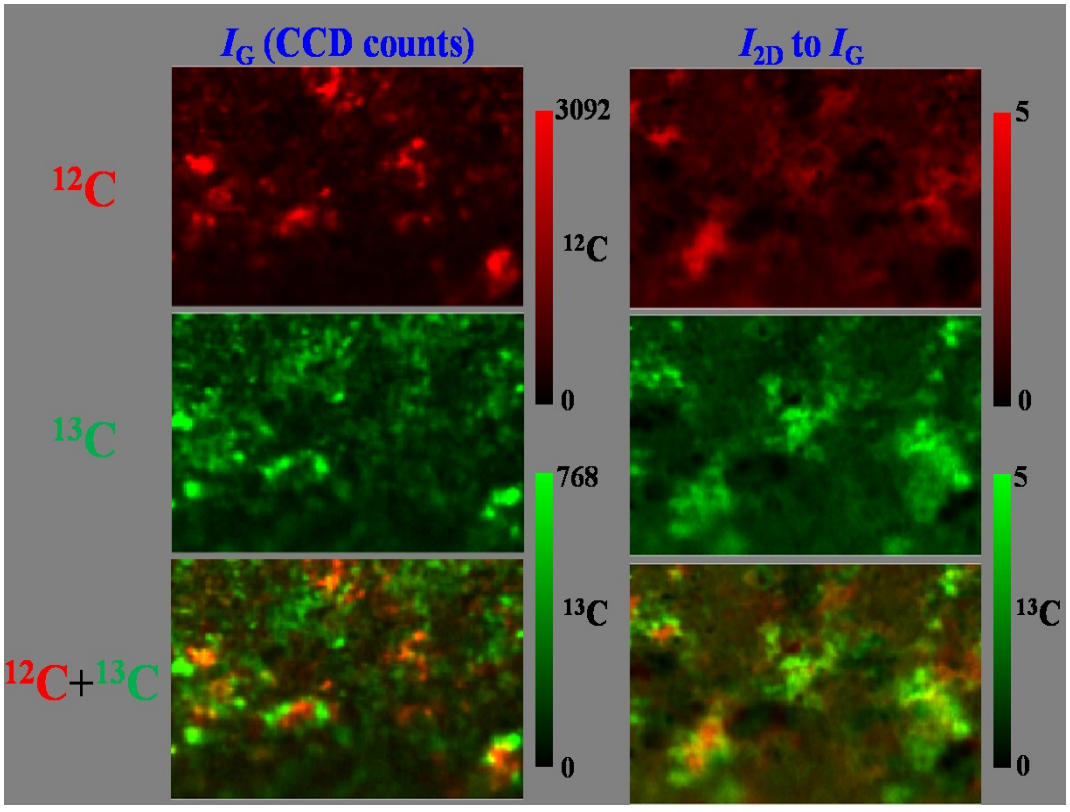

Figure 2.18. Typical Raman spectra for isotopic graphene samples. Spectra of single-layer graphene are shown on the right side, and spectra of few-layer graphene are shown on the left.

graphene always follows the growth site of ^{12}C graphene, suggests that there growth preference sites on Ni foil, which are obviously the imperfections on Ni surface such as step edges. In these experiments, firstly induced ^{12}C species start the growth on Ni foils, secondly induce ^{13}C species continue to grow on the growth preference sites occupied by ^{12}C graphene, and this procedure strongly suggests a surface procedure.

On the basis of the above results and discussion, we propose a non-segregation growth model to interpret the graphene formation on Ni surface from ethanol at high temperature. In this process, decomposition products of ethanol are partially catalyzed by Ni and form small carbon fragments on the surface. Due to the rapid surface saturation of Ni by the reactive carbon or buffering effects from the oxygen-containing decomposition products [59-60], instead of being dissolved into the bulk Ni, these small carbon fragments nucleate into graphene the growth. The nucleated carbon chains or hexagonal lattices rapidly expand to form SLG flakes. This rapid expansion of SLG forms a thermally stable equilibrium with the Ni system at high temperature, analogous to the "segregation" state of the Ni-C system. Graphene flakes formed on step edges quickly expand until a full cover of graphene layers are completed on the Ni surface. Extended growth time results in the formation of additional graphene layers when the carbon flux goes through the formed layers and in contact with the Ni surface. [61-62]

Note that our results don't necessarily contradict to the dissolution-segregation-precipitation model, since the mechanism could be very different for different carbon sources. For methane, which is the most commonly used precursor for graphene growth, the size of its molecules is small, and the dissociation energy is high, thus it is easier to be dissolved in Ni and less likely to react on the surface on Ni when energy is not sufficiently high (such as in low-temperature cases); and for some other non-hydrocarbon precursors, such as ethanol, benzene and acetylene[58, 63], the dissociation energy is low, combining with low reaction temperature, demonstrating a majority of surface-mediated reaction, resulting in a more uniform graphene film.

2.4 Summary

In this chapter, the basic structure and work function of ACCVD system is introduced. More importantly, the most powerful tool for graphene characterization, Raman spectroscopy, is introduced. And all the Raman characteristics for graphene are summarized and discussed, providing detailed information on the quality of CVD graphene film.

Moreover, with optimized CVD conditions, we proved ethanol as a replacement carbon source is equally capable in the synthesis of graphene. The resultant graphene films are mainly double layers, and 41% among them are AB-stacked, as confirmed by scanning Raman. The mechanism behind the CVD growth is explored via carbon-isotope labeling. With sequentially induced ^{12}C and ^{13}C ethanol vapor, the atoms of these two isotopes are not mixed, so we propose a surface adsorption model to explain the growth mechanism

Chapter 3
ACCVD synthesis of graphene on Cu

3.1 Background

Parallel to the works on Ni, many other groups tried to grow graphene on Cu substrates. The most successful results were published by the Ruoff group from UT at Austin, which they demonstrated that homogeneous single-layer graphene can be grown on Cu foils. Later, they showed that the growth behavior, *i.e.*, the evolution, the nucleation density, and the shapes of graphene flakes can be controlled by tuning CVD conditions. [64]

The major difference between these two transition metals is the solubility of C. In Ni, at typical CVD reaction temperature (900 ˚C), the solubility of C is ~0.9 at.% [65-66], thus a major dissolution of C atoms in the bulk Ni is entirely possible; while in Cu the C solubility is only ~4.8 at.ppm at 1000 ˚C [67], almost 2000 times lower than in Ni, thus a majority of C species would remain on the Cu surface, and the CVD reaction is refrained on the surface, which leads to a good control of number of layers. Many other transition metals may also be suitable for graphene growth, but Cu and Ni are obviously the low-cost choices, which is very important for both many repeating experiments and future industrial manufacture.

3.2 Single-layer graphene from ethanol on Cu

3.2.1 Growth procedure

Commercially available Cu foils (10-μm-thick, Nippon Denkai) were adopted as substrates. Thermally evaporated ethanol vapor was utilized as carbon source. The growth procedure (Figure 3.1) began with the cleaning of the substrate. Cu foils were washed with HCl solution, acetone and 2-proponal for 10 minutes each. Then

the Cu foils were placed into a quartz tube, and heated to 1000°C. We annealed the Cu foils for 40 minutes to increase the grain sizes and obtain a smooth surface. A 300 sccm flow of 3% H_2 diluted in Ar was used throughout the heating and annealing processes. After annealing, we cooled the system to the reaction temperature, optimally 900°C, and cut off the H_2/Ar flow. The Cu foils were then exposed to a 100 sccm flow of ethanol vapor for 20 seconds, at 70 Pa. Next, the ethanol flow was cut off and the system was cooled down to room temperature, with a 300 sccm H_2/Ar flow.

After growth, we transfer the graphene film to Si/SiO_2 via wet etching of the underlying Cu foils using poly(methyl methacrylate) (PMMA) as mediator. We spin-coat one PMMA (4% solution in anisole) layer on one side of the Cu foil, and stiffen the PMMA layer by baking it at 120°C for 2 minutes. The other side of the Cu foil was treated with O_2 plasma for 1 minute in order to remove the graphene. We immersed the sample into copper etchant (1 M $FeCl_3$) to etch the Cu foil, which would result in a PMMA/graphene film floating on the surface of the solution. The PMMA/graphene film was then washed with HCl solution and DI water for several

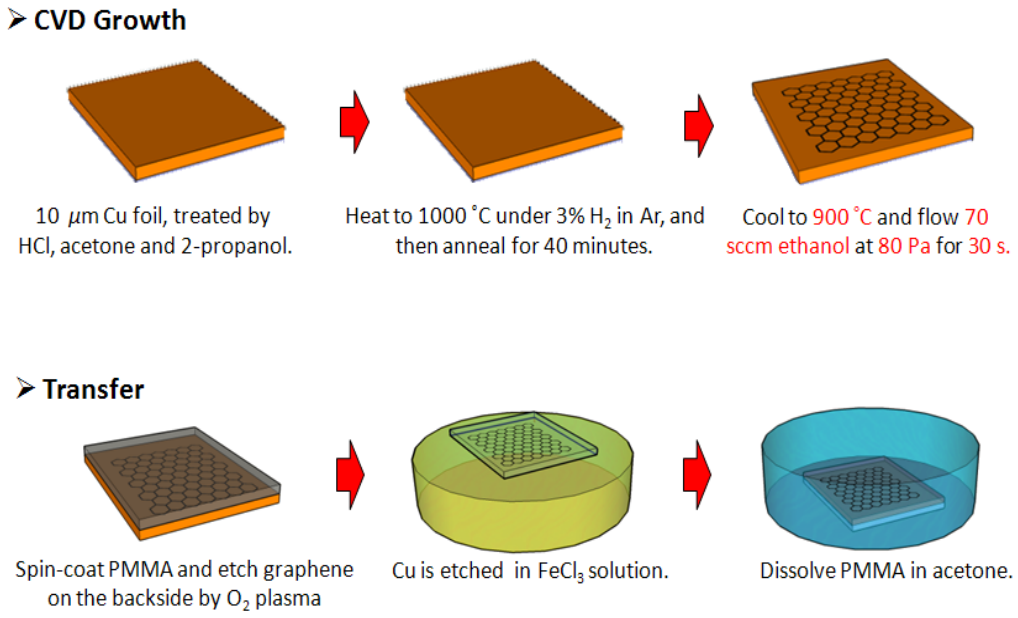

Figure 3.1 The basic CVD growth and transfer procedures that we apply in our experiments.

times and was transferred on to Si/SiO_2 substrate. Finally, we dissolved the PMMA film with a warm acetone bath to yield a graphene film on silicon substrate. The transferred graphene samples were characterized with Raman spectroscopy to evaluate the quality and the layer number.

3.2.2 Annealing of Cu foils

In the growth procedure introduced above, Cu foils are annealed in high temperature (~1000 ˚C) for 40 minutes. This procedure is due to the fact that Cu-foil surfaces are mostly rough, with lots of wrinkles and steps, and the sizes of Cu grains are very small. Annealing at high temperature can effectively smooth the

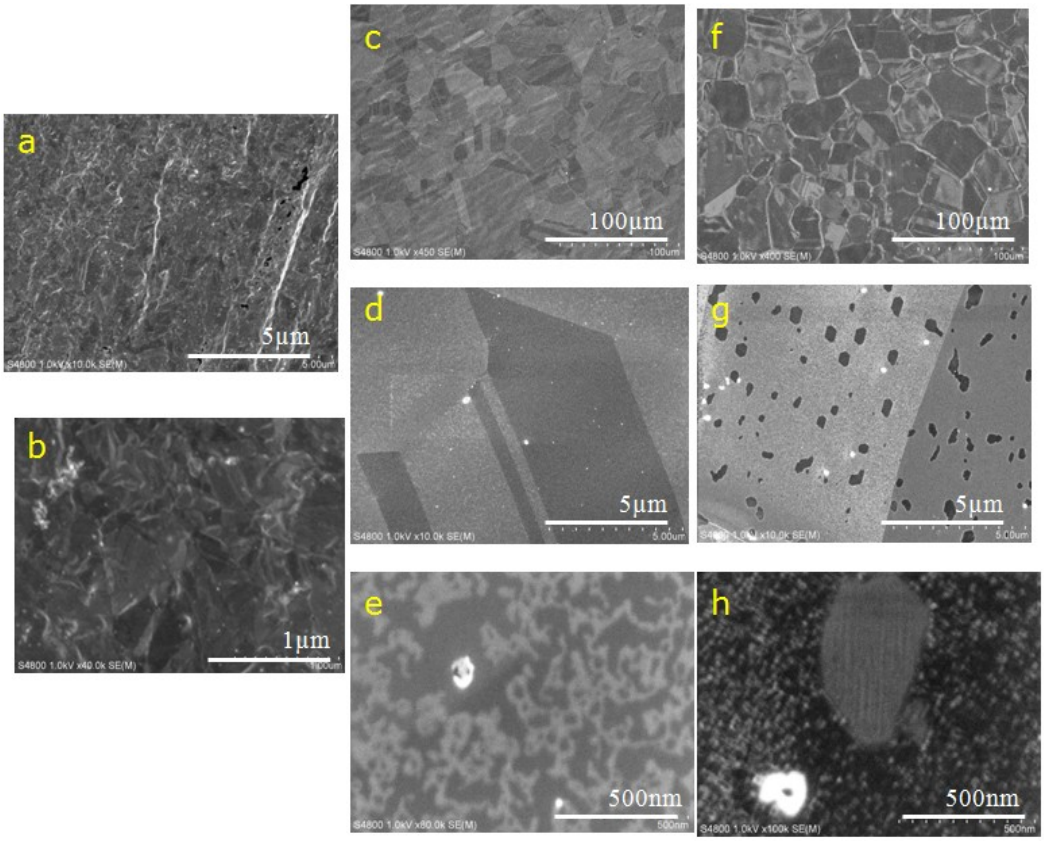

Figure 3.2 SEM images of Cu surfaces with different annealing times. a) and b) are pristine Cu surfaces, c), d) and e) are Cu surfaces after heating to 1000 ˚ C and immediately cooled down, f), g) and h) are Cu surfaces after a 40-minutes annealing process at 1000 ˚ C.

Cu surface, and enlarge the Cu-grain sizes, because of the low general energy statues of smoother surfaces as high temperature. [68] Figure 3.2 shows the effect of annealing. Here we understand that AFM observation may be a better method for such study on surface roughness, but we only applied SEM observation, since this improvement on the quality of Cu surfaces were already obvious under SEM; a more thorough investigation about the influence of annealing on Cu-surface roughness in shown in a published paper by our group [69].

Initially, pristine Cu surfaces are very rough (Figure 3.2-a, b), many step edges, grain boundaries, cracks, and so on are clearly visible with SEM. These imperfections in Cu surfaces are the preferred sites for the nucleation of multi-layer graphene, which would result in the low quality of graphene films. After heated to 1000 ℃ and immediately cooled down, some larger Cu grains and soother surface can be seen (Figure 3.2-c, d, e). The effect of annealing is very obvious; even without any annealing duration, barely the heating up process can effectively increase the surface condition of Cu foils. Figure 3.2-f, g, h show the Cu surfaces after a 1-hour annealing. The grain size of Cu is much larger, and the surfaces become much smoother.

Many have proved that the formation of graphene films can be affected by the underlying Cu surfaces, for example, the shape of graphene flakes can be six-lobed snowflake-like structures [2, 70], four-lobed star-like structures, or sometimes irregular shapes, and these patterns are believed to be related to the underlying Cu-surface morphology, such as the roughness or the crystal orientations. But generally, the interaction between graphene and Cu foils is relatively weak [71-73], compared with graphene on Ru(0001), where exclusively single perfect Moiré super-structures were observed.[74] Also, the reported growth results on single-crystal Cu (111) showed no much improvement compared with the results on poly-crystal Cu foils, and it is widely know that graphene flakes can continuously grow across Cu grain boundaries. So in general, we consider that the influence of Cu-surface morphology on the formation of graphene is only miner, so the pursuing of extremely smooth Cu surfaces with hours of annealing durations is unnecessary. We do acknowledge the importance on Cu lattice orientation towards the shape of graphene flakes, as shown in a published paper by our group.[69] But

we wouldn't emphasize too much on its affect for the quality of graphene films, so we only anneal the Cu foil for 40 minutes each time, resulting in a relatively smooth Cu surface. In this chapter, all growth procedures include a 40-minute annealing unless mentioned otherwise.

3.2.3 Results

A typical result of ACCVD graphene on Cu is shown in Figure 3.3. The SEM images of graphene before and after transfer (Figure 3.3-a, b) indicate good homogeneity and uniformity. The optical microscopic image (Figure 3.3-c) shows a clean and continuous transferred graphene film. We measured the light transmittance rate as a function of wavelength. When the wavelength of the light is 550 nm, the transmittance rate is ~96.95%, which is the signature of single-layer graphene.

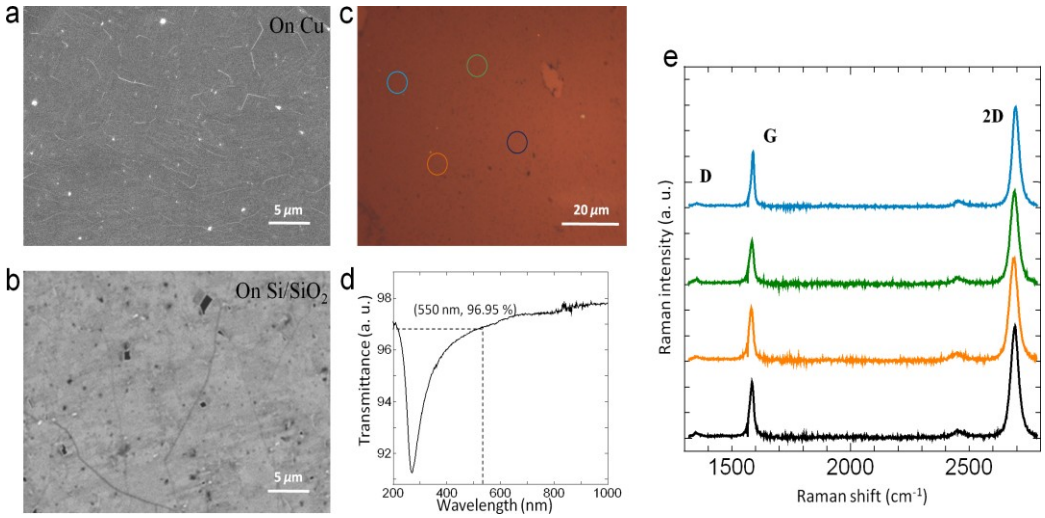

Figure 3.3. Characterization of ACCVD graphene grown at an optimized condition. SEM images of graphene on (a) Cu foil and on (b) Si/SiO_2 substrate. (c) Optical Microscopic image of graphene on Si/SiO_2 substrate. (d) Transparency rate of a graphene film transferred onto a quartz substrate. The transmittance rate is ~96.95% when the wavelength of the light source is 550 nm. (e) Raman spectra of four random points on the graphene film. All four spectra exhibit similar characteristics: I_{2D}/I_G is ~1.9, $I_G/I_D > 20$, and the FWHMs of 2D peaks are 35-39 nm^{-1}.

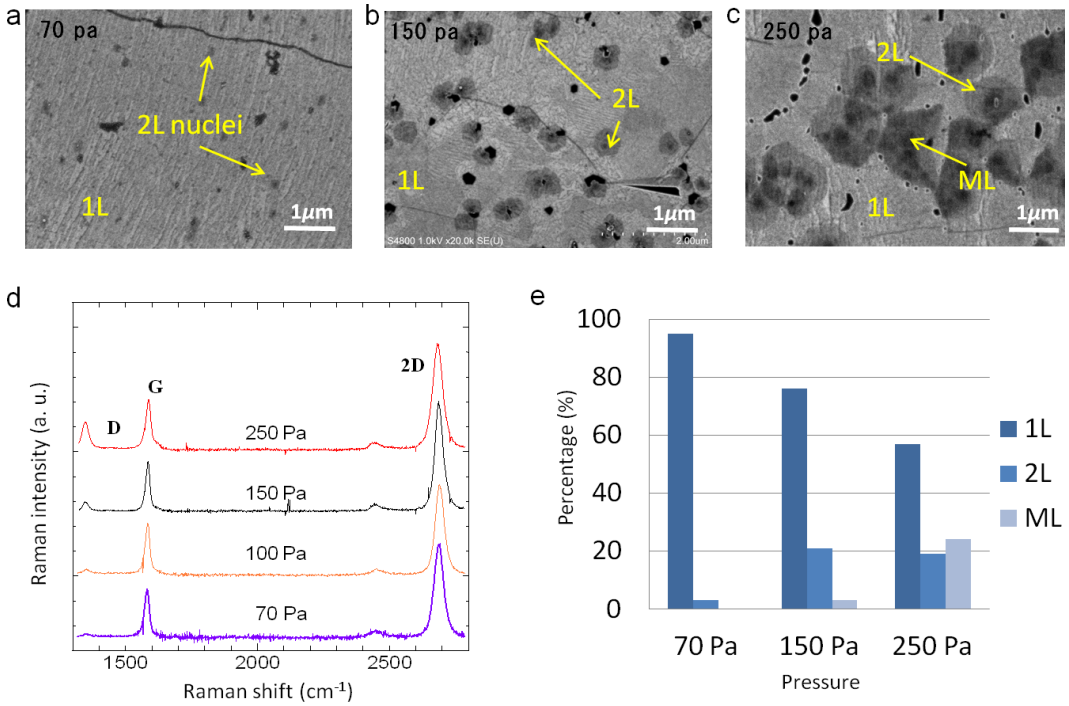

Figure 3.4. Graphene growth as a function of pressure. SEM images of graphene grown at (a) 70 Pa, (b) 150 Pa, and (c) 250 Pa. Single-layer graphene (1L), double-layer graphene (2L) and multi-layer (ML) graphene can be directly distinguished with SEM observation. (d) Raman spectra of graphene grown at different pressures. (e) Persentages of different layer numbers dependent on growth pressure.

Raman spectroscopy was conducted at four random points (Figure 3.3-e) in the transferred graphene film to show the quality, the layer number and the homogeneity of the graphene film. The 2D band exhibits a symmetric and narrow Lorentzian peak at ~2690 cm^{-1}, with a FWHM of ~35 cm^{-1}. The intensity ratio of the 2D-band peak to G-band peak (I_{2D}/I_G) is ~1.9. These are the clear evidences of single-layer graphene. The G peak/D-band intensity ratio (I_G/I_D) is higher than 20 at any random point, which indicates good quality of the graphene across the whole surface.

We studied the growth of graphene with Raman spectroscopy as a function of pressure. Figure 2d shows a general trend of the pressure dependence. The spectra are normalized so that the G peaks are of the same intensity. The intensity of the D

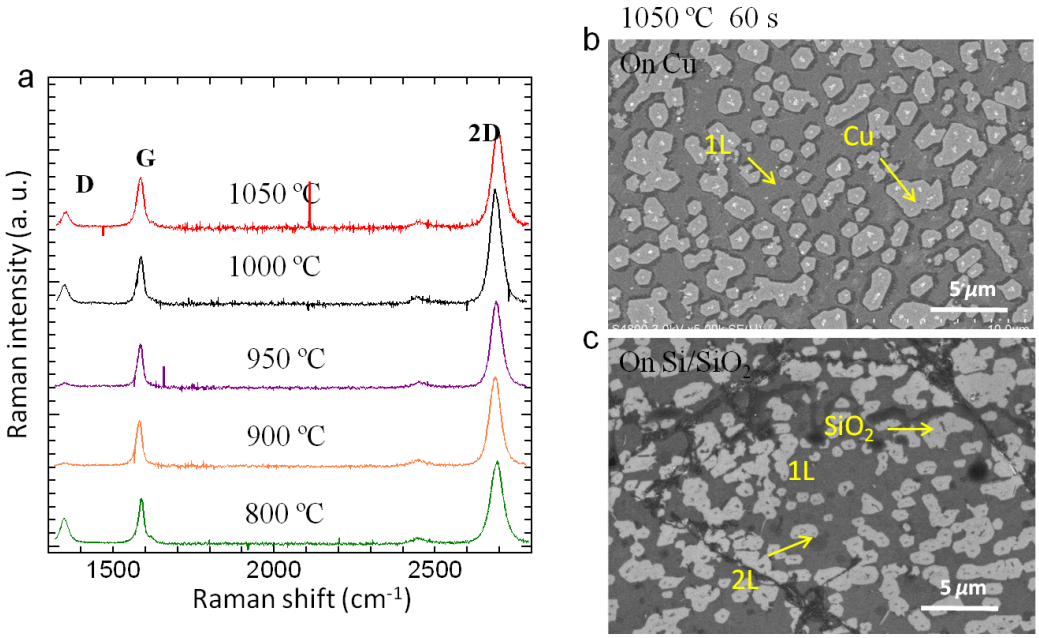

Figure 3.5. Graphene growth as a function of temperature. (a) Raman spectra of graphene grown at different temperatures. SEM images of graphene grown at 1050°C, 60 seconds before (b) and after (c) transfer.

peak increases dramatically with an increasing pressure. When the pressure is lower than 100 Pa, we observed the good quality of graphene (I_G/I_D>20). After transferred to Si/SiO_2 substrate, graphene with different layer numbers exhibit good contrast in SEM observation. At 70 Pa, only few multi-layer graphene nucleation seeds can be observed on the surface of the first layer of graphene (Figure 3.4-a). When the pressure was higher than 100 Pa, the growth rate of multi-layer graphene became dramatically high, due to a higher concentration of carbon source. At 150 Pa, arbitrary double-layer/multi-layer islands, which appeared to be thicker and darker in the SEM image, were clearly visible (Figure 3.4-b). At 250 Pa, multi-layer formation grew rapidly, to cover the majority of the graphene film within a growth time of 20 seconds (Figure 3.4-c). No appreciable D-band (G/D ratio is more than 20) was observed throughout the graphene film grown at a pressure lower than 100 Pa. When the pressure was 250 Pa, D-band became much stronger (G/D ration decreased to ~2), which was mainly caused by the boundaries of multi-layer domains.

We calculated the ratio of different numbers of layer dependent on reaction pressure based on SEM observation (Figure 3.4-e). At 70 Pa, more than 95% of the graphene film was, but when the pressure was enhanced to 250 Pa, only 56% was single-layer, and we observed 19% and 24% of double-layer and multi-layer graphene respectively.

We found that the growth result of graphene was strongly related to the reaction temperature. Figure 3.5-a shows the Raman spectra of graphene film grown at different temperature. Base on the intensity of D-band, we believe we acquired the best quality of graphene at the temperature around 900°C and 950°C. On the other hand, when we increase the temperature to 1000°C or 1050°C, which are the suitable conditions for graphene growth from methane, we observed a high D peak (G/D ~2.5), indicating the bad quality of graphene. In further SEM spectroscopy study, we found that when the growth temperature was higher than 1000°C, it was very difficult to make a full coverage of graphene film on the Cu substrate. We kept observing a lot of "holes" with hexagonal shape in the as-grown graphene film (Figure 3.5-b), where Cu surface was uncover with graphene, even with a longer CVD duration (60 seconds). In Figure 3b, the relatively brighter areas are Cu surface. After transferred to Si/SiO_2 substrate, the morphology of the graphene film correspond to that on Cu substrate, and we could also observe these holes in the graphene film where SiO_2 surface was uncovered (Figure 3.5-c), which proved that the judgment that there were uncovered holes in Figure 3b was accurate. These holes could be explained as the result of hydrogen etching, for the fact that the morphology of in Figure 3.5-b is very close to that observed by Y. Zhang et al [29] after a graphene hydrogen etching process. In our CVD reaction, the participation of hydrogen is unavoidable because it is a decomposition product of ethanol, and with higher reaction temperature, the amount of hydrogen is enhanced [30], thus we observed a hydrogen etching after the CVD reaction at high temperature (>1000°C) rather than at lower temperature (900°C).

In several different experiments, we halted the reaction after different CVD durations to study the formation of graphene domains at different growth stage. Because we used a relatively high flow rate (100 sccm) of carbon source compare with other groups, and ethanol decomposes much easier than methane, growth rate

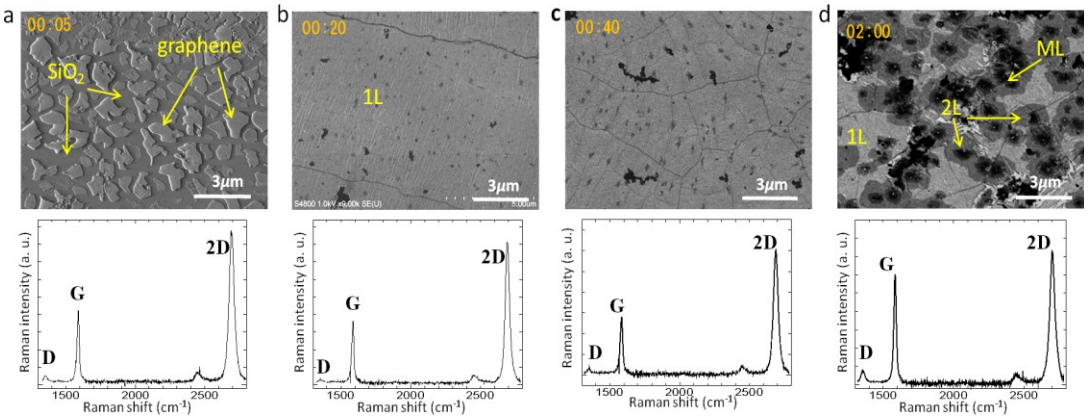

Figure 3.6. Graphene growth as a function of CVD duration. SEM images and Raman spectra of graphene grown in (a) 5 seconds, (b) 20 seconds, (c) 40 seconds, and (d) 2 minutes. SEM images and Raman spectra were taken after we transferred graphene onto Si/SiO_2 substrates.

was much higher than previous results. At early growth stage of 5 seconds, small domains of single-layer graphene formed randomly over the whole surface (Figure 3.6-a), and already nearly half of the area was covered with graphene within such a short CVD duration. Strangely, unlike previous results, the shape of these graphene domains was polygonal, rather than leaf-like or hexagonal, which might due to higher concentration of carbon gradients provided by the carbon source. A small D-band (G/D is ~10) could be observed in Raman spectrum at this stage, which was caused by the edges of these graphene islands.

With an increasing growth time of 20 seconds, a full coverage of single-layer graphene could be achieved (Figure 3.6-b), while almost no double layer region formed, except for few multi-layer nuclei, as we already demonstrated that single-layer graphene and double-layer graphene showed clear contrast under SEM observation. This indicates that under this optimized condition, the growth rate of the second layer of graphene was well limited, and was much slower than that of the first graphene layer. The Cu substrate served as catalyst in the CVD reaction, and since the Cu surface had been covered with a single layer of graphene, which

blocked the contact of carbon source and Cu, so the nucleation rate and growth rate of the second layer were much slower than those of the first layer. The Raman spectrum at this stage proved that the graphene film consisted of high-quality, and almost pure single layer.

Although we were able to control the growth of single-layer graphene to a self-limited process to some extent, due to the high concentration of carbon gradients in the reaction process, given longer reaction time, the expansion of double-layer region was unavoidable. Figure 3.6-c shows a sample with a CVD reaction time of 40 seconds. In this stage, although most of the area was still single-layer graphene, the multi-layer regions were expanding already. From the SEM image, we can observe that the sizes of the second layer domains are obviously larger than those in Figure 3.6-b. The Raman spectra also display a little higher D-band. When the CVD duration was extended to 2 minutes (Figure 3.6-d), more than half of the film was double- or multi-layer graphene. Multi-layer graphene domain boundaries also resulted in the high D-band intensity (G/D is ~6). The relatively higher G-band (2D/G ~1.1) indicated that the majority of the graphene film is multi-layer.

The growth condition we used in this study was similar to the low-pressure CVD (LPCVD) condition of graphene growth from methane. According to the detailed parametric study, graphene growth from ethanol displays three behaviors: first, lower CVD pressure results in higher quality of graphene. This is due to that lower concentration of carbon source causes lower graphene nucleation rate and lower growth rate in general, thus the graphene domains are relatively larger and the formation of the second layer is well limited. This point is consistent with graphene growth from methane. So the growth mechanism can be well explained with simple surface adsorption process which is utilized to disclose the formation of single-layer graphene by LPCVD from methane. Secondly, the growth rate is much higher compared with methane. This may be related to the fact that ethanol can be decomposed much easier than methane, which provide a higher concentration of carbon gradients, hence, once the condition of graphene nucleation is reached, the growth of graphene domains is much faster. Thirdly, the self-limited growth behavior is not as good as methane with the similar CVD conditions. For methane

precursor with similar CVD conditions, it is reported that the self-limited behavior could be preserved with CVD duration as long as 1 hour, but it is only 30 seconds in our case. Thus, the growth time is very important to synthesize single-layer graphene from ethanol, but still, it is controllable.

3.3 Improved growth with Cu pocket

As mentioned above, graphene growth on Cu from ethanol may result in severe etching due to certain SiO_2 particles from the quartz tube and the strong etching effect at high temperature (Figure 3.5). To solve this problem, we begin to fold Cu foils into pockets, so that the cu surface in the inside of the pocket is well protected from SiO_2 contamination. Also, according to R. Jacobberger and M. Arnold [75], there are at least two more advantages of this Cu pocket: a more steady flux of carbon source can be obtained, and the partial pressure of carbon source is further decreased, due to the narrow path at the pocket edge for carbon source to go through to reach the inside. A photo of the Cu pocket is shown in Figure 3.7.We believe more advantages are brought by this Cu pocket, including restraining sublimation of Cu, which would result in a much stable environment inside the pocket, and longer the possible CVD durations, which is very important as we will discuss later.

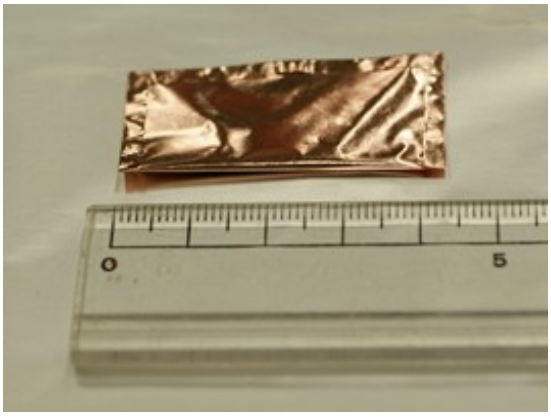

Figure 3.7. Photo of a Cu pocket

By utilizing the Cu pocket, and a small decrease in flow rate, we found that the nucleation density of graphene is significantly reduced (Figure 3.8). Without the Cu pocket, the shape of graphene flakes are almost random, and the nucleation density is about 0.5 μm^2, allowing a graphene grain size of about 2 μm in average (Figure 3.8 b). Besides, after these small graphene flakes emerge together into a big continuous graphene film, lots of those white particles can be observed, and these contaminations are one major origin of defects due to growth preference of multi-layers and etching. On the other hand, after using the Cu pocket, we find that

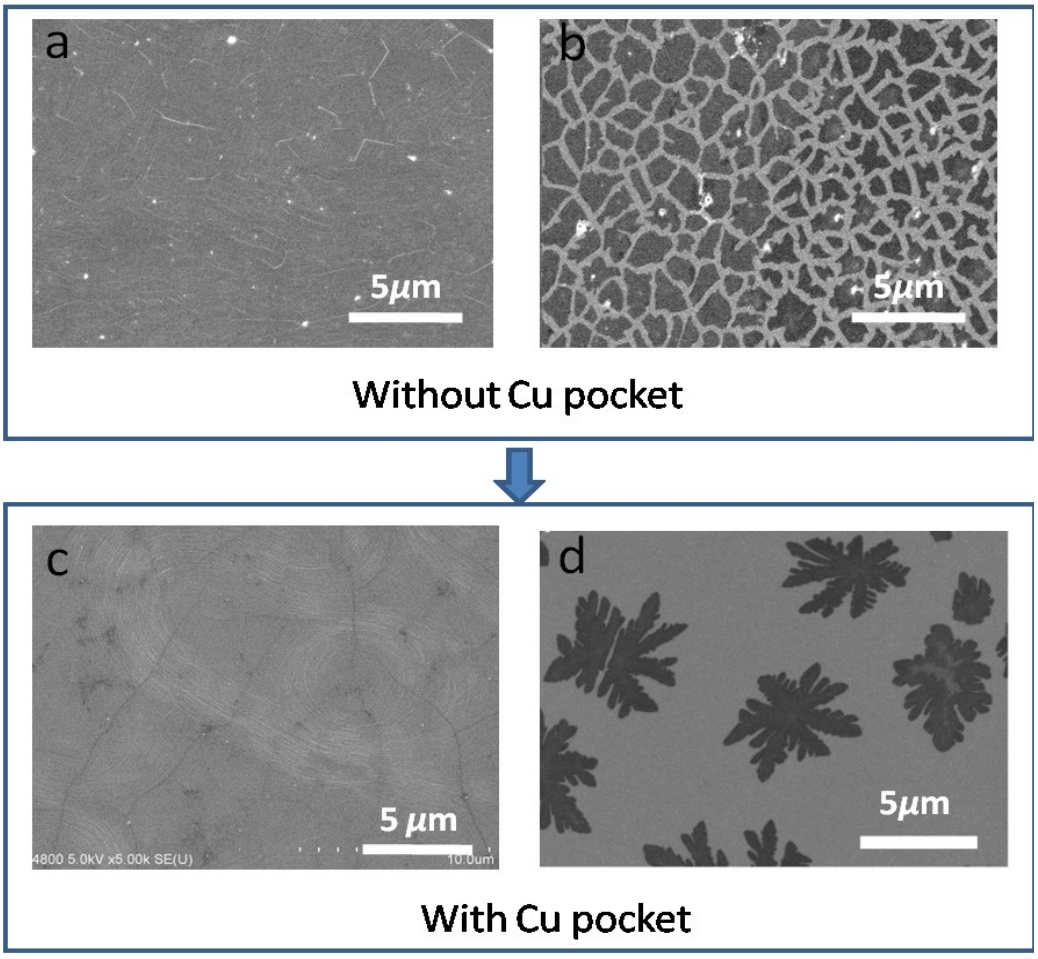

Figure 3.8. SEM images of graphene grown on Cu foils a), b) with and c), d) without Cu pocket. a) and c) are continuous graphene films grown at the same CVD conditions as b) and d) respectively.

the nucleation density is reduced to nearly 0.1μm^2, resulting in a graphene domain sized of 10 μm (Figure 3.8 d), so the amount of grain boundaries after graphene flakes grow together is dramatically reduced. Also, the continuous graphene film grown in this way is very clean, and no obvious contamination is observed (Figure 3.8 c). .

The quality of graphene films grown using Cu pocket is further confirmed after transferring it to Si/SiO2 substrates. We show the photograph (inset of Figure 3.9 a) and the optical image (Figure 3.8 a) of graphene transferred to a Si/SiO_2 substrate. A clear boundary of this graphene film can be observed in this optical image, and the whole film looks continuous and homogeneous. Furthermore, by using scanning Raman spectroscopy, we confirm the homogeneity of this graphene film (Figure 3.9 b). For an area as large as 15 μm × 15 μm, the 2D to G intensity map demonstrates that nearly 90% is single-layer graphene.

The evolution of graphene growth depending on CVD duration is shown in Figure 3.10. In merely 2 seconds after we flow in the ethanol vapor, some nuclei of graphene are observed. Initially, the shape of these small graphene flakes is more circular. From 5 to 30 seconds, these graphene islands expand rapidly, and the

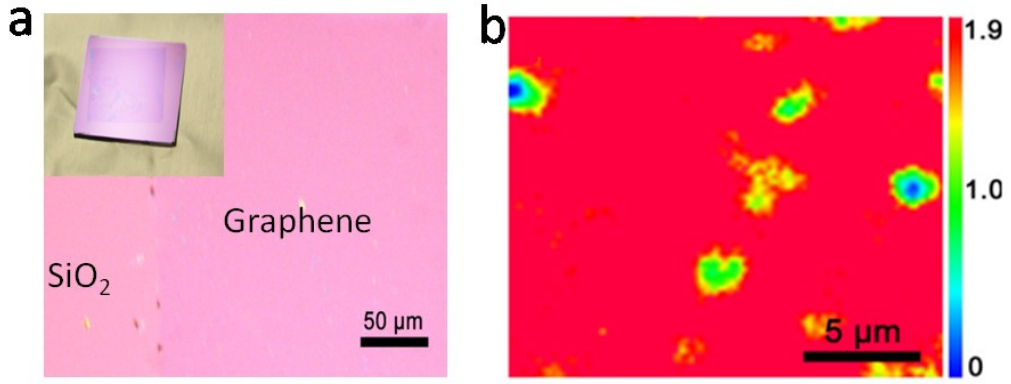

Figure 3.9. a) Photo (inset) and optical image of graphene on Si/SiO2 substrate. b) Raman map plotted based on the 2D to G intensity. This sample is grown using Cu pocket.

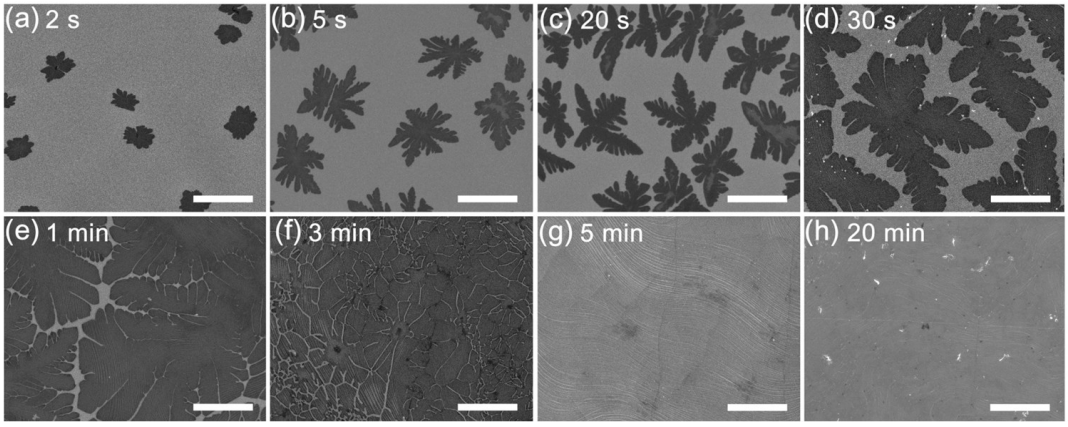

Figure 3.10. SEM images of graphene on Cu foil with different CVD durations

shape becomes very dentritic. In 5 minutes, the graphene domains emerge together, forming a continuous graphene film. If we keep flowing the carbon source for another 15 minutes, the morphology changes very little.

From this evolution based on CVD durations, we find two interesting points. First, the shape if graphene flakes is very dentritic, suggesting strong diffusion-limited growth behavior. Second, after we acquire continuous graphene film at 5 minutes, even if we continue to flow ethanol vapor, the there wouldn't be any growth of the second layer, this means that by applying this Cu pocket, we gain a much bigger window for the high percentage of single-layer graphene, which we refer to as self-limited growth.

Six-lobed dendritic shapes of graphene domains demonstrate that the growth is a substrate-mediated process rather than a direct adsorption of carbon atoms from the gas phase. Based on the observations above, we propose the growth mechanism as follows: i) Ethanol decompose into different products, which are catalyzed into active carbon species by copper and chemically adsorbed on its surface, and nucleate at supersaturation sites. ii) The diffused carbon atoms on the copper surface are captured by the edge of the nuclei and form a circular shape due to initial "capillarity limitation". iii) When the nucleated islands grow further, the

anisotropy of surface diffusion on the copper surface depending on the crystallographic orientation results in the dendritic shapes.

3.4 Summary

In this chapter, the CVD growth of graphene on Cu substrates using ethanol as carbon source is discussed. With optimized conditions, we were able to synthesize large-scale single-layer homogeneous graphene films on Cu foils. Small Raman D bands at random locations indicate the low defect level. With parametric study, we show that the formation of bi-layer and multi-layer graphene can be restrained be lowering the CVD reaction pressure. To solve the problem of high-temperature etching, we utilized Cu pockets. By Cu pockets and raising growth temperature, graphene with higher quality, i.e., fewer contamination, bigger graphene domain size, more dominant single layer, is synthesized. Furthermore, we find the growth can be self-limited, giving us a much bigger window and thus better control of the good quality of single-layer graphene.

Based on the observations, we propose the mechanism of a diffusion-limited growth procedure to explain graphene growth on Cu from ethanol.

Chapter 4
Synthesis of large single-crystal graphene

4.1 Approaches to increase the size of graphene flakes

As shown in Chapter 3, typically, CVD-derived graphene is polycrystalline, which is the merging of many small single-crystal graphene flakes. As has been proved by literature and the observation of ourselves, the orientation of each graphene flake is almost random, rather than corresponding to the lattice direction of the Cu facet underneath them. Thus, the boundaries between these small graphene flakes become a major origin of defect, because obviously C atoms located at the boundaries are disoriented. Former studies showed that, not only the electrical properties are decreased due to the existence of grain boundaries [76], but also mechanical strength is reduced [77]. The most obvious way to reduce grain boundaries is to increase the sizes of single-crystal graphene flakes, which almost equals to minimizing the number of graphene nuclei, as would be explained next. Other aspects, such as the shape of graphene flakes, also affect the amount of grain boundaries, for that obviously dentritic graphene flakes contain more boundaries than round or hexagonal ones, but we will see that this problem would be automatically solved once we are able to increase the size of graphene flakes. On the other hand, if graphene flakes are epitaxially grown on the substrate, their orientation would correspond to the metal substrate below, so even if the size of each graphene flake is small, they could merge together without creating any disoriented boundaries, given the fact that the substrate itself is single-crystal. A very recent work showed that wafer-scale single-crystal graphene can be realized by merging epitaxial small graphene flakes on single-crystal germanium substrates [78]. But this method is beyond the research of this thesis, and in this chapter, we focus on the growth of graphene large flakes using poly-crystal Cu substrates.

To achieve this, we must understand the mechanism of nucleation and growth of graphene flakes on metal substrates, and how each factor in this mechanism is governed by the microscale CVD conditions. The mechanism of 2D nucleation and growth of graphene is discussed intensively in recent years, and a widely accepted mode is explained as following: i) the carbon source is adsorbed on the Cu surface, and decompose to form carbon species; ii) the carbon species are defused on Cu surfaces, due to a relatively low surface-diffusion energy of C on Cu (~0.06 eV) [79-80]; desorption of these carbon species exist simultaneously on the Cu surface; iii) As the flow of carbon source continues, the concentration of carbon species increases, until the critical supersaturation concentration (C_{nucl}) is reached, and graphene nuclei are formed; iv) Carbon species near each nucleus are likely to be captured by the nucleus, resulting in a lower concentration of adatoms around the stable nucleus as a result of spontaneous growth, forming a so-called nucleation exclusion zone in which the formation of another nucleation is practically impossible [81]; v) As each nucleus depletes the carbon species close to it, the concentration of surface carbon species decreases to an equilibrium level (C_{eq}), at which the competition among the attachment of C on graphene edges, C surface diffusion and the desorption of C reaches equilibrium [82]. The exact form of C_xH_y defused on Cu surfaces is not well-defined,[83] so they are referred to as “carbon species” in this thesis. This mode is derived from the conventional 2-dementinal nucleation mode as explained by V. Robinson and J. Robins [84], and it enables us to simplify the problem. For instance, it is often observed that, despite of the nucleation density, almost all nuclei are formed at the initial stage of the CVD reaction, and afterwards, during the long duration of the growth of graphene flakes, hardly any new nuclei are formed, even if the coverage of graphene on Cu surface is still very low. By this mode, we explain this phenomenon through the fact that C_{eq} at the steady growth stage is lower than C_{nucl} which is required for nucleation. So increasing the size of graphene single crystals almost equals to decreasing the nucleation density. By applying the V. Robinson and J. Robins’s mode to the nucleation of graphene, H. Kim et al. derived the relationship for the saturation nucleus density:

$$N_S^2 \sim P_{CH_4} \times \exp\left(\frac{E_{des}+E_{att}-E_d-E_{ad}}{kT}\right) \quad (1)$$

where P_{CH_4} is the partial pressure of methane, E_{des} is the desorption energy of carbon species, E_{att} is the energy barrier of attachment for the capture of carbon species by supercritical nucleus, E_d is the activation energy of surface diffusion of a carbon species, and E_{ad} is the activation energy for adsorption of carbon source on the Cu surface [85]. Tuning the factors in (1) by microscale processes would directly affect the nucleation density. For this purpose, early efforts have been focused on smoothing Cu surface, reducing partial pressure of carbon source, and tuning C : H ratio.

As proved both experimentally and theoretically, nucleation often occurs at imperfections on Cu surfaces, such as impurities, step edges, defects, etc, due to lower nucleation barrier at these sites. Hence, electro-chemical polishing and long-duration annealing, which considerably smooth the Cu surface and increase the size of Cu graphene, resulting in a smoother surface of Cu with less defects, step edges and impurities, became very effective methods in reducing nucleation density. Given enough CVD duration, the size of a graphene flake that expands from a single nucleus could be as large as 2.3 mm. On the other hand, although imperfections on Cu surfaces can be reduced significantly, they can hardly be eliminated. Furthermore, with Cu, the energy in C-Cu bond is low, so the nuclei are not restricted to imperfection sites; rather, it occurs on plain area on Cu terrace, only with a lower possibility than that on impurities. Thus, this smoothing surface procedure may not be able to reduce the nucleation density too much.

Very small flow of carbon source would also dramatically reduce the nucleation density; because low concentration of C diffused on Cu surface make it less possible for a local super-saturation nucleation. But a very important disadvantage of small flow of carbon source is that, it also slows the growth rate of graphene flakes, thus, as reported by previous work it takes more than 24 hours to reach millimeter size. Even if further lowering the flow rate can lead to even lower nucleation density (0.1 nuclei/mm^2), considering the evaporation of Cu foil in the

high-temperature environment, it became really unrealistic to grow very large graphene single crystals with only this way.

Tuning the ratio of hydrogen can also affect the nucleation density. Hydrogen is believed to have two roles in the CVD growth of graphene. First, it serves as a catalyst to form carbon species (C_xH_y), which are the reaction gradient for sp^2-bonded carbon lattices. Second, it is the etching reagent of graphene, and by etching away the active growth front on graphene edges, it makes the growth speed at different sites on graphene edges even, resulting in smoother edges and better crystalline.[86] For graphene growth from methane, it is crucial to find the optimized ration of C : H in CVD reaction in order to acquire high quality. But its influence in controlling the nucleation density is minor, compared with its effect on controlling the shape and orientation of graphene flakes.

4.2 Effect of heating without hydrogen

Base on the discussion above, beside these three ways, some new methods must be found in order to grow centimeter-size single-crystal graphene. A seem-to-be-random trail proved to be very effective in such matter. In my experiments, during the heating and growth processes of CVD procedure, a flow of 3% H_2 in Ar was often used in order to keep the Cu surface reduced (Here, the effect of H_2 for ethanol may not be a catalyst or an etching reagent, for the fact that the decomposition of ethanol is very easy and that the ration of H_2 that we use is very small). But when we use only Ar flow during the heating process, the nucleation density decreased significantly. Figure 4.1 shows the difference in growth procedure and the results, in which H_2 is not involved only in the heating stage, and 3% H_2 in Ar is still used in the growth stage. We observe a 5-time decrease in the nucleation density for this new procedure, which dramatically reduces the amount of grain boundaries.

Parallel to this study, some other groups published results using almost the same method. They show that they can grow graphene single-crystals to millimeter sizes when heating without hydrogen. But they had essential differences regarding the mechanism behind this phenomenon. L. Gan and Z. Luo proposed that during heating process, the Cu surface would be oxidized by O_2 from leakage, due to lack

of H_2. And afterwards, when CVD reaction temperature was reached, they flow H_2 again to anneal the Cu foil, and during this annealing and reduction, Cu particles were formed on the Cu surface, which would act as nucleation center in the later growth process, as they confirmed by AFM observation.[1] In another work, H. Zhou and colleagues argued that there was a pristine oxidation layer on the Cu foil, and due to lack of H_2 in the heating process, the oxide layer was unreduced and preserved until the growth process, which would passivate the activity of Cu, thus leaded to a low nucleation density.[6]

We tend to believe the second theory, since it is more straight forward and obvious. For the first theory, L. Gan et al. failed to explain the nature of these particles, *i.e.*, why the oxidation-and-reduction process would create these particles. I conducted more experiments to further investigate this phenomenon, which I will explain in detail in 4.4.

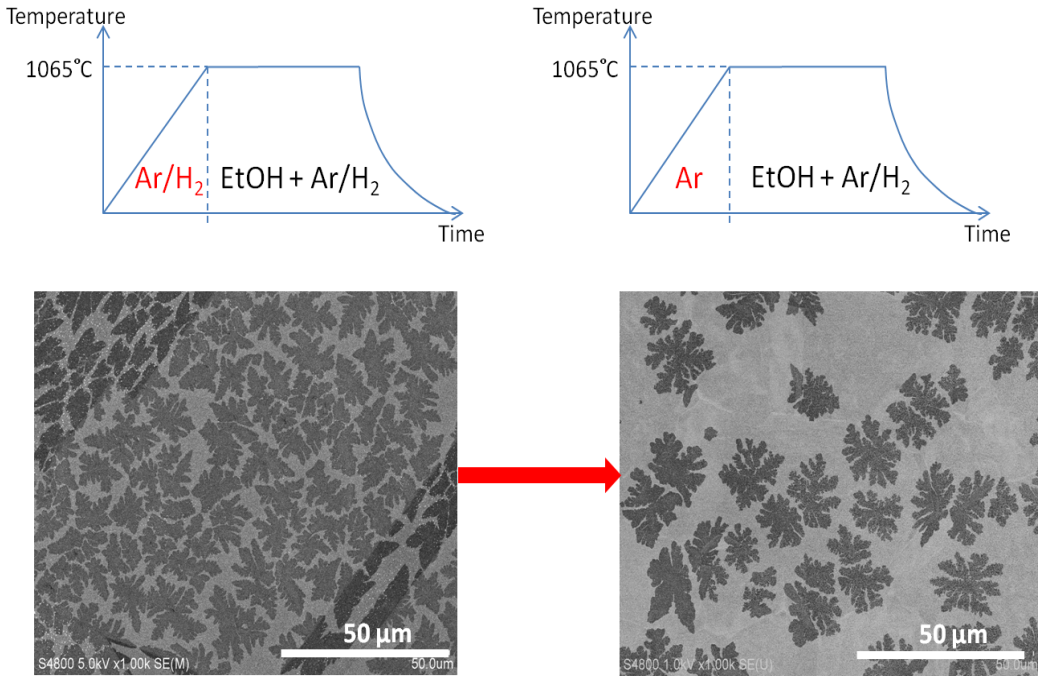

Figure 4.1. Schematic of a change in growth process and its effect on the nucleation density. More than 5-time reduction in nucleation density is observed without involving H_2 in the heating process.

4.3 Extremely low flow of ethanol

4.3.1 Low nucleation density using extremely low flow of ethanol

Although I've shown that heating without H2 can significantly reduce the nucleation density, but only allows the size of each flake to be as large as 20 microns at most. So I started to try to use very small flow of ethanol. Prior to this, we normally use a flow of more than 5 sccm. Now, I reduce the mass flow by 100 times, using only 0.05 sccm. With this procedure, the nucleation density decreased to about 0.8 nuclei/mm2, allowing the sizes of graphene flakes to be as large as hundreds of microns. In figure 4.2, we show several pieces of graphene flakes as large as 200 μm (this particular sample is grown at 1065 ˚C, with a flow of 0.05 sccm ethanol and 300 sccm Ar/H_2, using Cu pocket, 4 hour CVD duration). Moreover, the shapes of these graphene flakes are approximately hexagonal, in contrast with the dentritic shapes as shown before, indicating the good crystalline

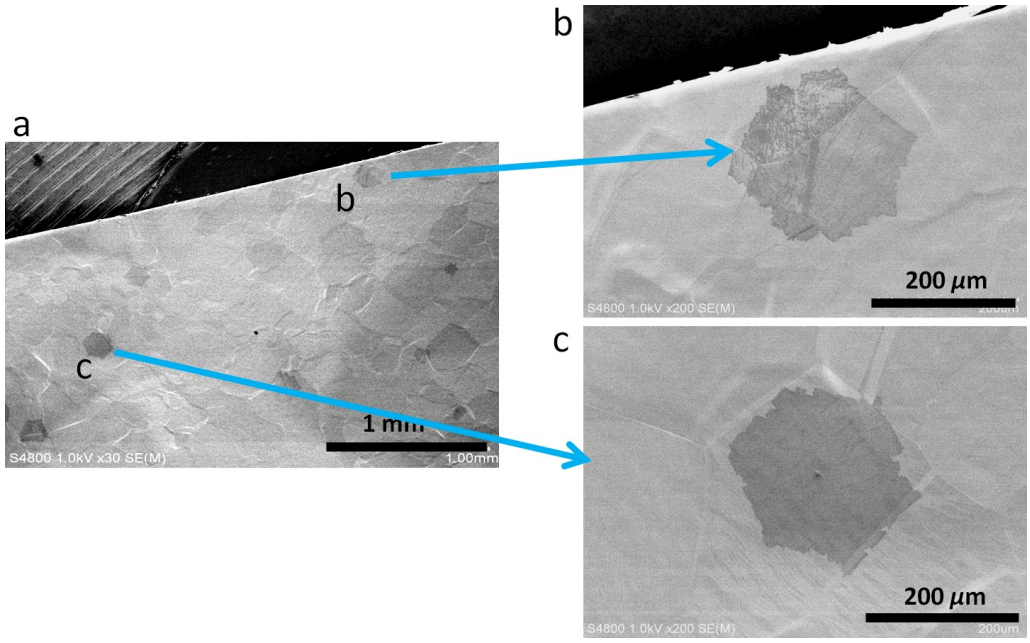

Figure 4.2. SEM images of graphene grown on Cu foil with extremely low mass flow of ethanol, and heating without H_2. b and c on the right side are images corresponding with two flakes in image a, only with a larger magnification.

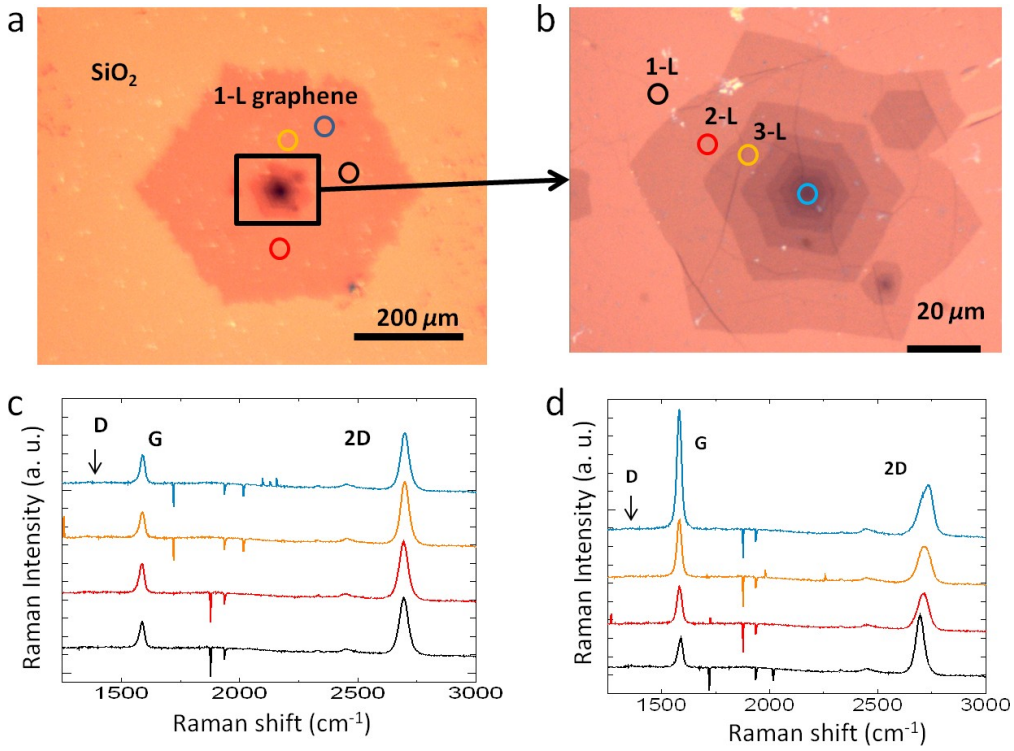

Figure 4.3. a. Optical image of graphene transferred to Si/SiO_2 substrate. b. higher-resolution image of the center part of the graphene flake in a. c and d are the Raman spectra of a and b, corresponding to the locations marked by circles with same colors.

within each flake. This is because by lowering the mass flow, the balance of growth and etching in the CVD reaction shifts towards etching, so the growth speeds at different sites along the graphene edges are more even, resulting in a better crystalline.

In order to further confirm the quality of this large graphene flakes, we transfer some samples to Si/SiO_2 substrates, and conduct Raman spectroscopy observation. Judging by the obvious contrast between graphene areas with different numbers of layers, we found that almost 90 percents of the whole graphene flake is single-layer, but at the core, there is about 10-percent area covered with bi-layer or multi-layer graphene. This is also confirmed by Raman spectroscopy. Four spectra from random locations are shown in Figure 4.3, showing typical signature for

single-layer graphene, each with a very small D-peak, indicating low defect level. Raman spectra taken at the center of this flake shows the existence of bi-layer and multi-layer graphene.

4.3.2 Dependence on growth temperature

Further study shows that the temperature of CVD reaction is essential in controlling the crystalline nature of resulting graphene flakes. In Figure 4.4, we show four SEM images of graphene flakes grown at different temperatures, while other conditions are the same. At 1000 ˚C, the shapes of flakes are almost random. At 1050 ˚C, the shape is typically six-lobed dentritic. At 1060 ˚C, the shape looks to be approximately hexagonal, but the edges are still very rough. At 1070 ˚C, the edges are very smooth, and the whole flake seems to be in good single-crystalline, following the orientation of graphene lattice.

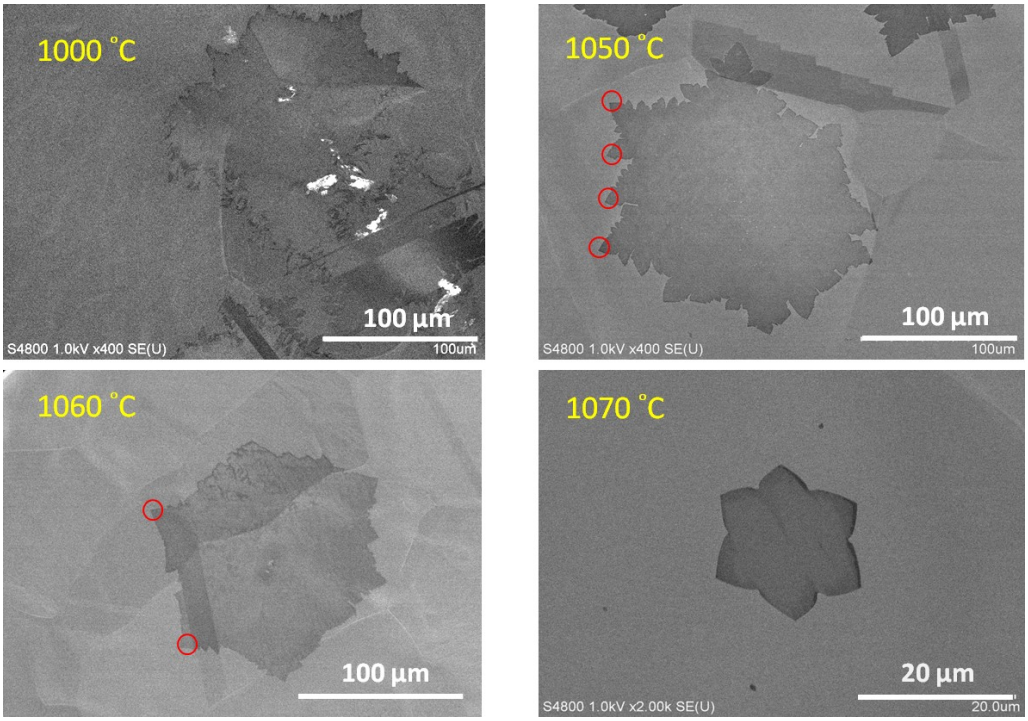

Figure 4.4. SEM images of graphene on Cu foil grown at different temperature. All the other parameters are the same for these samples except for the CVD temperature.

We believe this evolution depending on temperature is the result of shifting in the equilibrium of growth and etching. With higher temperature, the increase in etching effect is faster than that of growth speed. Although the balance is still in favor of growth, but etching becomes significantly strong and comparable to growth. For the fact that the growth active sites (marked by circles in Figure 4.4), such as growth front points on these dentritic branches, are also the etching active sites, the growth speed at these front points are reduced to the same level as other locations along the edges, so the growth speeds are even, resulting in a hexagonal shape depending on the orientation of the lattice of graphene. This result is corresponding to the observation in Chapter 3, where high temperature leads to etching holes across the graphene film. Only, in Chapter 3, the main etchant could be the decomposition product of ethanol, such as CO and H_2O, because the ratio of H_2 is very low compared with ethanol; but here, we are not sure what is the main etchant, for that the concentration of H_2 is much higher than that of ethanol, but ethanol could still provide enough etchant to maintain a etching speed same level as the growth speed, in which the carbon source is also provide by ethanol decomposition. This stronger etching effect at higher temperature can also be circumstantially proved by the sized of graphene flakes grown. Clearly, as the temperature increases, the size of graphene decreases, and the decrease is even faster when it's close to 1070 ˚C, suggesting that near 1070˚C, the etching rate is almost the same as growth rate.

Although we found that higher temperature is more favorable in maintaining the good shape of graphene flakes, we decided that the suitable temperature for the growth of graphene lager flakes should be 1065 ˚C, for that the melting point of Cu is 1086 ˚C, and near this temperature, the sublimation of Cu is strong, so with long-duration CVD, the thin Cu foil can be "burned through" with many holes, and eventually all sublimate out, leaving nothing behind, as has been confirmed by many experiments. 1065 ˚C is a relatively "safe" temperature allowing us to conduct CVD for many hours, but still forms graphene with good shapes on the other hand. So from here in this thesis, unless specially noted, all of our samples are grown at this temperature.

4.4 Millimeter-size graphene single crystals through pre-oxidation

4.4.1 Growth method

With low mass flow rate and heating without H_2, we can grow large graphene flakes to hundreds of microns. Following the discussion in 4.2, we still need to prove which theory is right regarding the effect of heating without H_2. So we think if the oxidation layer on Cu surface would deactivate the Cu, why not heat it in air to oxidize it even before the CVD procedure. So we begin to bring a new process in to the CVD growth of graphene. We heat the Cu on a hot plate in air (typically 200 ˚C) for several minutes before we fold it into a pocket and load it into the CVD chamber (Figure 4. 5 a). After heating in air, the surfaces of Cu foils are clearly oxidized, showing a darker color, close to that of CuO (Figure 4. 5 b).

After oxidation in air, we continue to conduct the rest of the CVD procedure, using all the positive tricks that discussed above, including heating without H_2, Cu pocket, extremely low flow of ethanol. The detailed procedure is shown in Figure 4.5 a.

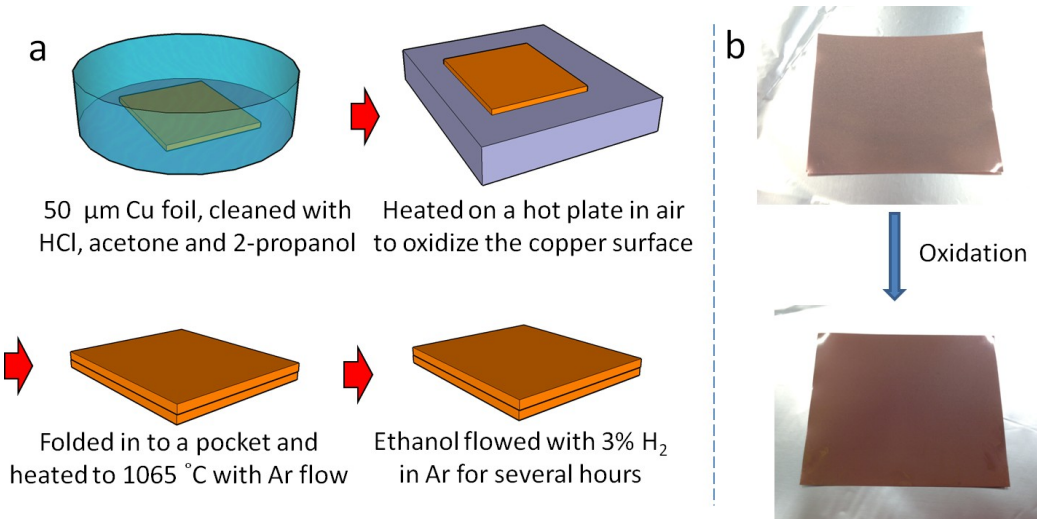

Figure 4.5. Pre-oxidation growth of graphene on Cu foil. a. schematic of the growth procedure. b. the photos of Cu foils before and after heating in air.

4.4.2 Characterization by Raman spectroscopy

By adding this process we found that the nucleation density is further reduced. In Figure 4.6, we show several SEM images of graphene growth at this condition. There graphene flakes are more than 2 mm in size, some are even larger than 3 mm. The shapes of these graphene flakes are generally hexagonal, but the edges are not very smooth, and the angle is sharper than 120 ° at points, as indicated by the optical image after we transfer the graphene flakes onto Si/SiO_2 substrates. We also conducted Raman spectroscopy at random locations, and they all exhibit typical single-layer graphene signature, and the D-peaks were very small compared with G-peak, suggesting the low defect level.

To further confirm the quality of our graphene samples, we use scanning Raman to obtain Raman signals over a relatively large area. We plot several maps based on the intensities of D peaks, G peaks and 2D peaks at 2 different locations. Based on these Raman maps, we observe that the graphene is homogeneous in large area. The intensity of 2D band is always nearly 2 times of the G band across the whole

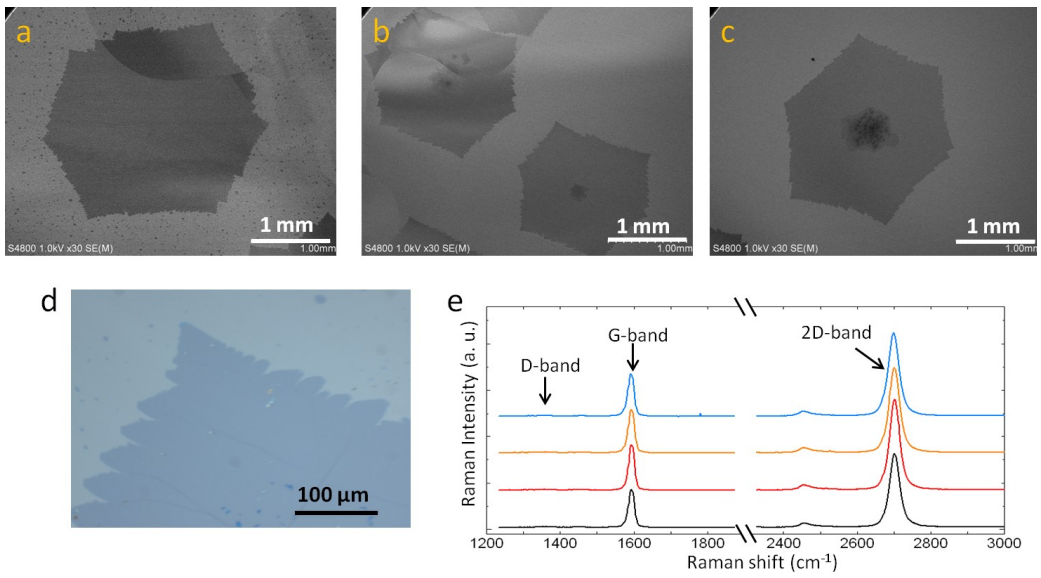

Figure 4.6. a), b) and c) are typical SEM images of large graphene flakes on Cu substrates. d shows one corner of a big graphene flake, after it is transferred to Si/SiO2 substrate. e shows Raman spectra of four random locations in the sample shown in d.

areas measured. The intensity of D band is very small, almost the same level as on Si/SiO_2, indicating low defect level on the whole flake. But we can observe a strong D band along the edge of this graphene flake, which is almost half the intensity of G band. This very strange considering the result of other groups, in which they show that even at graphene edges, the intensity of D band is still low, corresponding to a zigzag edge (Figure 4.8 a), and these zigzag edges are more stable than the armchair edges, so they are more favorable for the formation of smooth edges. But for our graphene, maybe the edges are not all zigzag, but rather armchair. On a closer look, we find that at the corners of the branches, i. e., at the growth front points, the D-band intensity is extremely high, meanwhile, at the withdrawn parts of the edges, the D-band intensity is very low (Figure 4.8 b). This

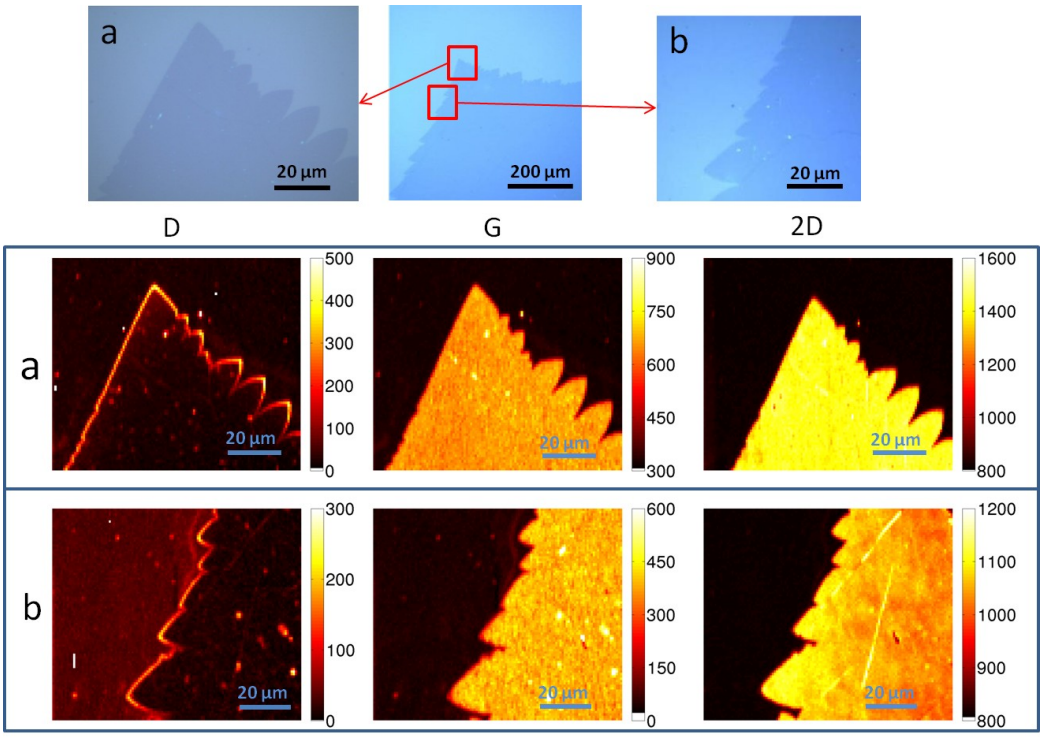

Figure 4.7. a, b and c are typical SEM images of large graphene flakes on Cu substrates. d shows one corner of a big graphene flake, after it is transferred to Si/SiO2 substrate. e shows Raman spectra of four random locations in the sample shown in d.

suggests that armchair edges dominate on the fast growing fronts, but at slower growing sites, zigzag edges are the major components.

This gives us a good insight on the growth kinetics. Conventionally, for the purpose of crystalline, when using methane precursor, other groups always use a high concentration of H_2 (200—400 times of CH_4) in the CVD reaction, thus the etching rate is almost the same as growth rate, resulting in a very smooth edge, but also greatly reduces the general growth speed. In this way, the attachment of C on graphene edges is reaction-limited, meaning there is a relatively high reaction barrier for Cs to be captured by graphene edges to form new sp^2 bonds. Even if the diffusion of C on Cu is high (this means for any location on graphene edges, more C atoms would reach this location in a certain period of time), many of these C atoms that reach graphene edges would not be captured, but just diffuse away, due to the high reaction barrier. In this case, the graphene edges are always zigzag, which is more stable because of its high reaction barrier for both growth and etching. Raman spectra on zigzag graphene edges only exhibit very little D-band intensity.

But in our case, the high D-band intensity on edges clearly suggests the

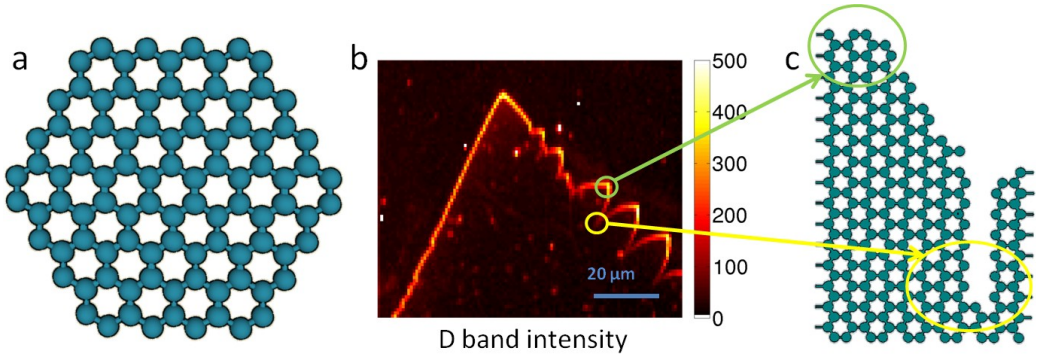

Figure 4.8. Edge orientations of graphene flakes. a. schematic of graphene flake with standard zigzag edges. b. D-band-intensity map of a corner of our graphene flake, in which growth front point and withdrawn point are marked by green and yellow circles respectively. c. schematics of edge orientations along one "branch" in b.

existence of armchair edges. In Figure 4.8 b, brighter color suggests armchair edges, but darker color along the withdrawn parts of the edge suggests possible existence of zigzag edges. Compared to zigzag edges, armchair edges are very active, which leads to a diffusion-limited growth mechanism. In diffusion-limited growth, diffused C atoms that reach the graphene edges are very likely to be captured and form new sp^2 bonds, so the reaction rate (growth rate) is predominantly limited by the supply (diffusion) of C, rather than the attachment of C atoms on graphene edges. In this way, given sufficient diffusion of C (enough involvement of carbon source), the growth rate could be much faster than that of reaction-limited growth (zigzag edges). But this often result in a dentritic shape of graphene flakes, due to the fact that graphene growth front corners have a much wider angle from which C species diffuse towards them, but at the withdrawn parts, the angle becomes very narrow, the chance of accepting diffused C species is much lower, thus the growth speed is also quite low. These uneven growth rates are not appreciable, for that not only they create rough edges, but also they may disorder the crystalline inside each graphene flakes. But in our case, we find our graphene flakes are still single-crystalline, which I would discuss later.

Interestingly, we may observe both armchair and zigzag edges along the same "branch" of the dentritic growth front. As marked by a green circle in Figure 4.8 b, high intensity of D band suggests the armchair orientation; but at the bottom of the same "branch", the D band is very weak, suggesting zigzag orientation, as marked by a yellow circle. The direction along this "branch" from top to bottom also roughly changes 30˚, which is exactly the angle between zigzag and armchair orientations. Their structure schematic is shown in Figure 4.8 c.

4.5 Growth-behavior dependence on CVD parameters

4.5.1 oxidation-level dependence

To find the optimize conditions for the growth of graphene large flakes, we investigated different conditions of the CVD reaction. The first parameter that we investigate is the level of oxidation. Since we lack any reliable equipment for detecting the exact oxidation level of Cu surface (such as thickness of oxide layer,

or the ratio of Cu atoms and O atoms), here we set the temperature for oxidation in air at 250 ˚C, and simply use the time of this heating in air to represent the level of oxidation, for that we do observe the change of color on Cu surfaces as we increase the time of oxidation.

Of course, different oxidation level results in different nucleation densities, as shown in Figure 4.9. With no pre-oxidation, the nucleation density is around 8 nuclei/mm^2, which would result in a maximum of graphene grain size of about 0.5 mm, when the flake is far for other ones by chance. Upon 10-minute oxidation, the improvement is already obvious, and we observe a 1-order lower nucleation density, letting us to grow graphene flakes as large as 1 mm in average. For 30-minute oxidation, the nucleation density is reduced to 0.3 nuclei/mm^2, and for 90 minutes,

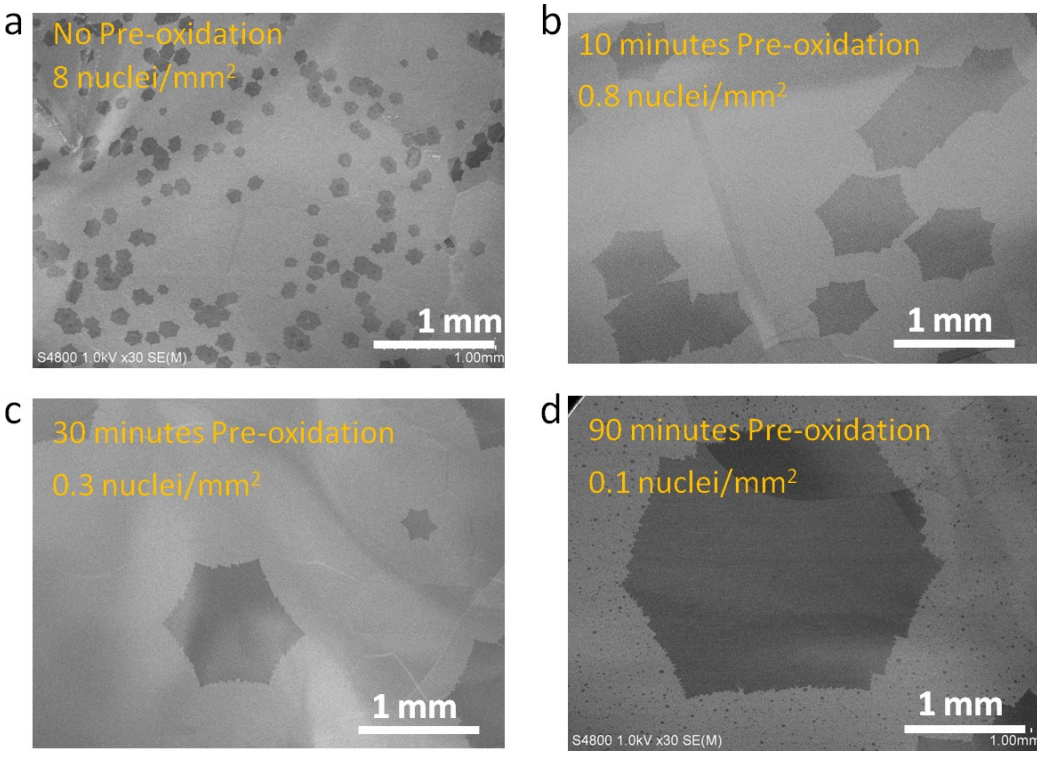

Figure 4.9. SEM images of graphene on Cu foils with different oxidation level. The CVD durations of these samples are different, for the convenience in counting nuclei. The nucleation densities are approximate numbers based on the statistics of an 1 cm×1 cm are for each sample.

we can decrease the nucleation density of 0.1 nuclei/mm^2, and grow graphene flakes more than 3 mm. We observe that although the nucleation density decreases as the oxidation time increases, this relation in not linear, because the after the surface of the Cu foil is oxidized, the dissolve of O in Cu is blocked by the oxide layer, so the rate of oxidation decreases as it continues, thus the actual oxidation level (such as thickness of oxide layer, or the ratio of Cu atoms and O atoms) at 30 minutes is far from 3 times of that at 10 minutes. Note that although the nucleation density allows us to grow graphene as large as 1 cm, but due to the growth rate and the sublimation of Cu, we can only grow 25 hours, resulting in a graphene flake as large as 5 mm, and this low growth rate is something we need to improve.

To further confirm the role of oxygen in this decrease of nucleation density, we

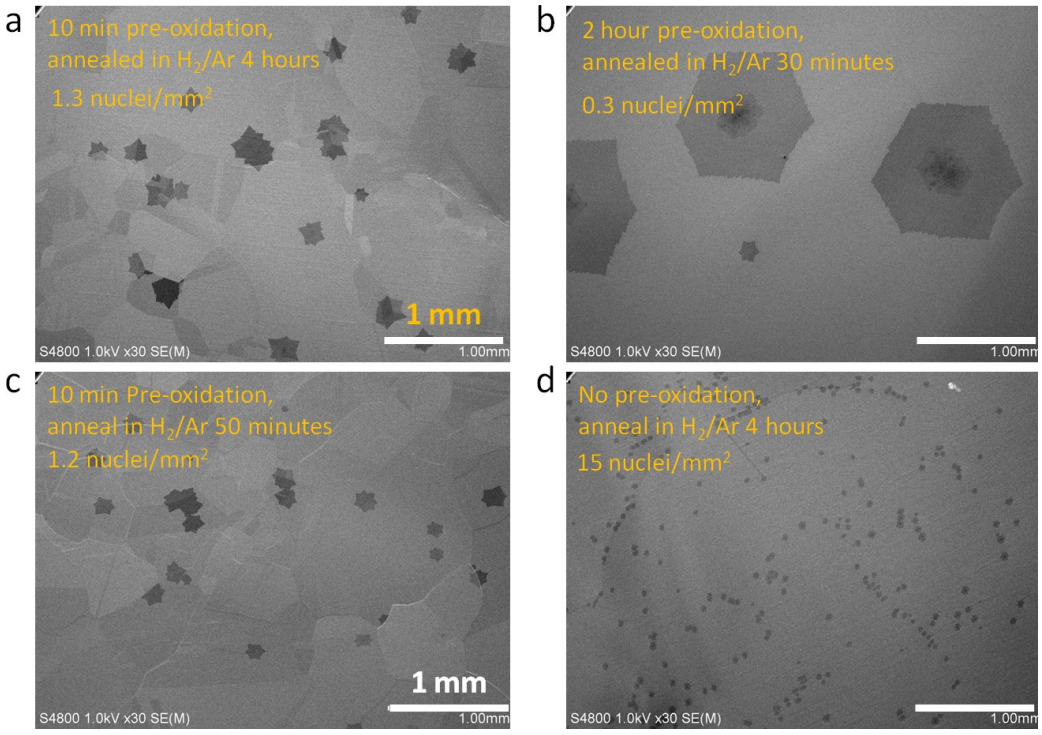

Figure 4.10. SEM images of graphene flakes on Cu foils after procedures combining pre-oxidation and annealing in H_2. The nucleation densities are approximate numbers based on the statistics of an 1 cm×1 cm are for each sample.

conducted several compare experiments. In these experiments, we first heat the Cu foils in air to oxidize it, than we anneal them in 1065 ˚C for some time before we introduce the ethanol flow to initiate CVD growth. In this way, the oxide layer would be reduced a little; since the annealing itself would smooth the Cu surface resulting in a decrease in nucleation density, but the reduction would increase the density, so we expect that the nucleation densities following this oxidation-and-reduction procedure would be in between of those of no oxidation at all and those of only oxidation.

Figure 4.10 shows the results. For the sample in Figure 4.10 a, we oxidize the Cu foil for 10 minutes, and anneal it in H_2/Ar for 4 hours, before we flow in the ethanol vapor to initiate the growth. We believe after this long duration of reduction, almost all the surface oxygen is removed. As a result, we observe 1.3 nuclei/mm^2, which is 1.5 times the density of only 10-minute oxidation (Figure 4.9 b), but still much lower than the one without any oxidation at all (Figure 4.9 a). Similar results are observed in Figure 4.10 c, for which we oxidize the Cu foil for 10 minutes, and reduce in H_2/Ar for 50 minutes. On the other hand, if we only anneal the Cu foils in H2/Ar for 4 hours, without any oxidation process, we observe a much higher nucleation density of more than 15 nuclei/mm^2. This indicates that if the Cu foil is pre-oxidized, even after long duration of reduction, some O would still be left in the Cu foil. For the sample in Figure 4.10 d, may be there is some small quantity of O on Cu surface, but after long-term annealing, these surface Os are most likely eliminated. For the case in Figure 4.10-a and c, after long-duration reduction, even if O on the surface of Cu is removed, there are still some dissolved in the Cu foil that cannot be removed completely. At 250 ˚C, the solubility of O in Cu is very low (less than 20 at. ppm), but as temperature increases to 1065 ˚C, the solubility also rises (several hundred at. ppm). Since we do not use H_2 during the heating process, when heated to 1065 ˚C, Os on the surface are preserved, and some of them would dissolve inside the Cu foil, which are hard to remove even by long-term reduction. And during CVD growth, it is possible that some of these Os dissolved inside the Cu foil would precipitate to the surface and deactivate the Cu surface, resulting in a lower nucleation density, but the concentration of these Os are not as high as without a reduction process at all, so the nucleation density is also higher.

In Figure 4.10 b, we oxidize the Cu foil for 2 hours, and anneal it for 30 minutes. The nucleation density is almost the same as the one only oxidized for 30 minutes. Obviously, some surface Os are removed, and nucleation density becomes higher. This further proved the surface oxide layer is the essential origin for the decrease in nucleation density. Now let's continue the discussion in chapter 4.2, where I summarize two opinions proposed by two different groups, regarding the reason why heating without H_2 would lower the nucleation density. Based on the evidence in Figure 4.9 and Figure 4.10, we believe that the idea provided by H. Zhou and colleagues is more convincing. By comparison of Figure 4.9 a and Figure 4.10 b, we find that without any oxidation, long term annealing can only reduce the nucleation density, and this is clearly caused by the lack of oxide layer on Cu surface. Besides, the origin of those particles as observed by L. Gan and Z. Luo is not clear, and the particles could be caused by contamination from the quartz tube, impurities in Cu foils, etc. Furthermore, even if these particles served as nucleation center in L. Gan and Z. Luo's experiments, it does not contradict to the explanation that oxide layer passivates the Cu surface and makes it harder for nucleation. L. Gan and Z. Luo themselves showed that nucleation forms only with large enough particles; so oxide layer might be the reason that small particle cannot initiate nucleation.

4.5.2 Ethanol partial pressure dependence

The pressure and flow rate of carbon sources can affect growth behavior greatly in CVD reactions. As mentioned in 4.5.1, the growth rate of our graphene flakes is very low, and the best way to accelerate it is increasing the pressure or flow rate of carbon source. Since our graphene grows in a Cu pocket, so we believe that there is almost no flow inside the pocket, and ethanol molecules or carbon species must dissolve into the pocket. Since as analyzed our graphene follows the diffusion-limited growth, by increasing the flow/partial pressure of ethanol, more carbon is provided and diffused, thus the growth rate can be increased. We conduct experiments with increased flow rate and pressure, as shown in Figure 4.11.

The lowest controllable flow for our mass flow controller is 0.03 sccm, and we have been using this low flow rate to realize low nucleation density. During growth, along with this 0.03 sccm ethanol flow, we also flow a 300 sccm 3% H_2 in Ar, and the total pressure is 300 Pa.. So the partial pressure of ethanol is around 0.03 Pa. Now we increase the flow rate a little to 0.04 sccm, so here the partial pressure of ethanol is also increased to 0.04 Pa. For another sample, we still use 0.03-sccm ethanol and 300 sccm H_2/Ar, but we increase the total pressure to 400 Pa, so the partial pressure of ethanol is also 0.04 Pa. The results are shown in Figure 4.11. Both samples are pre-oxidized for 30 minutes, so when applied with old conditions (partial pressure of ethanol is 0.03 Pa), the nucleation density is around 0.3 nuclei/mm^2. But with this increase in partial pressure, the nucleation density rises dramatically to about 4 nulei/mm^2 (Figure 9.11 a, b), more than 10 times higher. Figure 9.11 a and b exhibit almost the same morphology, suggesting that flow rate is not a variable inside the Cu case, and increasing flow rate is the same as increasing partial pressure of ethanol. But we are surprised to see that the nucleation density rises 10 times only with a 33% increase in partial pressure of

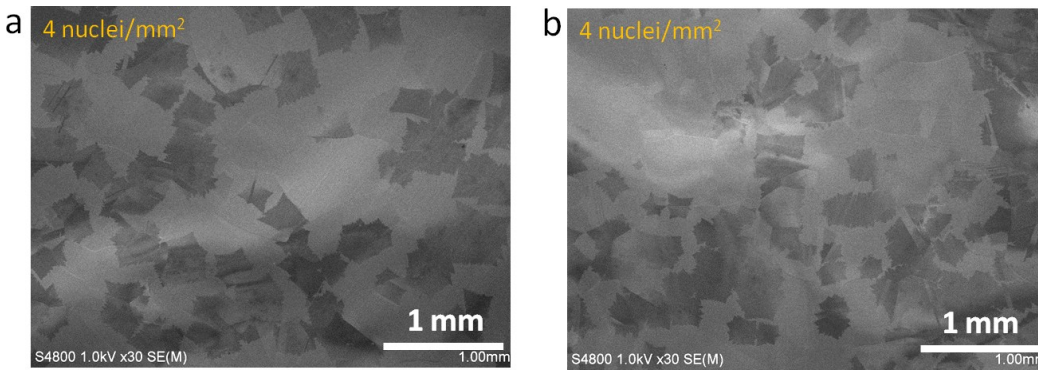

Figure 4.11. SEM images of graphene flakes on Cu. These samples are grown at 1065 ˚C, with a 30 minute pre-oxidation. The only difference is that during CVD growth, for a, the flow is 0.04 sccm ethanol and 300 sccm H_2/Ar at 300 Pa, and for b, the flow is 0.03 sccm ethanol and 300 sccm H_2/Ar at 400 Pa. The nucleation densities are approximate numbers based on the statistics of an 1 cm × 1 cm area for each sample.

ethanol. Not only the density rises, but also, the shapes of graphene flakes become very dentritic. The balance of growth and etching is somehow disturbed, and obviously growth rate at corners is much stronger than etching effect. Although we do observe a increase in growth rate (for one single flake, that growth rate increases nearly two times), this high nucleation density and uneven edges greatly lower the quality of graphene, thus this higher partial pressure of ethanol is not suitable for the growth of graphene single crystals.

4.5.3 Growth duration evolution

To get a more clear insight on how graphene nuclei gradually expand into large flakes, we conduct comparison experiment by stopping CVD growth at different duration, and observe them with SEM. Three results are shown in Figure 4.12. All three samples were pre-oxidized for 1.5 hours, and grown at 1065 ˚C, and they were stopped at 2 hours, 7 hours and 11 hours respectively. For graphene growth at this condition, within 2 hours, we can hardly observe any nucleation, and this is

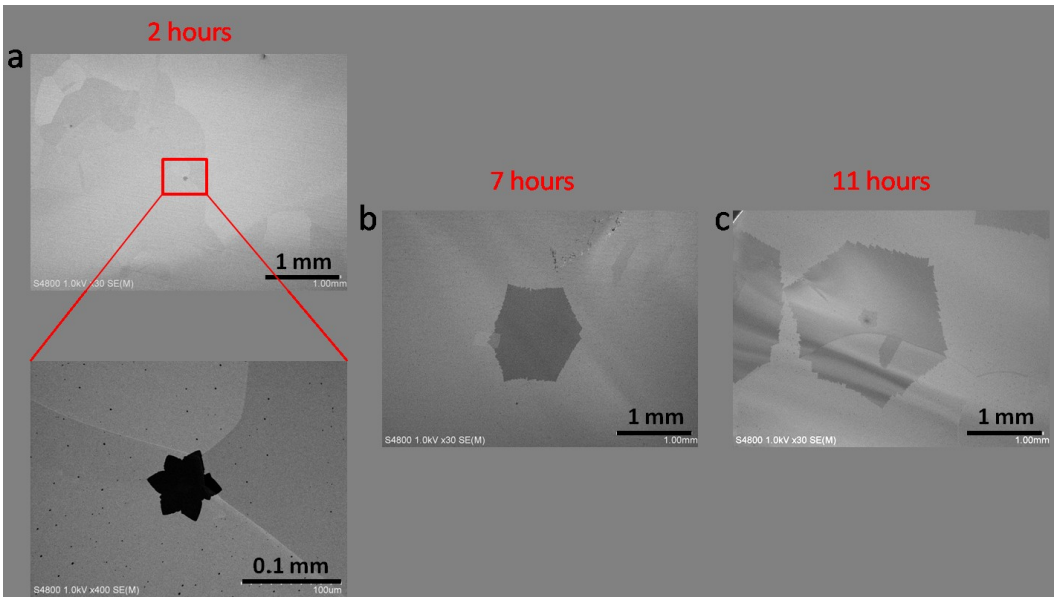

Figure 4.12. SEM images of graphene flakes on Cu with CVD durations of a) 2 hours, b) 7hours, and c) 11hours. These three samples are growth with same conditions except CVD durations. The conditions are: 1.5- hour pre-oxidation, 1065 ˚C, 0.03 sccm ethanol and 300 sccm H_2/Ar, and 300 Pa total pressure.

probably because that the nucleation density is very low, so if the nuclei are too small (less than 0.1 mm), it is very hard to find them by SEM. So here we show the evolution of growth for the stage of 2 hours.

In 2 hours, we start to observe graphene flakes with size of about 0.1 mm (Figure 4.12 a). It's with a typical six-lobed dentritic shape. The nucleation density at this stage is about 0.1~0.2 nuclei/mm^2. This particular graphene flake is near Cu edges, and it expends over the Cu grain boundaries easily. After seven hours, graphene flakes in this stage are dramatically bigger, with a size about 1 mm already. Also, the shape at this stage seems more hexagonal rather than dentritic. But on a closer look, we find the edge is still rough, and with dentritic branches, but the general shape is hexagonal. The nucleation density at this stage is also around 0.1~0.2 nuclei/mm^2. After 11 hours, the size of flakes becomes nearly 2 mm, still we see no change in nucleation density, and the general shape of the flakes is also hexagonal.

The fact that these SEM images taken at different growth stages show graphene flakes all with hexagonal shape, which might correspond to the graphene honeycomb lattice, and that the nucleation density doesn't not change through hours of growth durations, allow us to believe that these graphene flakes might be

Table 4.1: CVD conditions applied in the synthesis of large single-crystal graphene

Ref. #	CH_4 partial pressure	Total pressure	H_2: CH_4	Temperature	Cu enclosure	Surface oxygen	Size of largest single crystals	Growth duration	Growth rate
[2]	1 Pa	5 Pa	4	1035 ˚C	○		0.4 mm	75 min	6 μm/min
[3]	30 Pa	1.4 kPa	467	1077 ˚C			2.3 mm	125 min	18 μm/min
[4]	1.2 Pa	10 Pa	100	1035 ˚C	○		1.5 mm	6 hours	4 μm/min
[5]	4.6 Pa	100 kPa	2174	1075 ˚C			1 mm	5 hours	3.3μm/min
[6]	0.007 Pa	100 Pa	6000	1070 ˚C		○	5 mm	48 hours	1.7μm/min
[1]	21 Pa	100 kPa	2800	1050 ˚C		○	5.9 mm		
[7]	0.13 Pa	13.3 Pa	100	1035 ˚C	○	○	10 mm	800 min	12.5μm/min

single-crystal, a fact that we will prove nest. Another point is that it seems the growth rate is increasing trough the CVD duration, although CVD conditions are the same.

4.5.4 Results of higher total pressure

So far, the discussion has been restricted to LPCVD, with a total reaction pressure of about 300 Pa. The benefit of LPCVD is mainly about lower partial pressure of carbon source, so that the formation of graphene films is more controllable. On the other hand, many literatures reported the growth of graphene using ambient pressure CVD (APCVD) process [87-89]. At first, the purpose of developing this ambient pressure CVD is mostly for economic reasons or manufacture benefits, such that an roll-to-roll production can be realized [90-91]. But since the development on the growth of single-crystal graphene is drawing more attention, another benefit of APCVD becomes very clear, and that is the suppression of Cu sublimation. With a much higher total pressure than that of LPCVD (typically, around 300 times higher), the partial pressure of Cu vapor is also very high at this high temperature condition, thus the evaporation of the Cu substrate is well refrained. A systematically study showed that the activation energy for graphene nucleation at APCVD is 9 eV, more than twice the activation energy for LPCVD (4 eV) [92]. For this reason, even with a high partial pressure of carbon source (i.e., a high concentration of surface adatoms), the nucleation density could still be very low. Besides this change in activation energy, in APCVD, it is possible to bring the reaction temperature even closer to the melting point of Cu. As explained in 4.3.2, with higher temperature, the etching effect is stronger, the graphene flakes become more crystalline, and the only reason that we do not apply a temperature higher than 1065 ˚C is that we fear the Cu foils would be consumed before necessary CVD duration is reached due to the strong Cu sublimation. But with APCVD, even with higher temperature (or else, with melted copper, as shown by [5]), the rate of losing Cu is still lower than LPCVD with lower temperature. I summarize some important papers for the growth of large single-crystal graphene in Table 2. Generally, with APCVD, a higher temperature and a higher H_2: CH_4 ratio are applied, so that even with higher partial pressure of carbon sources, the

nucleation density is still low, and the shape of graphene flakes are often perfect hexagonal with very smooth edges.

In our study, although we believe with higher concentration of H_2, the growth result could be much improved, for safety reasons, we still use the 3% H_2 diluted in Ar. Figure 4.13 shows the evolution of graphene flakes dependent on the total pressure of the CVD system. Note that all other aspects in these experiments, such as the reaction temperature, the flow rate of each gas, the Cu enclosure and the oxidation procedure, remain the same as we used in LPCVD, but only the partial pressures of ethanol and H_2 increase along with the total pressure. Not only the edges of graphene flakes become much smoother with higher total pressure, the growth speed increases dramatically as well. These smooth edges can only be explained in the way that with higher total pressure, the etching effect on the growth front of graphene flakes is much stronger, so the balance between growth and etching along the edges are more even. But it is still unclear if the main etching agent in this process is H_2 or the decomposition products of ethanol. Although the general ratio of H_2 is low in our experiments, but since we apply a super low flow of ethanol, the ratio of H_2: EtOH is about 290, which is not very low compared with other groups parameters as shown in Table 4.1, so it is very possible that H_2 is the main etching agent that helps to maintain this balance of etching/growth of

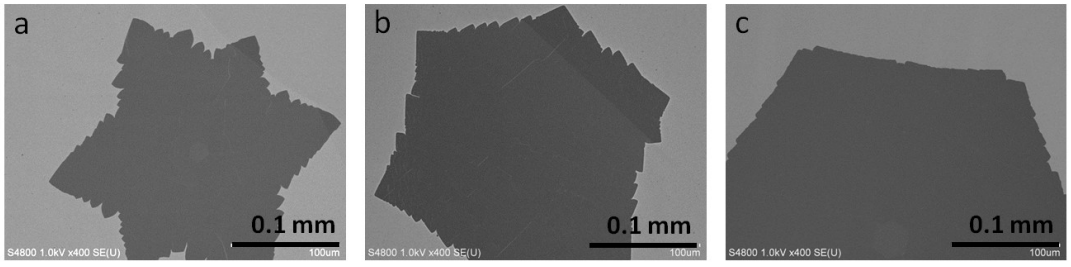

Figure 4.13. SEM images of graphene flakes on Cu with different CVD total pressures. The values of pressures are marked under each SEM image. These three samples were grown at 1065 ˚C, with a 300 sccm flow of H2/Ar and a 0.031 scccm flow of ethanol, for 3 hours.

graphene flakes, same as the cases reported by other groups using methane as the carbon source. And along with the increase in total pressure, the partial pressure of H_2 also increases dramatically, and the rate of etching obviously increases faster than that of growth. On the other hand, the decomposition products of ethanol, including H_2O, O_2, CO, etc., are also very strong etching reagents for graphene, which may also be mainly responsible for keeping this etching/growth balance instead of H_2. At current stage, we lack sufficient evidence to prove which way is right. More experiment regarding this, such as the dependence on different H_2 ratio, should be conducted to resolve this question.

Another important feature form higher total pressure is that the general growth

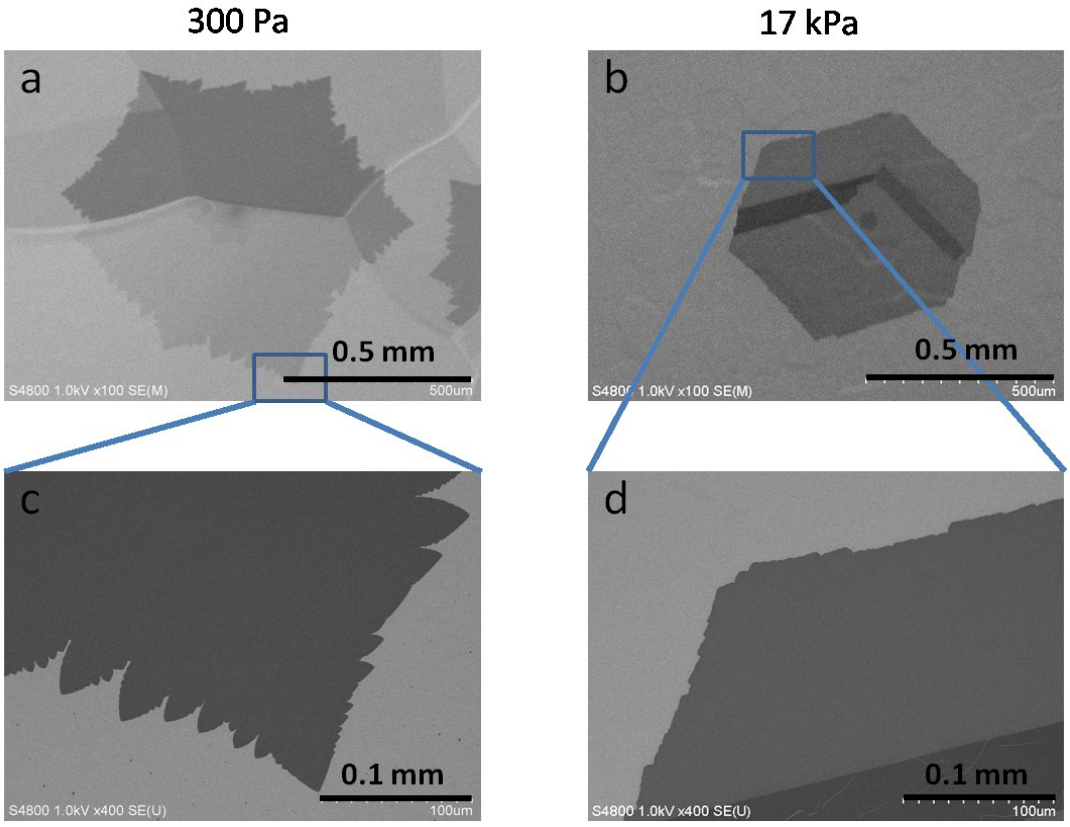

Figure 4.14. SEM images of graphene flakes on Cu grown at a total pressure of a), c) 300 Pa, and b), d) 17 kPa. Note that the growth duration for a) and c) was 7 hours, and for b) and d) was 5 hours. These two samples are shown here for their similarity in edge-to-edge sizes.

rate of graphene flakes increases. As shown in Figure 4.13, with same CVD duration (3 hours), the edge-to-edge size of graphene flakes at 17 kPa is almost twice the size of graphene flakes grown at 300 Pa. There are two possible origins of this evolution: first, with a higher partial pressure of ethanol, the concentration of surface C adatoms increases, resulting in a higher rate of edge attachment around each graphene flakes; second, the CVD duration of these three samples shown in Figure 4.13 is relatively short. Initially, the growth rate of graphene flakes is very low, due to the existence of surface oxygen. As shown in Figure 4.12, in 2 hour duration, we can only observe some 100 μm flakes, but in 7 hours, the size of graphene flakes is close to 1 mm, with a growth rate of about 0.15 mm from 2 hours to 7 hours, and it maintains the same rate from 7 hours to 11 hours. This could be explained in the way that after 2 hours, the oxygen on Cu surfaces are mostly reduced by H_2, thus the growth speed increases after 2 hours. So the size difference shown in Figure 4.13 could be contributed by the fast reduction of Cu surfaces due to higher H_2 concentration. Again, I am sorry to say that we still lack sufficient evidence to prove which is correct.

We show large graphene flakes grown at 300 Pa and 17 kPa in Figure 4.14. With LPCVD, with enough growth duration, although the shape of large graphene single crystals is generally hexagonal, but the edges are very rough as shown in Figure 4.14-a. A higher magnification image (Figure 4.14-c) reveals that the corner of the hexagonal flake is very sharp, close to 60 °, much smaller than the value of a hexagonal-shape corner angle, 120 °, of which the possible reason has been explained in 4.4.2. On the other hand, even for larger graphene flakes, samples grown at 17 kPa still maintain a perfect hexagonal shape, with very smooth edges (Figure 4.14-b). A closer look at the corner also shows a nearly 120 ° angle, suggesting the good crystalline of this graphene flake. This result is consistent with the discussion above.

In Figure 4.13 and Figure 4.14, we only increase the total pressure to 17 kPa, still much lower than the real atmospheric pressure, and this is because when we increase the pressure of ethanol in the ethanol tank, we have to heat it, thus condensation may occur along the tubes that guiding the ethanol vapor, so with our current setup, 17 kPa is the highest possible pressure. Still, this high –pressure

CVD seems promising enough for further exploration, which we would conduct in the near future. All the application and characterization results after this point are still based on LPCVD graphene.

4.6 Prove of single-crystal nature by SEAD

Merely the shape and the nucleation density of these graphene flakes are not enough in proving that these flakes are single-crystal. Here we apply the popular method of electron-diffraction pattern as the proof for single-crystal nature. Graphene flakes as large as several millimeters are transferred to TEM grids, and

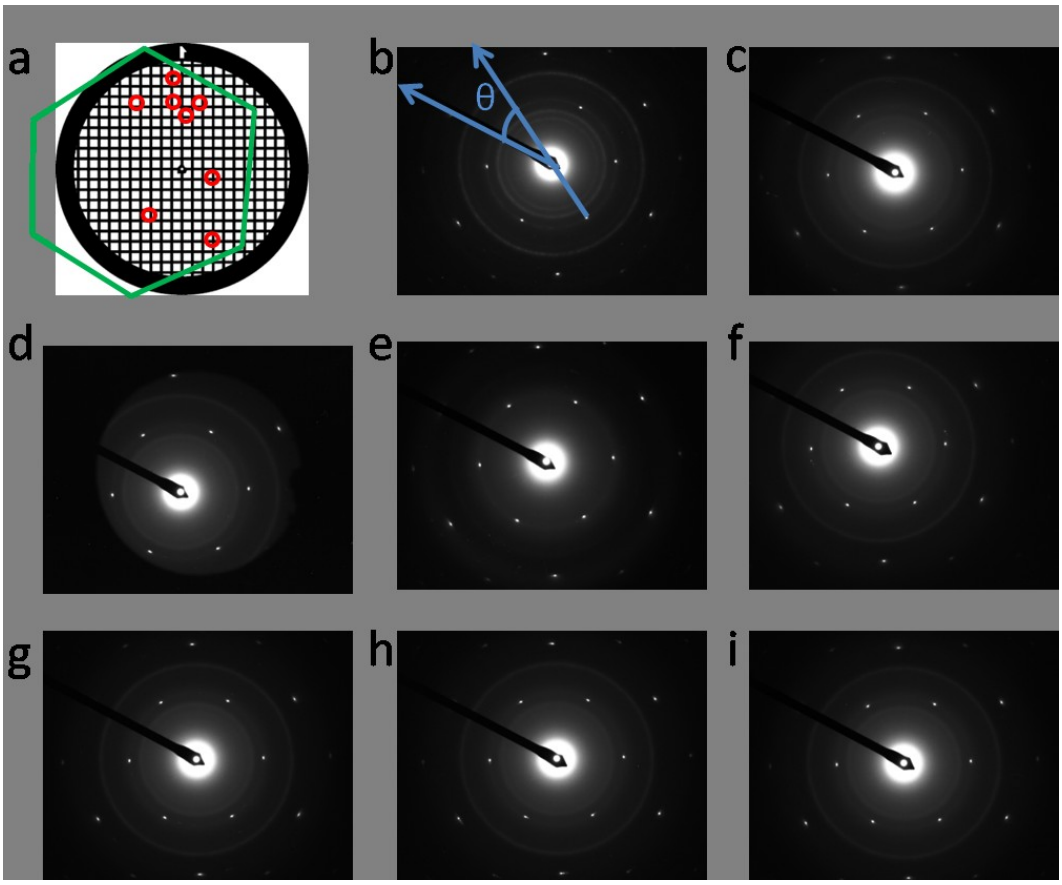

Figure 4.15. SAED patterns of graphene flake. b) – i) are SAED patterns of 8 randomly picked locations on this graphene sample. Their approximate locations are marked with red circles in a). The approximate contours of this graphene flake and the TEM grid is also drawn in a). The maximum diversion of θ in b) – i) is 1.4˚

using the Selected Area Electron Diffraction (SAED) function of TEM, we acquired the SAED patterns at random location on the graphene flake, as shown in Figure 4.15 and Figure 4.16.

Figure 4.15 and Figure 4.16 show two different graphene flakes transferred to TEM grids. For each sample, 8 random locations on these graphene flakes are selected and SAED patterns are taken (Figure 4.15-a and Figure 4.16-a). The SAED patterns are shown in Figure 4.15 b-i and Figure 4.16-b to i. We chose the black bar as x axis, and the angle between one certain crystal direction and the x axis in each pattern (marked as θ in Figure 4.15 b and Figure 4.16 b) is measured. The maximum diversion of θ in Figure 4.15 is 1.4˚ and the maximum diversion of θ

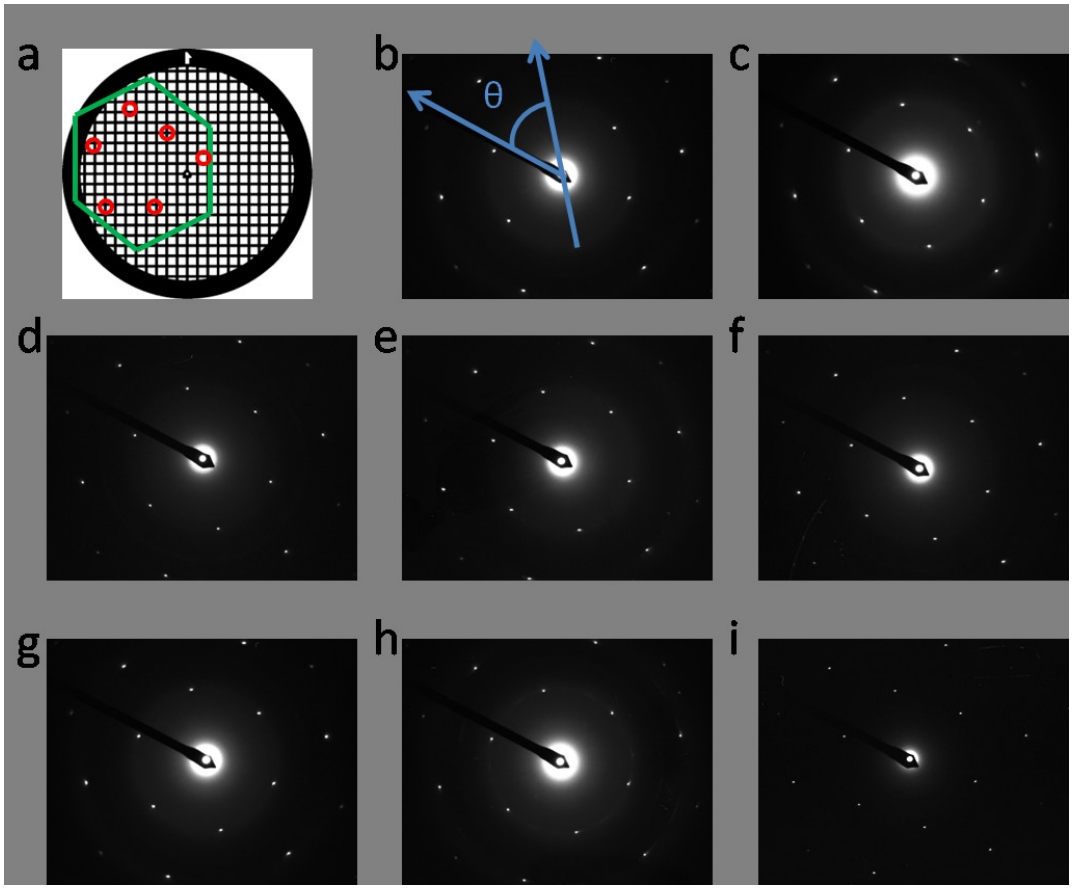

Figure 4.16. SAED patterns of another graphene flake. b) – i) are SAED patterns of 8 randomly picked locations on this graphene sample. Their approximate locations are marked with red circles in a). The approximate contours of this graphene flake and the TEM grid is also drawn in a). The maximum diversion of θ in b) – i) is 1.7˚.

in Figure 4.16 is 1.7˚. This mean that the orientation of graphene lattice changes less than 1.7˚ for locations with a distance as large as 2 mm, suggesting that these graphene flakes are indeed single-crystal. Since these two samples are randomly picked, and are the only two that we measured, and they are both single-crystal, so we have confidence that all of our graphene flakes synthesized in similar methods are single-crystal.

4.7 Discussion about growth mechanism of graphene large single crystals

Finally, we have enough evidences to discuss about the mechanism of the growth of graphene single crystals from ethanol. Mostly the detailed growth kinetics is the same as graphene growth from methane, but there are several points that are very different. The detailed mechanism is explained as follows:

1. After oxidation in air for tens of minutes, there is an oxide layer on the Cu foil. For the fact that we lack reliable equipment for detection of oxidation level, we suspect that the color changing during the oxidation represents the rising of the ratio between O atoms and Cu atoms. In our case, Cu is still the dominant atom on the Cu foil surface, because if the ratio of O:Cu is 1:1, the color should be black as the compound CuO. Since we heat the Cu foil in Ar only, the surface oxygen is well reserved till ethanol and H_2/Ar is introduced into the system to initiate the growth.
2. When ethanol vapor is flowed into the reaction chamber, it immediately decomposes into products such as, C_2H_2, C_2H_4, H_2O, CO, etc. These decomposition products are then adsorbed onto the Cu surface, and under the catalytic effect of cu, they further decompose into even smaller molecules, such as CO, C, CH, etc. These smaller decomposition produces would travel across the Cu surface due to surface diffusion, for the fact that C solubility in Cu is extremely low. [67] This process is exactly the same as the corresponding stage described in Chapter 3.
3. Due to surface oxygen on Cu surface, the activity of Cu surface is reduced, thus, the nucleation of graphene is restrained. We are still not quite clear of what exactly happens here. Either, the catalytic activity of Cu is reduced,

and ethanol cannot decompose to small molecules, which are the main gradients for graphene synthesis; or, there are small C species diffused on Cu surface, but only without the activity of Cu, they cannot form into honeycomb sp^2-bonded structures. This is the stage that we will continue to investigate.

4. Although it becomes very difficult for nucleation on Cu surface due to existence of surface oxygen, by small possibilities, there are still nuclei on Cu surface with very low density. After the formation of some initial nuclei, new diffused carbon atoms are much more likely to be captured by graphene edges, rather than reaching super-saturation and forming new nuclei, for the fact that the reaction barrier for graphene edge growth is much lower [85]. Here, although lacking convincing evidence, we have to believe that despite of surface oxygen, the diffusion length of C species on Cu/CuO surface is still very high, in order that these very discrete nuclei can capture C atoms and expand at this stage.
5. The role of H_2 in this reaction is very interesting. Because of the relatively low partial pressure of H_2 that we use in our experiments, we believe that the etching effect of H_2 is not a major one here. Another reason for this is

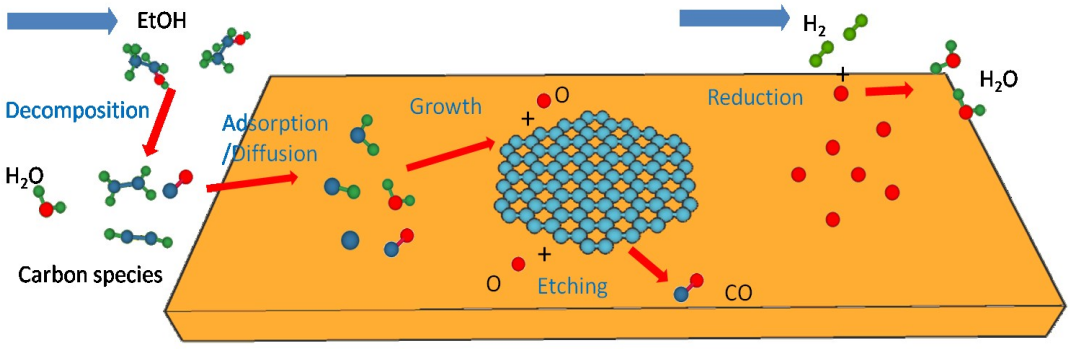

Figure 4.17. Schematics of the growth mechanism. Processes explained here happen simultaneously in the CVD reaction. The forms of ethanol decomposition products are only possible structures, more complex C species (C_xH_y) could also be generated under the catalytic effect of Cu and diffused on Cu surface to be involved in the growth of graphene.

that as explained in 4.5.2, by raising the partial pressure a little (0.03 Pa to 0.04 Pa), the shape of graphene flakes becomes very dentritic, indicating severe insufficient etching effect, but the partial pressure of H_2 is not changed (9 Pa). So we believe that the main function of H_2 in this reaction is to reduce the Cu surface. Surface oxygen can also exhibit strong etch effect, due to their high concentration initially in stage 3. This would severely reduce the growth rate of graphene growth, which is the reason that we only observe graphene flakes of less than 0.1 mm in 2-hour CVD duration (Figure 4.12 a). This growth rate is too low, and we would need several days in order to grow millimeter size graphene flakes. But for the reduction effect of H_2, the concentration of O on Cu surface is gradually reduced, and the etching effect of O becomes small, so the growth rate increases dramatically. As a result, we observe an increase in size of 1 mm for duration of 5 hours (Figure 4.12 a, b). But there are still some oxygen atoms that dissolved into Cu foil, and they are not reduced by H_2, and would precipitate to the surface to act as etchant. Still, the general etching effect that comes from either H_2 or O is very low, considering the diffusion-limited growth behavior and the armchair edges of our graphene flakes.

The 5 processes described above are the main growth mechanism for our CVD growth of graphene large single-crystals from ethanol precursor. In short words, they can be summarized as decomposition, surface diffusion, nucleation, growth and etching, and reduction. The schematic of these processes is shown in Figure 4.17.

4.8 Application: graphene/n-Si solar cells

For its transparency (about 97% for 550 nm wavelength) and good conductivity, graphene is considered to be a wonderful candidate for the application of transparent electrodes, especially for photovoltaic devices. The first generation solar cells based on heterojunction has been a major solar energy harvest technique in the past few decades. And for the sake of environment preservation and economical benefits, heterojunction solar cell based on new materials, especially

new nano-carbon materials. Recently, heterojunction solar cell using SWNT [93-97] or graphene [98-106] electrodes have produced exiting results, but their general performances are still far from theoretical value. One big problem with graphene-based heterojunction solar cell is that the size of this heterojunction is about 3 mm × 3 mm, which is nearly 2 orders larger than former single-crystal graphene flakes, thus the conductivity of graphene film is much decreased by the existence of grain boundaries. Here we fabricate graphene/n-Si Schottky junction solar cell to demonstrate the supreme improvement of power conversion efficiency (PCE) brought by the large single-crystal solar cell.

A typical schematic of graphene/Si heterojunction solar cells is shown in Figure 4.18. Graphene and n-type Si act as electrodes of a diode, and at the small contact window located at the center of the solar-cell chip, graphene and the n-type silicon form a heterojunction. When light hits this contact window, exited electrons would initiate a current. The fabrication process of such structure is as follows:

First, lightly doped n-type silicon wafer is cut into small pieces with the size of 5 mm × 5 mm each, and they are rinsed in concentrated NaOH solution to remove the oxide layer.

Second, after the removal of oxide layer, a piece of scotch tape with a size of 3 mm × 3mm is stuck at the center on one side of each silicon piece, and a 50 nm SiO_2 layer and a 50 nm Pt layer are deposited on the same side sequentially to serve as isolator and electrode. The other side of the chip is deposited with a 10 nm

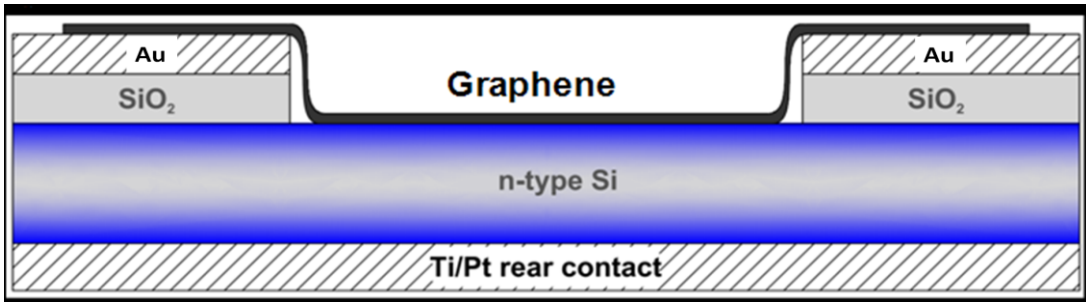

Figure 4.18. Schematic of graphene-Si solar cell

thick Ti layer and a 50 nm thick Pt layer, which act as the opposite electrode.

Third, after the deposition of electrodes, the small scotch tape is removed, and the whole chip is cleaned thoroughly with acetone, IPA, and DI water. Afterwards, graphene is transferred to completely cover the contact window as shown in Figure 4.19, using a wet-etching procedure as explained in 3.2.1.

The fabricated solar cell must be left in air to dry for at least 24 hours before testing. The PCE is the most important value for demonstration of the quality of the solar cell. Figure 4.19 shows the IV curves of the solar cells fabricated with poly-crystal graphene and single-crystal graphene. The poly-crystal graphene is synthesized using the CVD procedure as proposed in Chapter 3. Based on the I-V curves, the PCE and fill factor (FF) are calculated. The PCE of poly-crystal

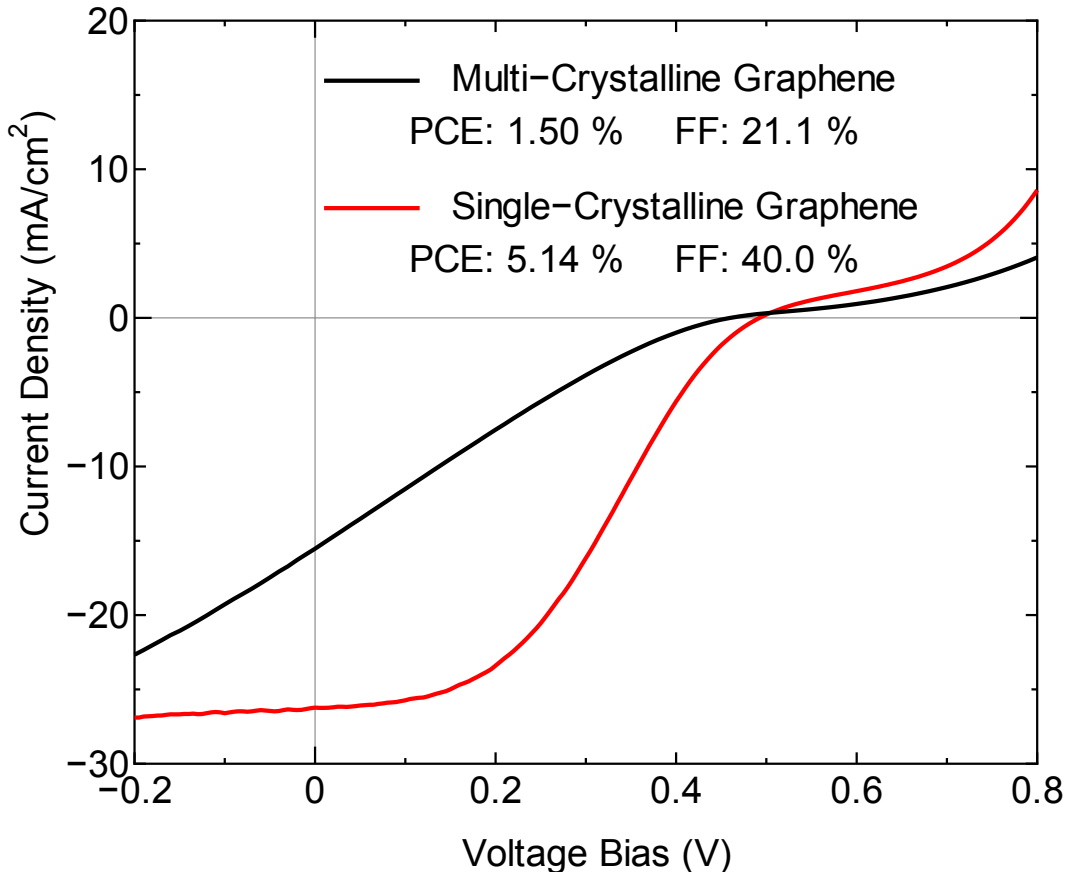

Figure 4.19. J-V curves of graphene/n-Si solar cells

graphene/n-Si solar cell is about 1.50%, which is close to the value that has been reported before. Meanwhile, the PCE of single-crystal graphene/n-Si solar cell is 5.14%, which is the highest value for pristine (undoped) graphene so far. The FF also improved from 21 % to 40 % when adopting the single-crystal graphene.

The PCE for Schottky junction solar cells is mainly affected by three factors: the electrical conductance of graphene, the optical transparency of graphene, and the contact between graphene and metal electrodes. Since the transmittances of both poly-crystal graphene and single-crystal graphene for 550 nm light are about 97%, and the basic solar cell structures are the same, this big improvement in both the PCE and the FF can only be explained as the result of increase in conductance by the absence of graphene grain boundaries in single-crystal graphene. Typically, the conductance can be measured by the 4-point method, but unfortunately we have not conducted this measurement yet.

The performance of graphene/Si solar cells can be easily improved by chemical doping (such as doping with HNO_3, as shown by E. Shi et al. [100]), or by adding the layer number of graphene (disoriented 4-layer graphene is believed to possess both the benefits of high transmittance and high conductivity). Since currently we have shown the best performance of pristine graphene/Si solar cells, we believe it is the most potential application for large single-crystal graphene, and the experiments to enhance the performances shall be conducted shortly.

4.9 Summary

The work described in this chapter is my main contribution as a doctoral candidate. Here, we propose and investigate several key processes for increasing the size of graphene flakes using ethanol as CVD precursor, including heating without H_2, extremely small flow rate (0.03 sccm), and pre-oxidation. The influence of each CVD parameter is carefully investigated, including flow rate and partial pressure of carbon source, reaction temperature, CVD duration, and oxidation level. These systematic studies give us a good insight on how to control the growth behavior, and provide us evidence for demonstrating a growth mechanism that emphasizes the role of oxygen in controlling the nucleation density. Raman maps and SAED observation helped us to understand the quality and

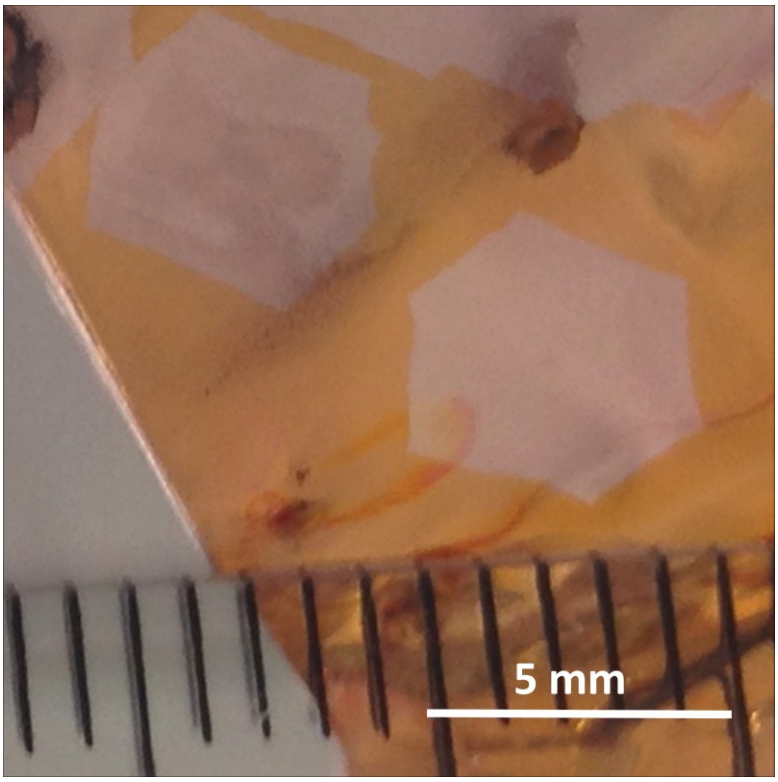

Figure 4.20. Photograph of 5mm graphene single crystals on Cu foil. Graphene/Cu foil is heated in air at 180˚C for 5 minutes to oxidize the Cu surface that is not covered by graphene, in order to create contrast. This

morphology of graphene flakes, and we are proudly proclaim that we grow single-crystal graphene flakes with relatively easy procedure, and the size of our biggest graphene single-crystal sample is 5 mm (Figure 4.20), which is one of the biggest individual hexagonal-shaped graphene single crystals currently.

Besides, the proposed mechanism based on experiment evidences would create an enlightening prospect for the possible realization of wafer-scale single-crystal graphene in the future.

Chapter 5
Closing Remarks

5.1 Summary of this thesis

The research in this Ph. D thesis includes many improvements in the synthesis of graphene on transition metals using ethanol as carbon source. Especially, since almost all the other groups that conducting CVD growth of graphene are applying methane as carbon source, following the successful initial trials by K. Kim et al. [32] and X. Li et al. [33], we proved that another carbon source, ethanol, are equally capable in the synthesis of high-quality graphene, and might bring procedure simplicity. This opens a brand new road to the synthesis of wafer-scale graphene single crystals. Ethanol can be an economic and safe alternative for graphene synthesis in future industrial manufacture.

After a brief introduction on the structure, the properties, and the early synthesis methods of graphene in Chapter 1, the ACCVD method, including the equipments and basic principles, is explained in Chapter 2. Especially, Raman spectroscopy, the most powerful tool in detection of the quality and numbers of layer of graphene, is introduced in detail. Some preliminary work using Ni substrates is shown in this chapter. We successfully synthesized graphene with low defect level on Ni surfaces, and by carbon-isotope labeling we proved that the growth is a surface mediated process, rather than a dissolving-and-precipitation process as conventionally believed. But the control over numbers of layers of the resultant graphene is not ideal, despite our effort on tuning the CVD conditions, due to the fact that the dissolving-and-precipitation process still exists as a miner process for the high solubility of carbon in Ni.

In Chapter 3, the CVD growth of graphene on Cu substrates using ethanol as carbon source is discussed. With optimized conditions, we were able to synthesize

large-scale single-layer homogeneous graphene films on Cu foils. Small Raman D bands at random locations indicate the low defect level. With parametric study, we show that the formation of bi-layer and multi-layer graphene can be restrained be lowering the CVD reaction pressure. To solve the problem of high-temperature etching, we utilized Cu pockets. By Cu pockets and raising growth temperature, graphene with higher quality, i.e., fewer contamination, bigger graphene domain size, more dominant single layer, is synthesized. Furthermore, we found the growth can be self-limited, giving us a much bigger CVD-duration window and thus better control of the good quality of single-layer graphene. Based on the observations, we propose the mechanism of a diffusion-limited growth procedure to explain graphene growth on Cu from ethanol.

To further improve the quality of graphene films, especially the grain size of single-crystal graphene, methods including extremely small ethanol flow, heating without hydrogen are explored. Finally, we realized the importance of surface oxygen in reducing the nucleation density of graphene on Cu foils, and utilizing this advantage, 5 mm single-crystal graphene is synthesized. A complete mechanism model is proposed to explain the detailed procedure of the nucleation and growth of graphene flakes. Furthermore, graphene/n-Si solar cells are fabricated, and the preliminary results of them are very promising, which is considered a major prospect of this thesis.

5.2 Objective fulfillment

The objective of this thesis as proposed in 1.5 is to investigate of mechanism of graphene growth on metal surfaces and to grow high-quality graphene using ethanol as the precursor.

For the first objective, a series of isotope labeling experiments were conducted on Ni substrates, and the adsorption growth model was proposed based on these results. For Cu substrates, influence of wide CVD parameter ranges was explored, and based on the systematic study, the detail procedure of nucleation and expansion

of graphene flakes were explained.

For the second objective, 5 mm single-crystal graphene flakes are synthesized. Their single-crystal nature has been confirmed by SAED patterns. Scanning Raman shows that graphene flakes are uniform, with very low D-band across the whole film. The electrical property of the large single-crystal graphene film is demonstrated by its application in graphene/Si solar cells, and the good performance of these solar cell compared with the ones formed by poly-crystal graphene shows great improvement on conductance..

5.3 Prospects

Although a 5 mm single-crystal graphene film is already supreme compared with the growth results from merely two years ago, wafer-size single-crystal graphene by simple CVD method on Cu substrates is yet to be realized. Techniques to further decrease the nucleation density and increase the growth speed is required, such as seeded growth, two-step growth, and a more detailed optimization on the surface oxygen. Since it has become very clear that surface oxygen can directly and efficiently refrain the nucleation, it is entirely possible to control the location and the occasion of the nucleation by manipulating the morphology of the surface oxygen and the oxygen inside the Cu foil.

Second, for graphene films grown on metal substrates, a transfer procedure is necessary for the applications, and graphene is more or less damaged in this process either by wet-etching or mechanical force. So we think a very important work for the next step could be the direct growth of graphene on dielectric materials, such as SiO_2. Since it has been proved that graphene grown on Cu is not epitaxial and Cu is barely involved in the attachment of C atoms onto graphene edges, the metal substrates may not be necessary after the nucleation stage. Transfer free growth on dielectric materials could be realized using a similar method of the cloning of single-walled carbon nanotubes.

Third, with involvement of surface oxygen, the nucleation and growth processes of graphene flakes become more complex, and the mechanism behind this is still unclear. Further investigation involving evolved characterization technique is required. For instance, an in-situ Raman observation of these two processes could

greatly help to understand the role of oxygen on reducing the nucleation density and increasing the growth speed.

Forth, the application of large single-crystal graphene is the major challenge for the research of this material. For FET devices, the synthesis of AB-stacked double-layer graphene is required, for the natural band gap possessed by it. Double-layer graphene has been reported to be successfully synthesized with small grain size [62, 107-113], and the biggest single-crystal double-layer graphene reported is about 200 μm [6]. We believe with our experience and skill in the synthesis of large single-crystal graphene, the size of single-crystal double-layer graphene can also be improved, which is critical for future large-scale FET applications, for its supreme homogeneity. Another major application is the transparent electrode for solar cells, as mentioned in 4.8. After improving the performance of graphene/Si solar cells, other types of solar cell including polymer solar cells can also be fabricated using graphene electrode.

Bibliography

1. Gan, L.; Luo, Z., Turning off Hydrogen To Realize Seeded Growth of Subcentimeter Single-Crystal Graphene Grains on Copper. *ACS Nano* **2013,** *7* (10), 9480-9488.

2. Li, X.; Magnuson, C. W.; Venugopal, A.; Tromp, R. M.; Hannon, J. B.; Vogel, E. M.; Colombo, L.; Ruoff, R. S., Large-Area Graphene Single Crystals Grown by Low-Pressure Chemical Vapor Deposition of Methane on Copper. *Journal of the American Chemical Society* **2011,** *133* (9), 2816-2819.

3. Yan, Z.; Lin, J.; Peng, Z.; Sun, Z.; Zhu, Y.; Li, L.; Xiang, C.; Samuel, E. L.; Kittrell, C.; Tour, J. M., Toward the Synthesis of Wafer-Scale Single-Crystal Graphene on Copper Foils. *ACS Nano* **2012,** *6* (10), 9110-9117.

4. Chen, S.; Ji, H.; Chou, H.; Li, Q.; Li, H.; Suk, J. W.; Piner, R.; Liao, L.; Cai, W.; Ruoff, R. S., Millimeter-Size Single-Crystal Graphene by Suppressing Evaporative Loss of Cu During Low Pressure Chemical Vapor Deposition. *Advanced Materials* **2013,** *25* (14), 2062-2065.

5. Mohsin, A.; Liu, L.; Liu, P.; Deng, W.; Ivanov, I. N.; Li, G.; Dyck, O. E.; Duscher, G.; Dunlap, J. R.; Xiao, K.; Gu, G., Synthesis of Millimeter-Size Hexagon-Shaped Graphene Single Crystals on Resolidified Copper. *ACS Nano* **2013,** *7* (10), 8924-8931.

6. Zhou, H.; Yu, W. J.; Liu, L.; Cheng, R.; Chen, Y.; Huang, X.; Liu, Y.; Wang, Y.; Huang, Y.; Duan, X., Chemical vapour deposition growth of large single crystals of monolayer and bilayer graphene. *Nat Commun* **2013,** *4*.

7. Hao, Y.; Bharathi, M. S.; Wang, L.; Liu, Y.; Chen, H.; Nie, S.; Wang, X.; Chou, H.; Tan, C.; Fallahazad, B.; Ramanarayan, H.; Magnuson, C. W.; Tutuc, E.; Yakobson, B. I.; McCarty, K. F.; Zhang, Y.-W.; Kim, P.; Hone, J.; Colombo, L.; Ruoff, R. S., The Role of Surface Oxygen in the Growth of Large Single-Crystal Graphene on Copper. *Science* **2013,** *342* (6159), 720-723.

8. Kroto, H. W.; Heath, J. R.; O'Brien, S. C.; Curl, R. F.; Smalley, R. E., C60: Buckminsterfullerene. *Nature* **1985,** *318* (6042), 162-163.

9. Iijima, S.; Ichihashi, T., Single-shell carbon nanotubes of 1-nm diameter. *Nature* **1993,** *363* (6430), 603-605.

10. Bethune, D. S.; Klang, C. H.; de Vries, M. S.; Gorman, G.; Savoy, R.; Vazquez, J.; Beyers, R., Cobalt-catalysed growth of carbon nanotubes with single-atomic-layer walls. *Nature* **1993,** *363* (6430), 605-607.

11. Novoselov, K. S.; Geim, A. K.; Morozov, S. V.; Jiang, D.; Zhang, Y.; Dubonos, S. V.; Grigorieva, I. V.; Firsov, A. A., Electric Field Effect in Atomically Thin Carbon Films. *Science* **2004,** *306* (5696), 666-669.

12. Geim, A. K.; Novoselov, K. S., The rise of graphene. *Nat Mater* **2007,** *6* (3), 183-191.

13. Zhang, Y.; Tan, Y.-W.; Stormer, H. L.; Kim, P., Experimental observation of the quantum Hall effect and Berry's phase in graphene. *Nature* **2005,** *438* (7065), 201-204.

14. Bolotin, K. I.; Sikes, K. J.; Jiang, Z.; Klima, M.; Fudenberg, G.; Hone, J.; Kim, P.; Stormer, H. L., Ultrahigh electron mobility in suspended graphene. *Solid State Communications* **2008,** *146* (9–10), 351-355.

15. Dean, C. R.; Young, A. F.; MericI; LeeC; WangL; SorgenfreiS; WatanabeK; TaniguchiT; KimP; Shepard, K. L.; HoneJ, Boron nitride substrates for high-quality graphene electronics. *Nat Nano* **2010,** *5* (10), 722-726.

16. Zhao, H.; Aluru, N. R., Temperature and strain-rate dependent fracture strength of graphene. *Journal of Applied Physics* **2010,** *108* (6), -.

17. Lee, C.; Wei, X.; Kysar, J. W.; Hone, J., Measurement of the Elastic Properties and Intrinsic Strength of Monolayer Graphene. *Science* **2008,** *321* (5887), 385-388.

18. Van Bommel, A. J.; Crombeen, J. E.; Van Tooren, A., LEED and Auger electron observations of the SiC(0001) surface. *Surface Science* **1975,** *48* (2), 463-472.

19. Charrier, A.; Coati, A.; Argunova, T.; Thibaudau, F.; Garreau, Y.; Pinchaux, R.; Forbeaux, I.; Debever, J.-M.; Sauvage-Simkin, M.; Themlin, J.-M., Solid-state decomposition of silicon carbide for growing ultra-thin heteroepitaxial graphite films. *Journal of Applied Physics* **2002,** *92* (5), 2479-2484.

20. Berger, C.; Song, Z.; Li, T.; Li, X.; Ogbazghi, A. Y.; Feng, R.; Dai, Z.; Marchenkov, A. N.; Conrad, E. H.; First, P. N.; de Heer, W. A., Ultrathin Epitaxial Graphite: 2D Electron Gas Properties and a Route toward Graphene-based Nanoelectronics. *The Journal of Physical Chemistry B* **2004,** *108* (52), 19912-19916.

21. Eda, G.; Fanchini, G.; Chhowalla, M., Large-area ultrathin films of reduced graphene oxide as a transparent and flexible electronic

material. *Nat Nano* **2008,** *3* (5), 270-274.

22. Stankovich, S.; Dikin, D. A.; Piner, R. D.; Kohlhaas, K. A.; Kleinhammes, A.; Jia, Y.; Wu, Y.; Nguyen, S. T.; Ruoff, R. S., Synthesis of graphene-based nanosheets via chemical reduction of exfoliated graphite oxide. *Carbon* **2007,** *45* (7), 1558-1565.

23. Hagstrom, S.; Lyon, H. B.; Somorjai, G. A., Surface Structures on the Clean Platinum (100) Surface. *Physical Review Letters* **1965,** *15* (11), 491-493.

24. Bartelt, N. C.; McCarty, K. F., Graphene growth on metal surfaces. *MRS Bulletin* **2012,** *37* (12), 1158-1165.

25. N'Diaye, A. T.; Bleikamp, S.; Feibelman, P. J.; Michely, T., Two-Dimensional Ir Cluster Lattice on a Graphene Moiré on Ir(111). *Physical Review Letters* **2006,** *97* (21), 215501.

26. Sutter, P. W.; Flege, J.-I.; Sutter, E. A., Epitaxial graphene on ruthenium. *Nat Mater* **2008,** *7* (5), 406-411.

27. Gao, L.; Ren, W.; Xu, H.; Jin, L.; Wang, Z.; Ma, T.; Ma, L.-P.; Zhang, Z.; Fu, Q.; Peng, L.-M.; Bao, X.; Cheng, H.-M., Repeated growth and bubbling transfer of graphene with millimetre-size single-crystal grains using platinum. *Nat Commun* **2012,** *3*, 699.

28. Daiyu, K.; Shintaro, S.; Katsunori, Y.; Naoki, H.; Motonobu, S.; Mizuhisa, N.; Naoki, Y., Low-Temperature Synthesis of Graphene and Fabrication of Top-Gated Field Effect Transistors without Using Transfer Processes. *Applied Physics Express* **2010,** *3* (2), 025102.

29. Ago, H.; Ito, Y.; Mizuta, N.; Yoshida, K.; Hu, B.; Orofeo, C. M.; Tsuji, M.; Ikeda, K.-i.; Mizuno, S., Epitaxial Chemical Vapor Deposition Growth of Single-Layer Graphene over Cobalt Film Crystallized on Sapphire. *ACS Nano* **2010,** *4* (12), 7407-7414.

30. Bae, S.; Kim, H.; Lee, Y.; Xu, X.; Park, J.-S.; Zheng, Y.; Balakrishnan, J.; Lei, T.; Ri Kim, H.; Song, Y. I.; Kim, Y.-J.; Kim, K. S.; Ozyilmaz, B.; Ahn, J.-H.; Hong, B. H.; Iijima, S., Roll-to-roll production of 30-inch graphene films for transparent electrodes. *Nat Nano* **2010,** *5* (8), 574-578.

31. Reina, A.; Jia, X.; Ho, J.; Nezich, D.; Son, H.; Bulovic, V.; Dresselhaus, M. S.; Kong, J., Large Area, Few-Layer Graphene Films on Arbitrary Substrates by Chemical Vapor Deposition. *Nano Letters* **2008,** *9* (1), 30-35.

32. Kim, K. S.; Zhao, Y.; Jang, H.; Lee, S. Y.; Kim, J. M.; Kim, K. S.; Ahn, J.-H.; Kim, P.; Choi, J.-Y.; Hong, B. H., Large-scale pattern growth of graphene films for stretchable transparent electrodes. *Nature* **2009,** *457* (7230), 706-710.

33. Li, X.; Cai, W.; An, J.; Kim, S.; Nah, J.; Yang, D.; Piner, R.; Velamakanni, A.; Jung, I.; Tutuc, E.; Banerjee, S. K.; Colombo, L.; Ruoff, R. S., Large-Area Synthesis of High-Quality and Uniform Graphene Films on Copper Foils. *Science* **2009,** *324* (5932), 1312-1314.

34. Li, X.; Cai, W.; Colombo, L.; Ruoff, R. S., Evolution of Graphene Growth on Ni and Cu by Carbon Isotope Labeling. *Nano Letters* **2009,** *9* (12), 4268-4272.

35. Coraux, J.; N'Diaye, A. T.; Busse, C.; Michely, T., Structural Coherency of Graphene on Ir(111). *Nano Letters* **2008,** *8* (2), 565-570.

36. Guermoune, A.; Chari, T.; Popescu, F.; Sabri, S. S.; Guillemette, J.; Skulason, H. S.; Szkopek, T.; Siaj, M., Chemical vapor deposition synthesis of graphene on copper with methanol, ethanol, and propanol precursors. *Carbon* **2011,** *49* (13), 4204-4210.

37. Miyata, Y.; Kamon, K.; Ohashi, K.; Kitaura, R.; Yoshimura, M.; Shinohara, H., A simple alcohol-chemical vapor deposition synthesis of single-layer graphenes using flash cooling. *Applied Physics Letters* **2010,** *96* (26), -.

38. Sun, Z.; Yan, Z.; Yao, J.; Beitler, E.; Zhu, Y.; Tour, J. M., Growth of graphene from solid carbon sources. *Nature* **2011,** *471* (7336), 124-124.

39. Ruan, G.; Sun, Z.; Peng, Z.; Tour, J. M., Growth of Graphene from Food, Insects, and Waste. *ACS Nano* **2011,** *5* (9), 7601-7607.

40. Maruyama, S.; Kojima, R.; Miyauchi, Y.; Chiashi, S.; Kohno, M., Low-temperature synthesis of high-purity single-walled carbon nanotubes from alcohol. *Chemical Physics Letters* **2002,** *360* (3–4), 229-234.

41. Murakami, Y.; Chiashi, S.; Miyauchi, Y.; Hu, M.; Ogura, M.; Okubo, T.; Maruyama, S., Growth of vertically aligned single-walled carbon nanotube films on quartz substrates and their optical anisotropy. *Chemical Physics Letters* **2004,** *385* (3–4), 298-303.

42. Ferrari, A. C.; Meyer, J. C.; Scardaci, V.; Casiraghi, C.; Lazzeri, M.; Mauri, F.; Piscanec, S.; Jiang, D.; Novoselov, K. S.; Roth, S.; Geim, A. K., Raman Spectrum of Graphene and Graphene Layers. *Physical Review Letters* **2006,** *97* (18), 187401.

43. Malard, L. M.; Pimenta, M. A.; Dresselhaus, G.; Dresselhaus, M. S., Raman spectroscopy in graphene. *Physics Reports* **2009,** *473* (5–6), 51-87.

44. Ferrari, A. C.; Basko, D. M., Raman spectroscopy as a versatile tool for studying the properties of graphene. *Nat Nano* **2013,** *8* (4),

235-246.

45. MacDonald, A. H.; Bistritzer, R., Materials science: Graphene moire mystery solved? *Nature* **2011,** *474* (7352), 453-454.

46. Ni, Z.; Wang, Y.; Yu, T.; You, Y.; Shen, Z., Reduction of Fermi velocity in folded graphene observed by resonance Raman spectroscopy. *Physical Review B* **2008,** *77* (23), 235403.

47. Casiraghi, C.; Hartschuh, A.; Qian, H.; Piscanec, S.; Georgi, C.; Fasoli, A.; Novoselov, K. S.; Basko, D. M.; Ferrari, A. C., Raman Spectroscopy of Graphene Edges. *Nano Letters* **2009,** *9* (4), 1433-1441.

48. Graf, D.; Molitor, F.; Ensslin, K.; Stampfer, C.; Jungen, A.; Hierold, C.; Wirtz, L., Spatially Resolved Raman Spectroscopy of Single- and Few-Layer Graphene. *Nano Letters* **2007,** *7* (2), 238-242.

49. You, Y.; Ni, Z.; Yu, T.; Shen, Z., Edge chirality determination of graphene by Raman spectroscopy. *Applied Physics Letters* **2008,** *93* (16), 163112-163112-3.

50. Cançado, L. G.; Jorio, A.; Ferreira, E. H. M.; Stavale, F.; Achete, C. A.; Capaz, R. B.; Moutinho, M. V. O.; Lombardo, A.; Kulmala, T. S.; Ferrari, A. C., Quantifying Defects in Graphene via Raman Spectroscopy at Different Excitation Energies. *Nano Letters* **2011,** *11* (8), 3190-3196.

51. Huang, M.; Yan, H.; Chen, C.; Song, D.; Heinz, T. F.; Hone, J., Phonon softening and crystallographic orientation of strained graphene studied by Raman spectroscopy. *Proceedings of the National Academy of Sciences* **2009,** *106* (18), 7304-7308.

52. Kudin, K. N.; Ozbas, B.; Schniepp, H. C.; Prud'homme, R. K.; Aksay, I. A.; Car, R., Raman Spectra of Graphite Oxide and Functionalized Graphene Sheets. *Nano Letters* **2007,** *8* (1), 36-41.

53. Jorio, A.; Cançado, L. G., Raman spectroscopy of twisted bilayer graphene. *Solid State Communications* **2013,** *175–176* (0), 3-12.

54. Righi, A.; Venezuela, P.; Chacham, H.; Costa, S. D.; Fantini, C.; Ruoff, R. S.; Colombo, L.; Bacsa, W. S.; Pimenta, M. A., Resonance Raman spectroscopy in twisted bilayer graphene. *Solid State Communications* **2013,** *175–176* (0), 13-17.

55. Campos-Delgado, J.; Cançado, L.; Achete, C.; Jorio, A.; Raskin, J.-P., Raman scattering study of the phonon dispersion in twisted bilayer graphene. *Nano Research* **2013,** *6* (4), 269-274.

56. Wang, Y.; Su, Z.; Wu, W.; Nie, S.; Xie, N.; Gong, H.; Guo, Y.; Hwan Lee, J.; Xing, S.; Lu, X.; Wang, H.; Lu, X.; McCarty, K.; Pei, S.-s.; Robles-Hernandez, F.; Hadjiev, V. G.; Bao, J., Resonance Raman spectroscopy of G-line and folded phonons in twisted bilayer

graphene with large rotation angles. *Applied Physics Letters* **2013,** *103* (12), -.

57. Kalbac, M.; Frank, O.; Kong, J.; Sanchez-Yamagishi, J.; Watanabe, K.; Taniguchi, T.; Jarillo-Herrero, P.; Dresselhaus, M. S., Large Variations of the Raman Signal in the Spectra of Twisted Bilayer Graphene on a BN Substrate. *The Journal of Physical Chemistry Letters* **2012,** *3* (6), 796-799.

58. Weatherup, R. S.; Dlubak, B.; Hofmann, S., Kinetic Control of Catalytic CVD for High-Quality Graphene at Low Temperatures. *ACS Nano* **2012,** *6* (11), 9996-10003.

59. Horgan, A. M.; King, D. A., Oxygen adsorption, reconstruction, and thin oxide film formation on clean metal surfaces: Ni, Fe, W and Mo. *Surface Science* **1970,** *23* (2), 259-282.

60. Allen, G.; Tucker, P.; Wild, R., Surface oxidation of nickel metal as studied by X-Ray photoelectron spectroscopy. *Oxid Met* **1979,** *13* (3), 223-236.

61. Nie, S.; Walter, A. L.; Bartelt, N. C.; Starodub, E.; Bostwick, A.; Rotenberg, E.; McCarty, K. F., Growth from Below: Graphene Bilayers on Ir(111). *ACS Nano* **2011,** *5* (3), 2298-2306.

62. Li, Q.; Chou, H.; Zhong, J.-H.; Liu, J.-Y.; Dolocan, A.; Zhang, J.; Zhou, Y.; Ruoff, R. S.; Chen, S.; Cai, W., Growth of Adlayer Graphene on Cu Studied by Carbon Isotope Labeling. *Nano Letters* **2013,** *13* (2), 486-490.

63. Entani, S.; Matsumoto, Y.; Ohtomo, M.; Avramov, P. V.; Naramoto, H.; Sakai, S., Precise control of single- and bi-layer graphene growths on epitaxial Ni(111) thin film. *Journal of Applied Physics* **2012,** *111* (6), -.

64. Li, X.; Magnuson, C. W.; Venugopal, A.; An, J.; Suk, J. W.; Han, B.; Borysiak, M.; Cai, W.; Velamakanni, A.; Zhu, Y.; Fu, L.; Vogel, E. M.; Voelkl, E.; Colombo, L.; Ruoff, R. S., Graphene Films with Large Domain Size by a Two-Step Chemical Vapor Deposition Process. *Nano Letters* **2010,** *10* (11), 4328-4334.

65. Singleton, M.; Nash, P., The C-Ni (Carbon-Nickel) system. *Bulletin of Alloy Phase Diagrams* **1989,** *10* (2), 121-126.

66. Nishitani, S. R.; Ishihara, K. N.; Suzuki, R. O.; Shingu, P. H., Metastable solid solubility limit of carbon in the Ni-C system. *J Mater Sci Lett* **1985,** *4* (7), 872-875.

67. López, G. A.; Mittemeijer, E. J., The solubility of C in solid Cu. *Scripta Materialia* **2004,** *51* (1), 1-5.

68. Cho, J.; Gao, L.; Tian, J.; Cao, H.; Wu, W.; Yu, Q.; Yitamben, E. N.; Fisher, B.; Guest, J. R.; Chen, Y. P.; Guisinger, N. P., Atomic-Scale

Investigation of Graphene Grown on Cu Foil and the Effects of Thermal Annealing. *ACS Nano* **2011,** *5* (5), 3607-3613.

69. Zhao, P.; Kumamoto, A.; Kim, S.; Chen, X.; Hou, B.; Chiashi, S.; Einarsson, E.; Ikuhara, Y.; Maruyama, S., Self-Limiting Chemical Vapor Deposition Growth of Monolayer Graphene from Ethanol. *The Journal of Physical Chemistry C* **2013,** *117* (20), 10755-10763.

70. Zhang, Y.; Zhang, L.; Kim, P.; Ge, M.; Li, Z.; Zhou, C., Vapor Trapping Growth of Single-Crystalline Graphene Flowers: Synthesis, Morphology, and Electronic Properties. *Nano Letters* **2012,** *12* (6), 2810-2816.

71. Giovannetti, G.; Khomyakov, P. A.; Brocks, G.; Karpan, V. M.; van den Brink, J.; Kelly, P. J., Doping Graphene with Metal Contacts. *Physical Review Letters* **2008,** *101* (2), 026803.

72. Khomyakov, P. A.; Giovannetti, G.; Rusu, P. C.; Brocks, G.; van den Brink, J.; Kelly, P. J., First-principles study of the interaction and charge transfer between graphene and metals. *Physical Review B* **2009,** *79* (19), 195425.

73. Rasool, H. I.; Song, E. B.; Allen, M. J.; Wassei, J. K.; Kaner, R. B.; Wang, K. L.; Weiller, B. H.; Gimzewski, J. K., Continuity of Graphene on Polycrystalline Copper. *Nano Letters* **2010,** *11* (1), 251-256.

74. Marchini, S.; Günther, S.; Wintterlin, J., Scanning tunneling microscopy of graphene on Ru(0001). *Physical Review B* **2007,** *76* (7), 075429.

75. Jacobberger, R. M.; Arnold, M. S., Graphene Growth Dynamics on Epitaxial Copper Thin Films. *Chemistry of Materials* **2013,** *25* (6), 871-877.

76. Yu, Q.; Jauregui, L. A.; Wu, W.; Colby, R.; Tian, J.; Su, Z.; Cao, H.; Liu, Z.; Pandey, D.; Wei, D.; Chung, T. F.; Peng, P.; Guisinger, N. P.; Stach, E. A.; Bao, J.; Pei, S.-S.; Chen, Y. P., Control and characterization of individual grains and grain boundaries in graphene grown by chemical vapour deposition. *Nat Mater* **2011,** *10* (6), 443-449.

77. Huang, P. Y.; Ruiz-Vargas, C. S.; van der Zande, A. M.; Whitney, W. S.; Levendorf, M. P.; Kevek, J. W.; Garg, S.; Alden, J. S.; Hustedt, C. J.; Zhu, Y.; Park, J.; McEuen, P. L.; Muller, D. A., Grains and grain boundaries in single-layer graphene atomic patchwork quilts. *Nature* **2011,** *469* (7330), 389-392.

78. Lee, J.-H.; Lee, E. K.; Joo, W.-J.; Jang, Y.; Kim, B.-S.; Lim, J. Y.; Choi, S.-H.; Ahn, S. J.; Ahn, J. R.; Park, M.-H.; Yang, C.-W.; Choi, B. L.; Hwang, S.-W.; Whang, D., Wafer-Scale Growth of Single-Crystal Monolayer Graphene on Reusable Hydrogen-Terminated Germanium. *Science* **2014,** *344* (6181),

286-289.

79. Yazyev, O. V.; Pasquarello, A., Effect of Metal Elements in Catalytic Growth of Carbon Nanotubes. *Physical Review Letters* **2008,** *100* (15), 156102.

80. Wu, P.; Zhang, W.; Li, Z.; Yang, J.; Hou, J. G., Communication: Coalescence of carbon atoms on Cu (111) surface: Emergence of a stable bridging-metal structure motif. *The Journal of Chemical Physics* **2010,** *133* (7), -.

81. Markov, I.; Kashchiev, D., The effect of substrate inhomogeneity on the kinetics of heterogeneous nucleation from vapours. *Thin Solid Films* **1973,** *15* (2), 181-189.

82. Loginova, E.; Bartelt, N. C.; Feibelman, P. J.; McCarty, K. F., Factors influencing graphene growth on metal surfaces. *New Journal of Physics* **2009,** *11* (6), 063046.

83. Zhang, W.; Wu, P.; Li, Z.; Yang, J., First-Principles Thermodynamics of Graphene Growth on Cu Surfaces. *The Journal of Physical Chemistry C* **2011,** *115* (36), 17782-17787.

84. Robinson, V. N. E.; Robins, J. L., Nucleation kinetics of gold deposited onto UHV cleaved surfaces of NaCl and KBr. *Thin Solid Films* **1974,** *20* (1), 155-175.

85. Kim, H.; Mattevi, C.; Calvo, M. R.; Oberg, J. C.; Artiglia, L.; Agnoli, S.; Hirjibehedin, C. F.; Chhowalla, M.; Saiz, E., Activation Energy Paths for Graphene Nucleation and Growth on Cu. *ACS Nano* **2012,** *6* (4), 3614-3623.

86. Vlassiouk, I.; Regmi, M.; Fulvio, P.; Dai, S.; Datskos, P.; Eres, G.; Smirnov, S., Role of Hydrogen in Chemical Vapor Deposition Growth of Large Single-Crystal Graphene. *ACS Nano* **2011,** *5* (7), 6069-6076.

87. Liu, L.; Zhou, H.; Cheng, R.; Chen, Y.; Lin, Y.-C.; Qu, Y.; Bai, J.; Ivanov, I. A.; Liu, G.; Huang, Y.; Duan, X., A systematic study of atmospheric pressure chemical vapor deposition growth of large-area monolayer graphene. *Journal of Materials Chemistry* **2012,** *22* (4), 1498-1503.

88. Vlassiouk, I.; Fulvio, P.; Meyer, H.; Lavrik, N.; Dai, S.; Datskos, P.; Smirnov, S., Large scale atmospheric pressure chemical vapor deposition of graphene. *Carbon* **2013,** *54* (0), 58-67.

89. Bi, H.; Huang, F.; Liang, J.; Xie, X.; Jiang, M., Transparent Conductive Graphene Films Synthesized by Ambient Pressure Chemical Vapor Deposition Used as the Front Electrode of CdTe Solar Cells. *Advanced Materials* **2011,** *23* (28), 3202-3206.

90. Bhaviripudi, S.; Jia, X.; Dresselhaus, M. S.; Kong, J., Role of

Kinetic Factors in Chemical Vapor Deposition Synthesis of Uniform Large Area Graphene Using Copper Catalyst. *Nano Letters* **2010,** *10* (10), 4128-4133.

91. Yao, Y.; Li, Z.; Lin, Z.; Moon, K.-S.; Agar, J.; Wong, C., Controlled Growth of Multilayer, Few-Layer, and Single-Layer Graphene on Metal Substrates. *The Journal of Physical Chemistry C* **2011,** *115* (13), 5232-5238.

92. Vlassiouk, I.; Smirnov, S.; Regmi, M.; Surwade, S. P.; Srivastava, N.; Feenstra, R.; Eres, G.; Parish, C.; Lavrik, N.; Datskos, P.; Dai, S.; Fulvio, P., Graphene Nucleation Density on Copper: Fundamental Role of Background Pressure. *The Journal of Physical Chemistry C* **2013,** *117* (37), 18919-18926.

93. Wei, J.; Jia, Y.; Shu, Q.; Gu, Z.; Wang, K.; Zhuang, D.; Zhang, G.; Wang, Z.; Luo, J.; Cao, A.; Wu, D., Double-Walled Carbon Nanotube Solar Cells. *Nano Letters* **2007,** *7* (8), 2317-2321.

94. Cui, K.; Chiba, T.; Omiya, S.; Thurakitseree, T.; Zhao, P.; Fujii, S.; Kataura, H.; Einarsson, E.; Chiashi, S.; Maruyama, S., Self-Assembled Microhoneycomb Network of Single-Walled Carbon Nanotubes for Solar Cells. *The Journal of Physical Chemistry Letters* **2013,** *4* (15), 2571-2576.

95. Tune, D. D.; Flavel, B. S.; Krupke, R.; Shapter, J. G., Carbon Nanotube-Silicon Solar Cells. *Advanced Energy Materials* **2012,** *2* (9), 1043-1055.

96. Jia, Y.; Cao, A.; Bai, X.; Li, Z.; Zhang, L.; Guo, N.; Wei, J.; Wang, K.; Zhu, H.; Wu, D.; Ajayan, P. M., Achieving High Efficiency Silicon-Carbon Nanotube Heterojunction Solar Cells by Acid Doping. *Nano Letters* **2011,** *11* (5), 1901-1905.

97. Jung, Y.; Li, X.; Rajan, N. K.; Taylor, A. D.; Reed, M. A., Record High Efficiency Single-Walled Carbon Nanotube/Silicon p–n Junction Solar Cells. *Nano Letters* **2012,** *13* (1), 95-99.

98. Li, X.; Zhu, H.; Wang, K.; Cao, A.; Wei, J.; Li, C.; Jia, Y.; Li, Z.; Li, X.; Wu, D., Graphene-On-Silicon Schottky Junction Solar Cells. *Advanced Materials* **2010,** *22* (25), 2743-2748.

99. Miao, X.; Tongay, S.; Petterson, M. K.; Berke, K.; Rinzler, A. G.; Appleton, B. R.; Hebard, A. F., High Efficiency Graphene Solar Cells by Chemical Doping. *Nano Letters* **2012,** *12* (6), 2745-2750.

100. Shi, E.; Li, H.; Yang, L.; Zhang, L.; Li, Z.; Li, P.; Shang, Y.; Wu, S.; Li, X.; Wei, J.; Wang, K.; Zhu, H.; Wu, D.; Fang, Y.; Cao, A., Colloidal Antireflection Coating Improves Graphene–Silicon Solar Cells. *Nano Letters* **2013,** *13* (4), 1776-1781.

101. Li, X.; Fan, L.; Li, Z.; Wang, K.; Zhong, M.; Wei, J.; Wu, D.; Zhu, H., Boron Doping of Graphene for Graphene–Silicon p–n Junction

Solar Cells. *Advanced Energy Materials* **2012,** *2* (4), 425-429.

102. Ye, Y.; Dai, L., Graphene-based Schottky junction solar cells. *Journal of Materials Chemistry* **2012,** *22* (46), 24224-24229.

103. Lin, Y.; Li, X.; Xie, D.; Feng, T.; Chen, Y.; Song, R.; Tian, H.; Ren, T.; Zhong, M.; Wang, K.; Zhu, H., Graphene/semiconductor heterojunction solar cells with modulated antireflection and graphene work function. *Energy & Environmental Science* **2013,** *6* (1), 108-115.

104. Chen, C.-C.; Aykol, M.; Chang, C.-C.; Levi, A. F. J.; Cronin, S. B., Graphene-Silicon Schottky Diodes. *Nano Letters* **2011,** *11* (5), 1863-1867.

105. Ye, Y.; Dai, Y.; Dai, L.; Shi, Z.; Liu, N.; Wang, F.; Fu, L.; Peng, R.; Wen, X.; Chen, Z.; Liu, Z.; Qin, G., High-Performance Single CdS Nanowire (Nanobelt) Schottky Junction Solar Cells with Au/Graphene Schottky Electrodes. *ACS Applied Materials & Interfaces* **2010,** *2* (12), 3406-3410.

106. Zhang, L.; Fan, L.; Li, Z.; Shi, E.; Li, X.; Li, H.; Ji, C.; Jia, Y.; Wei, J.; Wang, K.; Zhu, H.; Wu, D.; Cao, A., Graphene-CdSe nanobelt solar cells with tunable configurations. *Nano Research* **2011,** *4* (9), 891-900.

107. Lee, S.; Lee, K.; Zhong, Z., Wafer Scale Homogeneous Bilayer Graphene Films by Chemical Vapor Deposition. *Nano Letters* **2010,** *10* (11), 4702-4707.

108. Yan, K.; Peng, H.; Zhou, Y.; Li, H.; Liu, Z., Formation of Bilayer Bernal Graphene: Layer-by-Layer Epitaxy via Chemical Vapor Deposition. *Nano Letters* **2011,** *11* (3), 1106-1110.

109. Liu, X.; Fu, L.; Liu, N.; Gao, T.; Zhang, Y.; Liao, L.; Liu, Z., Segregation Growth of Graphene on Cu–Ni Alloy for Precise Layer Control. *The Journal of Physical Chemistry C* **2011,** *115* (24), 11976-11982.

110. Sun, Z.; Raji, A.-R. O.; Zhu, Y.; Xiang, C.; Yan, Z.; Kittrell, C.; Samuel, E. L. G.; Tour, J. M., Large-Area Bernal-Stacked Bi-, Tri-, and Tetralayer Graphene. *ACS Nano* **2012,** *6* (11), 9790-9796.

111. Liu, L.; Zhou, H.; Cheng, R.; Yu, W. J.; Liu, Y.; Chen, Y.; Shaw, J.; Zhong, X.; Huang, Y.; Duan, X., High-Yield Chemical Vapor Deposition Growth of High-Quality Large-Area AB-Stacked Bilayer Graphene. *ACS Nano* **2012,** *6* (9), 8241-8249.

112. Liu, W.; Kraemer, S.; Sarkar, D.; Li, H.; Ajayan, P. M.; Banerjee, K., Controllable and Rapid Synthesis of High-Quality and Large-Area Bernal Stacked Bilayer Graphene Using Chemical Vapor Deposition. *Chemistry of Materials* **2013,** *26* (2), 907-915.

113. Fang, W.; Hsu, A. L.; Caudillo, R.; Song, Y.; Birdwell, A. G.; Zakar, E.; Kalbac, M.; Dubey, M.; Palacios, T.; Dresselhaus, M. S.; Araujo, P. T.; Kong, J., Rapid Identification of Stacking Orientation in Isotopically Labeled Chemical-Vapor Grown Bilayer Graphene by Raman Spectroscopy. *Nano Letters* **2013,** *13* (4), 1541-1548.